6

SOLID EARTH GEOMAGNETISM

One of the fundamental issues in geosciences relates to formation and evolution of the crust, whose understanding has increased many-fold with advanced geophysical techniques. The geological history spans from Archaean, 3.8 Giga years (1 Giga=10^9), to the present (Neogene). Geophysical methods and techniques investigate the structure, composition and physical state of the Earth by mapping crustal anomalies associated with mineral deposits, structural features, and hydrocarbons. Since these constituents lie hidden beneath the surface, geophysics has become a preferred tool of exploration compared to geological techniques. The present section deals with crustal anomalies, and deliberates on their form and detection using appropriate geophysical procedures.

Geophysical methodology is used to detect anomaly in the crust arising essentially due to differences in physical properties of rock materials (Fig. 6.1a), which are related to structural setting of subsurface geological features. The principle of geophysical technique, regarding observed anomalies of magnetism, gravity and electrical resistivity, is employed to investigate crust-mantle relationship.

In general, geophysical surveys fall into two categories: (i) natural field methods, which measure physical properties of the Earth, e.g. gravity, magnetic, radioactive and geothermal and (ii) artificial source excitation methods, which generate pertinent signals used as input into the Earth. The response of input signal is then measured and analyzed to characterize physical properties, e.g. electrical, electromagnetic and seismic of host material. Natural field surveys are passive and easier to conduct, since they do not require large equipment. These surveys delineate the structures to greater depth, but suffer from severe limitations with regard to spatial resolution. Artificial source surveys, on the other hand, are techniques designed and organized to image the structures to a desired degree of accuracy and resolution in an optimal fashion.

N. Basavaiah, *Geomagnetism*

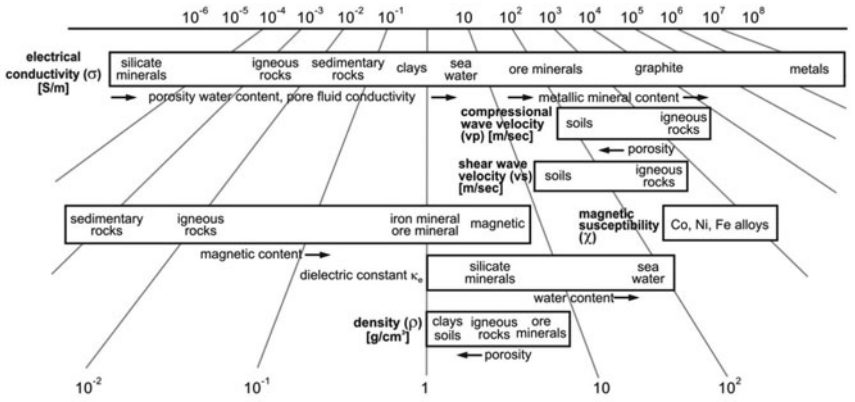

Figure 6.1a. The range of values for the physical properties that can be measured with the methods of applied geophysics (http://appliedgeophysics.lbl.gov/intro/figures fig_prop.jpg).

Seismic tomography with controlled resolution, for example, is a versatile technique capable to resolve complex structures in 3D. Among the various tomographic techniques, teleseismic wave tomography (TWT), local earthquake tomography (LET), and high resolution tomography (HRT) are commonly employed to delineate layered structure in association with seismic wave velocity perturbations. Wide angle seismic refraction and reflection data are acquired along several profiles using chemical explosions as artificial seismic sources. Analysis of teleseismic receiver functions of several P and S phase configurations produced by conversions at interfaces within the crust and upper mantle, using a large number of broad-band seismic stations, and azimuthally well distributed teleseismic sources, is more relied upon. The stacked receiver functions obtained essentially by waveform inversion give lithospheric structure with improved accuracy. The low velocity zones (LVZ) and plume conduits are also imaged well.

Geophysical surveys are carried out on land (magnetics and electromagnetics), at sea (ocean bottom magnetometry (OBM) and seismic reflection), and in air (aeromagnetics), over a range of scales: reconnaissance over 10 to >100 km, focussed mapping in 1 to 10 km range, and high resolution mapping (for finer details) in a few tens to few hundred metres range. The Indian subcontinent has been surveyed by a variety of geophysical tools and the data gained relate to analysis of ground, aerial and satellite potential field anomalies (gravity and magnetics), geoelectromagnetic inductive studies (geomagnetic depth soundings, OBM and magnetotellurics) on land and at ocean bottom, tectonomagnetism (repeat magnetometry for earthquake precursory changes and global positioning system for seismotectonics), rock and sediment magnetism (palaeomagnetic and mineral magnetics), and magnetic petrology. In this chapter, fundamental principles involved in the application

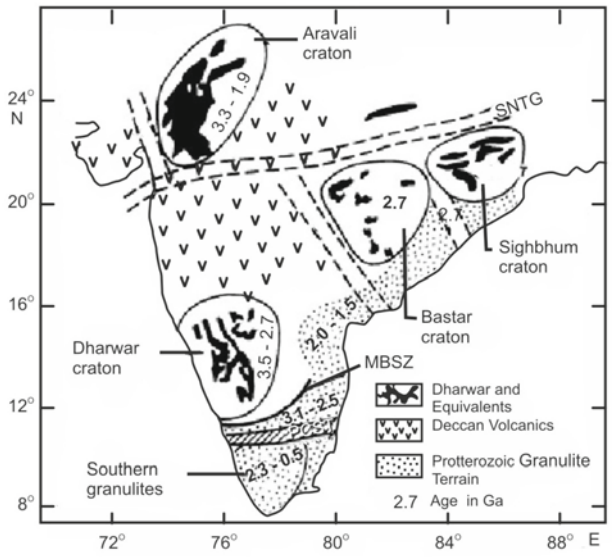

Figure 6.1b. Locations of Archean-Early Proterozoic cratons in the Indian peninsular shield. CG, SNTG, GG, MG, MBSZ and PCSZ refer to the Cambay graben, Sone-Narmada-Tapti graben, Godavari graben, Mahanadi graben, Moser-Bhavani shear zone and Palghat-Cauvery shear zone, respectively. Geologic ages are from S.M. Naqvi (pers comm) (courtesy: Pandey and Agrawal, 1999).

of these methods to the major tectonic and lithologic problems, are discussed with emphasis on comprehensive study of the Earth's interior.

The Indian shield is known to have grown through the nucleation of six widespread Archaean-early Proterozoic cratons separated by Gondwana rift valleys, sutures, and mega-lineaments (Fig. 6.1b). These distinct tectonic and lithostratigraphic assemblages differ in petrography, chemistry, thickness and seismic structures. The deeper structures beneath different geological provinces, which exhibit interesting cratonic formations, grabens with active and dormant geologic faults and shear zones are studied through geomagnetic methods and techniques.

Pure and applied geophysical studies: Geophysical methods employ natural and artificial sources. Earth's 'natural' signatures like gravity, magnetism and EM are employed for mapping anomalous structures in the Earth's deep interior, whereas induced electromagnetism involving geomagnetic deep sounding (GDS) and magnetotelluric (MT) techniques provide information supplementing the above methods. For example, the MT method is used in a large frequency or period range, which corresponds to a depth interval from the surface to some hundred km. The aim of exploration varies according to depth. In artificial source methods, the response of subsurface geological feature to artificial energization of the ground is attempted. Such approaches include artificial electrical, EM, seismic methods and microseismics.

Thus, geophysical studies have both fundamental and applied aspects, essential to enhance research and development in geosciences. These studies upgrade the basic understanding of regional tectonics, and considerably improve knowledge on the global geodynamical processes that drive the continents, control generation of energy, give rise to mineral deposits, earthquakes, volcanoes, and the like. A few of the applied aspects specifically relate to information on optimizing land-use, potential resource locations, and marking out earthquake prone areas by identifying active faults and conductive zones. However, both pure and applied aspects of a geophysical measurement are necessary to produce a holistic understanding of the dynamical processes at work in the Earth's interior. In this sense, they are complementary to each other.

6.1 GEOPOTENTIAL FIELD ANOMALY STUDIES

Geopotential field methods involve measurement of Earth's gravity and magnetic field to prepare anomaly maps. An anomaly is an abnormality, i.e. something different from the normal (theoretical value estimated from homogeneous Earth model) formed by spatial gravity and magnetic field variations, depending on the discrepancy in surface geology, and changes in composition, subsurface temperature, or thickness of the crust and mantle. Magnetic (gravity) anomalies are perturbations of the geomagnetic (gravity) field due to Earth structure. They are seen when one subtracts a regional magnetic (gravity) field from a series of observed readings.

I. Sources of Regional Anomalies

Many of the regional tectonic features of the study area appear coincident with satellite geopotential field anomalies. Sources for these anomalies may be generalized as lateral variations of the vertical integral of crustal density and magnetization. Hence, optimally reduced anomaly maps are used to detect these lateral variations. These variations in density and magnetization of the crustal column may in turn reflect petrological, structural, or thermal variations of the crust, resulting through active tectonic processes. Anomaly maps are used to constrain tectonic configuration of the lithosphere.

In general, long wavelength magnetic anomalies can be modelled by regional scale magnetization variations of the lithosphere, which lies between the surface and a lower boundary at which magnetic minerals do not occur. This boundary is defined as the topography of the Curie point isotherm of the crustal magnetic minerals. The location of this lower boundary is not unanimously agreed upon. Seismic velocities and analysis of upper mantle xenoliths indicate that lower crust is made up of granulite grade metamorphic rocks, and that the upper mantle is dominantly peridotite (Chapter 2). Mantle xenolith studies also indicate magnetite or serpentinized metals do not exist below the Moho, making it the magnetic basement except where a limiting Curie isotherm is above the Moho. Some invoke serpentinization as a source

of magnetic mineralogy below the crust extending the magnetic boundary to the upper mantle. However, the debate will continue till this problem is definitely sorted out.

Crustal conditions affecting regional scale magnetization generally involve variation in the amount, distribution, and magnetic properties of magnetite within the lower crust. The amount and distribution of magnetite are related to crustal composition and thickness, whereas the magnetic properties of magnetite are temperature dependent (Chapter 2). Thus petrologic, structural and thermal perturbations within the crust and upper mantle produce magnetization contrasts. These physical and lithologic variations often combine to produce anomaly superposition, and source ambiguity, which limits the interpretation of regional magnetic anomalies.

This is overcome by combining the gravity data. In general, gravity anomalies are related to density variations, formed from several sources. At satellite elevations, gravity signals with long wavelengths characterize crustal and upper mantle density contrasts due to regional variations in composition (bulk mineralogy), temperature or crustal thickness. Longer wavelength anomalies, which are of continental scale, commonly arise from deeper mass variations in the mantle and core, which occur below the magnetic lithosphere. The combined analysis of gravity and magnetic data is, however, more effective in bringing out crustal and mantle features, since they map the source fields at different depths. Hence, ground magnetic and gravity surveys are planned, wherein ground data can then be coupled with aeromagnetic and satellite data for a comprehensive subsurface picture.

II. Anomaly Contour Maps

The compilation of gravity and magnetic anomaly maps in this book are qualitatively presented in the form of contour maps (points having equal gravity and magnetic values). Presence of 3D bodies is suggested by more or less circular or elliptical contours, whereas elongated ones define the presence of 2D bodies. The contour map is then divided into zones of different magnetic characters, which are correlated with the known geology and these correlations are extrapolated to poorly mapped regions. The axes of the anomalies are usually drawn on the maps to derive information on major structural controls. Repetition of the contour pattern is suggestive of a folded sequence of sedimentary beds. Termination of the contours along a line, or the presence of flexures in the contours indicates a fault. Magnetic axes are also frequently displaced due to faulting. Individual bodies of the same rock type occurring within a single geological province show similar magnetic characteristics. Frequently, magnetite may be formed in some rocks due to effects of the adjacent igneous intrusives helping to outline the intrusive itself. A qualitative idea of the depth of the sources can also be obtained from some striking characteristics of the anomaly patterns; sharp anomalies indicate, for example, the anomalous bodies to be at very shallow depths.

III. Geopotential Problems

Solutions to geopotential problems are non-unique, and other available geophysical data are necessary to constrain the models. Hence, magnetic surveying is often done in conjunction with other geophysical techniques such as gravity, heat flow, seismic and MT to recognize different source field depths, and thereby help to reconstruct the plate history. Magnetic data together with integrated geophysical data have proved especially useful in studying several processes, such as intrusive bodies with different magnetization than the country rocks, the juxtaposition of crustal blocks of different magnetization through plate tectonics, and creation of the oceanic crust during different core field polarity periods.

IV. Ground, Aero and Satellite Magnetic Surveys

Magnetic survey is the measurement of EMF intensity or its components (such as vertical component) with the objective of measuring the magnetism over an area of interest. Magnetic measurements can be made from a variety of platforms (water, ground, air) and altitude (ocean bottoms to satellite heights). These measured magnetic data have contributions from source fields over several spatial scales. Due to the availability of the data at various scales and elevations (which generally represent geophysical variations at different depths), synergistic use of these data provides a unique opportunity to study similarities and variances of geologic and structural variations through the entire lithospheric column. Short-wavelength signal is generated by magnetic material that resides within the uppermost part of crust, medium-wavelength comes from materials at shallow depths, and long-wavelength component is generated from deep-seated structures. The ground data contain contribution from all these sources, but the air-borne data contain mostly medium and long wavelength components, basically limited by the size of the survey area. The satellite data, on the other hand, contain only long-wavelength module. As far as exploration of resources at exploitable depths is concerned, the ground data offer more information than the air-borne data. For pinpointing exact location of the geodynamic structure, long as well as medium-wavelength components derived from ground and air-borne data are subtracted.

Analysis of data for crustal magnetic anomalies is obtained from (1) satellite data of polar orbiting geophysical observatory (Pogo), and MAGnetic field SATellite (Magsat), (2) aeromagnetic maps, and (3) ground magnetic surveys conducted over petroliferous sedimentary basins of India.

6.2 SATELLITE MEASUREMENTS OF EARTH'S GRAVITY FIELD

Remote sensing of the Earth through satellites provides data to undertake studies that embrace virtually every aspect of the origin, dynamics and evolution of

the lithosphere. One of the earliest scientific uses of satellite technology has been the mapping of the Earth's gravity field and determining its shape (the Geoid). As early as in 1956, a new value for the flattening of the Earth was determined from tracking of Sputnik I. The gravity field is not easy to measure from air-borne sensors to an accuracy needed for a proper analysis of shallow subsurface structures. The gravity field is the result of mass and its distribution inside a body. Therefore, a spacecraft tracking, using its radio communication signal, determines its orbit or trajectory from which the gravitational field and a mass of the body can be inferred. For a proper analysis of shallow subsurface structures, gravity anomalies can be calculated from satellite orbital motions.

I. Satellite Free-air Gravity Anomaly Maps

This book uses free-air anomaly maps at ground level and 400 km height prepared by Rapp from the spherical harmonic analysis of the 1° by 1° averages of the measured free-air gravity anomalies and satellite tracking data. These maps are often called the satellite-derived free-air anomaly maps, or satellite gravity anomaly maps (Fig. 6.2). In essence, Fig. 6.2b is a downward continuation of Fig. 6.2a at ground level.

India is known for a thorough gravimetric coverage of its landmass, although major part of it still continues to be impervious to detailed geological and geophysical surveys. This is because of problems posed by the highly varying topography of Aravallis, Vindhyans, eastern and western ghats, Deccan plateau, and the Himalayas. The only recourse is satellite-based measurements, which can map surface and subsurface structures of the entire subcontinent,

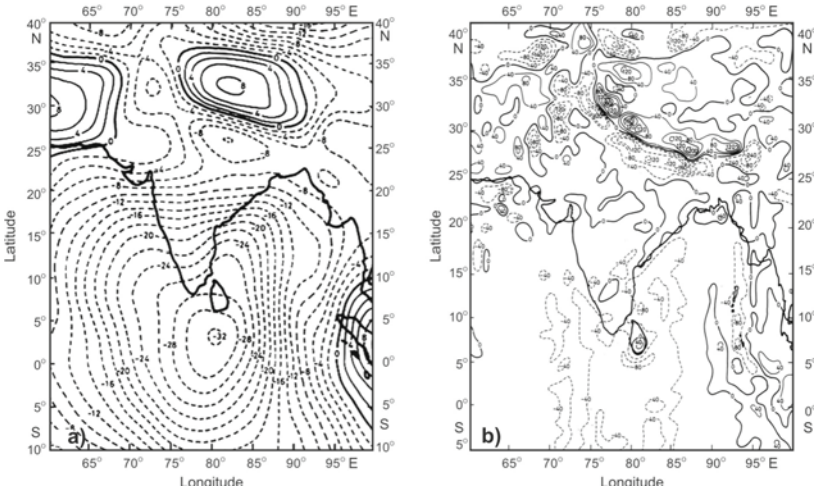

Figure 6.2. (a) Satellite free-air gravity field anomaly observed at a height of 400 km, contour interval 2 mgal. (b) Satellite free-air gravity field anomaly observed at ground level, contour interval 40 mgal (Singh et al., 1992a).

and its neighbouring oceanic realm; hence, satellite gravity anomaly maps are analyzed.

Satellite gravity anomaly, sources: Gravity anomalies are caused, in principle, by lateral density variations that can be located anywhere from the Earth's surface to the Earth's core. Anomaly components of a wide band of wavelengths are usually superimposed on each other on gravity anomaly maps. Generally, the Earth's gravity field can be considered to be distinctly composed of short-wavelength (a few to few tens of km), intermediate-wavelength (a few hundreds to few thousands of km), and long-wavelength (larger than described by spherical coefficients of degree and order 10) components. The short-wavelength anomalies, which are of interest in crustal studies are usually associated with the near-surface structures such as faults, intrusive bodies, sedimentary basins and others. In contrast, large-scale features such as mountain belts, isostatic processes, and inhomogeneities due to changes in composition, thermal state or thickness of the crust and mantle lead to long-wavelength anomalies. Short-wavelength anomalies overlap and dominate the ground gravity maps, making it difficult even to identify the trends of anomalies from deeper tectonic causes. However, anomalies measured at a few hundred km above the Earth's surface represent density variations at large depths only, since most of the short-wavelength components are automatically filtered out at these heights (Fig. 6.2a).

II. Ambiguity in Gravity Interpretation

Interpretation of gravity data means locating and determining various parameters of the sources responsible for the anomalies. A given gravity distribution on the ground surface can be explained by a variety of mass distributions at different depths. Following the theorem of equivalent stratum, the ground surface (or plane observation) can be replaced by a hypothetical mass distribution. The observed anomalies are actually continued downwards to different levels, and from these continued anomalies, a hypothetical mass distribution can be calculated at each level. Only one of these mass distributions is the correct solution to the observed anomalies, and this can be selected, if the depth to the mass distribution is known. In the absence of any outside information such as depth to the mass distribution, gravity interpretation is ambiguous, and no solution can be found that explains the observed anomalies uniquely.

To make the problem determinate, the unknown parameters must be reduced to a number less than the observations. This can be done in many ways, each pertinent to the problem in hand. The most important way of overcoming ambiguity is to assign a regular shape to the disturbing body, and to assume that the model has a uniform or uniformly varying density contrast. The important geometrical models very often used in gravity and magnetic interpretations are spheres, cylinders, faults, dykes, and others. A 2D fault structure, for instance, with a uniform density has only four parameters to be

determined from the gravity anomalies. These parameters are the density contrast, two depths (one each to the top and bottom interfaces), and the dip of the inclined face. The contour pattern of the anomaly map itself and the knowledge of local geology permit the assumption of the pertinent shape to the target.

III. Qualitative Interpretation of Satellite Gravity Anomaly Maps

The free-air anomaly map at 400 km height (Fig. 6.2a) shows only a couple of very broad highs and lows, formed by density variations at the boundary of the upper and lower mantle at 600 km. A major low over the southern part of India (specifically the Indian ocean low, IOL) and a high over the Kohistan-Himalaya high (KHH) are the two main prominent gravity features at satellite heights. The long wavelength of the IOL and its geographical coincidence with extreme geoidal minima of –104 m suggests the anomaly source to be in the crust or upper mantle.

On the other hand, the free-air anomaly at the ground level (Fig. 6.2b) is generally –40 mgal south of 15°N, and nearly zero over the northern portion of the peninsular shield. The latter observation signifies that the Indian peninsula is isostatically compensated. The region between 25° and 35°N is dominated by a strong negative anomaly reaching to <–120 mgal, and an equally strong positive anomaly north of it. These trends are attributed to the Himalayan mountain ranges and their overcompensation.

The free-air anomaly at the ground level shows several localized high and low anomaly values defining different blocks, which do not appear in 400-km height (Fig. 6.2a), since these anomalies have their roots in crust or upper mantle. For instance, the gravity high values up to 40 mgal, not seen at 400-km level, are associated with Sri Lanka and Shillong plateaus, Aravallis, Marwar and eastern ghats, suggesting their sources limited to the crust. Another significant feature of 90°E ridge gravity high does not reflect at 400-km level, implying a crustal anomaly. The long belt of negative anomalies of –40 to –80 mgal, covering the region between latitudes 5° and 18°N confined to 95°E longitude, corresponds to the trench system of Andaman Islands. These anomaly components are also missed at 400-km level. There is no obvious expression of Deccan traps, an extensive cover of the flood basalts, both at ground and at 400 km level.

IV. Anomalous Satellite Gravity over Himalayas and Its Isostatic Compensation

The satellite free-air gravity anomaly at ground level (Fig. 6.2b) is further used for studying the isostatic condition in many parts of Indian peninsula in general and the Himalayas in particular. The anomaly is consistently zero over

the northern portion of the peninsular shield, which implies major part of the peninsula being isostatically compensated. A strong positive free-air anomaly, initially trending NW-SE at 34°N and 75°E, and then turning E-W beyond 30°N and 80°E, correlates with the known trend of Himalayas (Fig. 6.2b). The high positive anomaly is bordered on the south by an equally strong negative anomaly. The Himalayas are generally considered isostatically overcompensated, and are expected to give rise to negative free-air anomalies. But, contrary to expectations, free-air anomalies over the Himalayas in satellite data are positive, ranging from 40 to 160 mgal. Some have explained this anomalous behaviour in terms of isostatically undercompensated processes.

To solve the riddle, free-air anomalies are calculated over typical models of trapezoidal topography depicting elevated masses and steep valleys following the local compensation theory of Airy-Heiskanen. The crust-mantle boundary outside the anomalous zone is assumed to be at 30 km depth. According to the Airy-Heiskanen system, a topographic height of 1 km increases the thickness of the crust by 6.67 km for a density of 2670 kg/m^3 of the topography and the universally accepted density contrast of 400 kg/m^3 at the Moho.

Figure 6.3 clearly indicates that free-air anomalies are positive over the topography, flanked by negative ones on either side, which are stronger on the flanks of a steep slope. This shows that the Himalayas are indeed overcompensated isostatically and it would be erroneous to presume that the positive satellite gravity anomalies over them prove undercompensation. It is also stressed that the true nature and extent of isostatic compensation of the Himalayas can only be decided by investigating both the positive and negative anomalies resulting from the mountains and their roots.

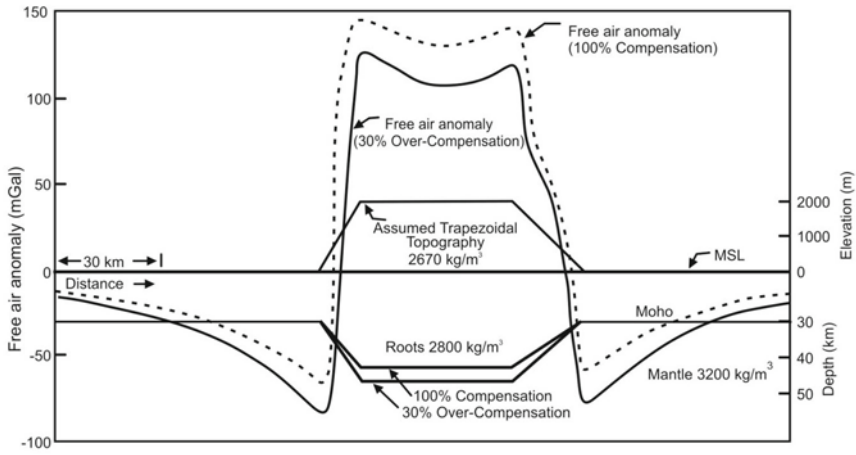

Figure 6.3. Calculated free-air anomalies over an assumed trapezoidal topography model depicting the Himalayas with an elevation of 2000 m and base width of 75 km for both cases of complete and 30% over-compensation (Basavaiah et al., 1991).

V. Preparation of Residual Free-air Anomaly Map

The anomalies at ground level (Fig. 6.2b) are composed of long-wavelength anomalies from distant deep sources, which are removed to study crustal and local features. The long-wavelength part estimated from the inversion of the gravity anomaly at 400-km level for an equivalent mass distribution at ~600-km depth is a fairly representative value for lateral heterogeneity in the upper mantle. Deep earthquakes have foci up to 600-km depth. The anomaly components due to such a mass distribution are used to recalculate the long-wavelength anomalies at ground level (Fig. 6.4).

It shows a pronounced minimum over the IOL, and three systematic maximum anomalies over Sumatra-Indonesia high (SIH), KHH and Baluchistan high (BNH). These anomalies are long wavelength components and are subtracted from Fig. 6.2b. The difference between observed total anomaly at ground level (Fig. 6.2b), and those calculated through the equivalent point source technique (Fig. 6.4) is called the 'residual anomaly'. Figure 6.5 shows the residual gravity anomalies, which give a better idea of sources at shallower than 600-km depth.

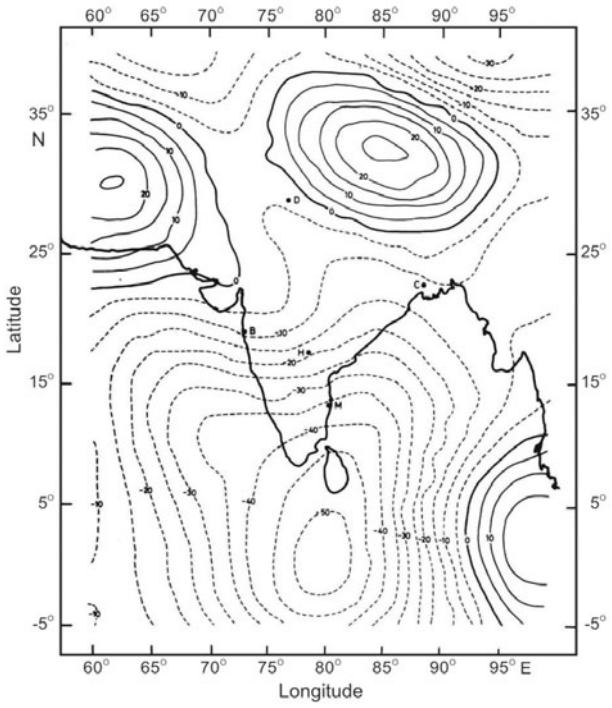

Figure 6.4. Gravity anomaly, in mgal, at the surface of the Earth recalculated from the equivalent mass distribution obtained by inverting gravity data at a height of 400 km, contour interval 5 mgal (Singh et al., 1992a).

VI. Residual Free-air Gravity Anomaly Map and Tectonic Implications

Figure 6.5 shows several highs and lows of different magnitudes, some extending to several hundred km, and others confined to small areas. The residual gravity map can identify geological lineaments, horst like structures, intra-cratonic basins, oceanic ridges, and transform faults that are caused by or associated with structures at the Conrad or Moho levels or both. Some localized closures characteristically identify the tectonic units. The high of 40 mgal near 25°N latitude defines the Shillong plateau (shown as SP in Fig. 6.5). Over Sri Lanka, a distinct positive anomaly closure is surrounded by negatives. The well-defined and isolated highs over Shillong plateau and Sri Lanka are due to their associated horst-like structures developed by deep faulting in Meso-Cenozoic time at Moho discontinuity. The Dharwar folding (DF) is also reflected on the residual map by a general NNW-SSE trending, partly superimposed by high grade granulites. The Cuddaph (CD) basin is seen as a major negative anomaly, indicating it to be the result of tectonic activity at deeper levels either

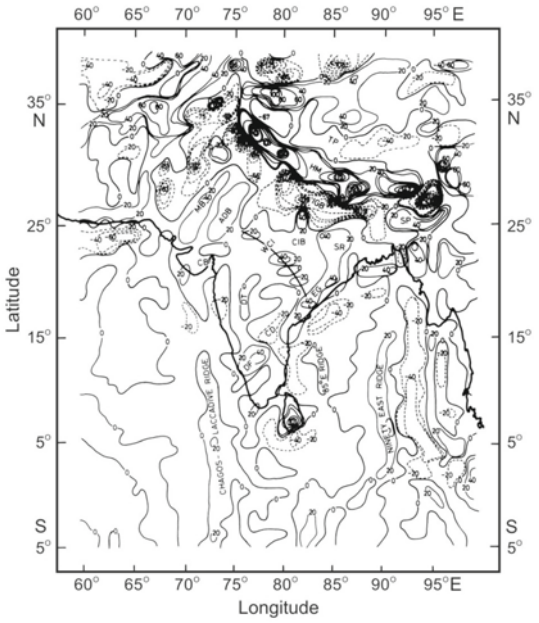

Figure 6.5. Residual gravity field anomaly, in mgal, after removal of the calculated long wavelength part due to sources in the upper mantle at a depth of 600 km from the observed gravity anomaly at the ground surface. Contour interval 20 mgal. DF - Dharwar Folding; DT - Deccan Traps; CB - Cambay Basin; MB - Marwar Block; ADB - Aravalli-Delhi Block; CIB - Central Indian Bijawars; SR - Singhbhum Region; EG - Eastern Ghats; CD - Cuddapah Depression; SP - Shillong Plateau; TP - Tibetan Plateau; HM - Himalayan Mountain ranges; IGB - Indo-Ganga-Brahmaputra basin, and WCI - West-Central Indian lineament (Singh et al., 1992a).

at Moho or Conrad or both. Importantly, Fig. 6.5 accentuates many features, which are not so obvious in Fig. 6.2b. Perhaps, the situation is unique for the Indian region, where sharp gradients of a strong long wavelength component masks the local features. The causative sources of all these residual gravity anomaly trends are wholly located within the crust.

In addition to long running anomaly closures, many localized closures are also seen to align in well defined trends that can be identified as lineaments. The most important ones are marked as Himalayas (HM), west-central Indian (WCI), eastern ghats (EG), and ridge features in the Indian ocean. Some of these lineaments coincide with or run parallel to the known major geological trends. The anomaly trends of the Himalayas, eastern ghats, Aravallis-Delhi block (ADB), Marwar block (MB), and 90°E ridge appear distinctly in the residual map, but are subdued in the ground map. In addition, this map brings out a few more important trends, and anomalies such as the Chagos-Laccadive ridge, 85°E ridge, west-central Indian lineament, Dharwar folding, and Cuddapah depression. It also gives clear demarcation of the Himalayas, Indo-Ganga-Brahmaputra basin and Tibetan plateau (TP).

VII. Residual Bouguer Gravity Anomaly Map and Crustal Thickness

A Bouguer anomaly map of India (Fig. 6.7) is prepared after removing the long wavelength component from the modified Bouguer gravity anomaly map (Fig.6.6). The calculated residuals are plotted in Fig. 6.7, and are used to estimate the thickness of the 'Indian' crust.

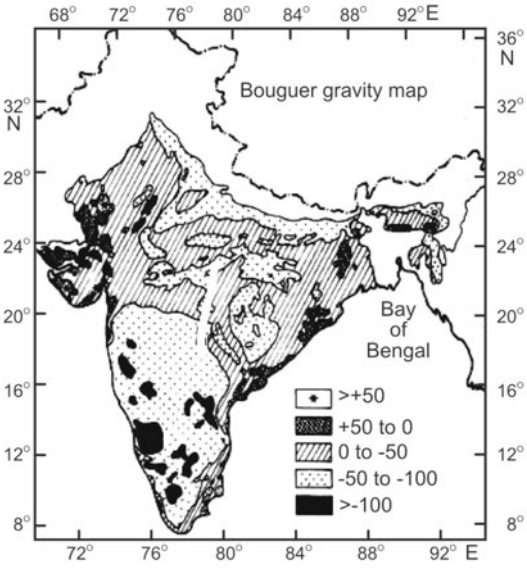

Figure 6.6. Modified Bouguer gravity anomaly map of India prepared by the National Geophysical Research Institute (1975). Contours are drawn at 50 mgal intervals.

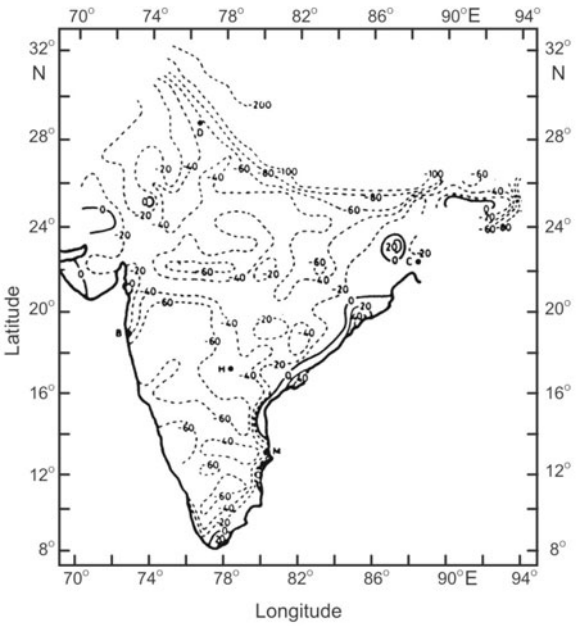

Figure 6.7. Residual Bouguer gravity anomaly map after removal of long wavelength component shown in Fig. 6.4 from Fig. 6.2b (Singh et al., 1989a).

Thin crust exists across the Delhi folding, Aravallis, the Bombay high, Cambay basin and eastern ghats (Fig. 6.7). The change in pattern and amplitude of anomalies is indicative of different crustal configuration along the east and west coasts. Although the data do not extend into the oceanic region on the east coast, closures of anomaly contours on the continental side are evident and a line of zero-anomaly coinciding with the coast line signifies a transition in the nature of the crust. The gravity pattern indicates a long linear trend along the eastern coast suggesting dimensional extent of the causative source. On the other hand, the contour loops on the west coast seem to continue into the oceanic side. These deductions of the continent-ocean boundary are corroborated using the satellite magnetic data.

6.3 SATELLITE MEASUREMENTS OF THE EARTH'S MAGNETIC FIELD

The Earth is heterogeneous in age from the land to ocean. Beneath oceanic realm, the crust is young, thin and layered. The continents, at places, have a crust as thick as 70 km (45 miles) with age up to 4,000 Ma. Research expeditions mounted through ingenious techniques such as seismic, geochemical, petrological and the like have been able to accumulate knowledge of its highly complex structure and composition. The continental crust is alternately seen to form and deform by the mechanism and processes that are still not well

understood. A new geophysical tool based on satellite measurements of the EMF (discovered almost by chance) offers a new avenue of testing models of the evolution and deformation of the continental, and to some extent oceanic crust. This methodology has already given some promising results in the exploration of cosmic bodies such as Mars or the Moon.

The first global EMF measurements encompassing all the sectors of the Earth were made by Cosmos (USSR) and a series of USA's Pogo 2, 4 and 6 satellites launched by NASA in the late 1960s. Cain and his associates in 1970 were the first to recognize long wavelength anomalies from the total field residuals obtained from Pogo data. Magnetic bodies of such magnitude were hard to predict, and difficult to conceive with the investigative tools at hand at those times. Scientists, then, were content with delineating micro-level features, and structures of the crust (fold/fault) as well as the compositional and temperature changes that were deciphered from rapid variations caused in the process of propagation of seismic waves.

The anomalies deciphered by Pogo were confirmed later by the Magsat satellite, launched by NASA in November 1979. This satellite had a lower and less elliptical orbit equipped with magnetometers that measured the Earth's magnetic field vector. NASA's Langel and his team were the first to publish new anomaly maps mounted from Magsat data, which were improved later by other groups. These long wavelength anomalies (product of Pogo and Magsat) gave newer insights into deformations and other tectonic imprints from innumerable areas that were inaccessible till then. Magsat has a unique place in global magnetic studies, since it churned out vector measurements. The total field measured by Cosmos and Pogo has a scalar component from which ionosphere components are difficult to separate out. Even for Earth resource survey, vector measurements are more potent than just the scalar ones. Because of this reason, Magsat data are extensively used by both space and geoscientists. The Magsat-like Oersted satellite launched in 1997 covered near-noon local time, and provided ideal conditions for studying ionospheric current systems. Such an effort is rewarding not only in an integrated use of Magsat data, but also in providing appropriate method for reduction of the data to be obtained through forthcoming missions.

Anomalies in the static part of the magnetic field as deduced from satellites establish the utility of space-borne measurements in studies of long wavelength anomalies, which originate largely within the lithosphere. Long wavelength anomalies are mostly recognized from near-Earth satellites at altitudes of 350-750 km, and these altitudes define the shortest wavelengths traditionally associated with such geomagnetic features. Virtually identical features have now been recognized in satellite magnetic field records from Pogo (1967-1971), Magsat (1979-1980), Oersted (1999-), CHAMP (2000-) and SAC-C (2004).

All masses contribute to gravity field, but only those materials that have a significant susceptibility contrast add to magnetic anomalies. The density variations of different layers within the lithosphere may change by less than one order of magnitude, but susceptibility variations contributing to

magnetization can change by three orders of magnitude, thus making magnetic data a very sensitive indicator of change within the lithosphere. With the advent of digital signal processing techniques, it is now possible to extract far greater information and gain accurate results.

I. Regional Magnetic Anomaly Map

Potentiality of satellite magnetic data in determining structure of geological significance and in identifying inhomogeneities in the lithosphere, has been proved beyond doubt. Identification of the Bangui anomaly in Africa from Pogo data is an excellent example of the importance of satellite magnetic data. The magnetic field residuals obtained from several passes of Pogo satellite over India reveal them to be positive over the southern part of India, and negative over the Himalayas. Boundary separating regions of positive and negative anomalies appear to be in line with the Narmada-Sone lineament, which extends from the western to eastern margins of Indian plate. To resolve the structural complexities of the Indian plate, regional geomagnetic reference field and magnetic anomaly maps are prepared using ground and Magsat data.

II. Magnetic Anomaly through Magsat

Data obtained during its passage over the Indian region (0° to 40°N geomagnetic latitude and 60° to 100°E longitude) with finer time resolution were used to draw anomaly maps. These data contain contributions from three sources: (1) Earth's core (~40,000 nT), (2) ionosphere-magnetosphere currents (up to 200 nT), and (3) geological structures within the crust (0 to 20 nT). Magsat data provide additional constraints to study oceanic basins and continental margins, besides giving an insight into deep crustal conditions, as well as providing useful framework for tectono-mineralogic analyses and synthesis along with surface and other satellite-based data. These datasets provide interesting information on the geodynamical structures and processes, which are discussed below.

III. Data Processing

Several processing and reduction procedures involving equivalent point source inversion modelling were synthesized and applied to satellite magnetic data. These yielded improved reduction techniques and better resolved anomaly maps suitable for geologic analysis. Observed satellite magnetic data came from the Magsat <2°> scalar and vector anomaly maps derived by Agarwal and his coworkers.

IV. Isolation of Crustal Origin Components and Reduction of Data

Data from Magsat measurements are reduced to isolate components of crustal origin of 10 to 20 nT. Considering that crustal component constitutes only

~0.5% of the total field, its isolation is an involved process. The normal procedure is to eliminate core field constituting ~99% of the main field through MGST (4/81) thirteenth order and degree spherical harmonic expansion. From the remainder, contribution of ionospheric-magnetospheric currents (which usually refer to as external field) is removed. The ionospheric contributions are neglected since Magsat orbits always confined to dawn-dusk meridian. The distribution of external field currents during disturbed conditions of magnetosphere is sufficiently complex to preclude a simple expression. However, when the magnetosphere is quiet, $P_1°(\cos \theta)$ is reasonably taken to represent the latitudinal dependence of external field, where P_1 is Legendre polynomial of 1° and θ is the dipole colatitude of the observation point. The data of 92 passes with $Kp<1_0$ are selected. Even after all these corrections, the residual data from overlapping passes show zero-level difference. This has been ascribed to lack of base-line control arising from the nature of measurements, which are made with a continuously moving magnetometer. To account for base-shift, a quadratic trend is subtracted. The residuals are then scrutinized, and values with magnitudes >20 nT are rejected. The remaining data are then isolated for 2° by 2° blocks, and data in each block are averaged. Values deviating by $>2\sigma$ (σ = standard deviation) from the block mean are rejected. A new average is then estimated, which represents the anomaly at the average height of 420 km for the block. The crustal part (often referred to as anomaly field): total (B), N-S (X), and vertical (Z) fields are shown in Figs. 6.8a, b.

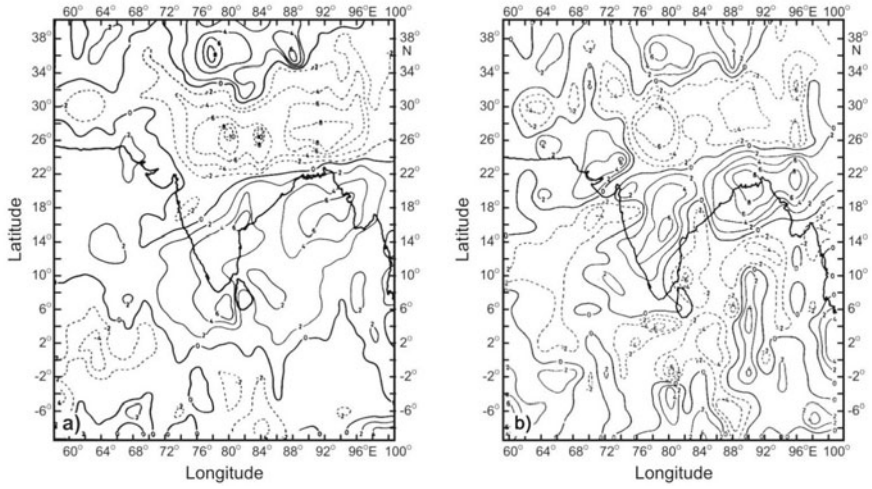

Figure 6.8. Data collected over the Indian subcontinet from the Magsat satellite are used to understand the crustal structure by determining crustal magnetic anomalies. Since the crustal component contributes only 0.05% to the total observed values, its isolation is a complex process. Here the anomaly shown is for: (a) vertical field (Z), and (b) scalar total field (B) computed from X, Y, and Z anomalies for an average Magsat height of 420 km. The values plotted are in units of nT (Agarwal et al., 1986).

The B-anomalies synthesized from X-, Y- and Z-anomalies are compared with B-anomaly estimated directly, and found the two to agree quite well. This gives credence to the data reduction technique, and at the same time establishes reliability of the anomaly maps.

V. A Tricky Magnetic Interpretation

Characterization of crust in terms of geological properties directly from the anomaly map is difficult, because the angle of inclination changes from zero over the southern end of peninsula to ~45° over the Himalayas. Apart from depending on the geological structure, the pattern of anomaly also depends upon the direction of magnetization. Hence, further reductions aimed at improving the resolution of geologically significant Magsat anomalies are applied. Most importantly, because magnetization of lower crustal and upper mantle sources are predominantly induced, the data are reduced for the variable geomagnetic field effects of inclination, declination and intensity to enhance geologic analysis.

The vector anomaly maps (particularly the X and Z) exhibit much larger amplitudes than the scalar anomalies, indicating that the scalar anomaly is not the total anomaly. Rather it is the projection on the direction of the main field. Thus, when the main field is wholly horizontal, the scalar anomaly can have no contribution from anomalies in vertical direction. Such a situation is seen over the southern portion of the Indian peninsula and the adjoining sea. Since the angle D over India is 1° to 2°, the scalar anomaly is independent of E-W direction anomalies. These regions have one or two components (X, Y and Z) as zero, hence utmost care should be taken when synthesizing models for geological structures from just total field measurement.

Further, geographical coincidence between the magnetic anomalies and various tectonic and geological structures need cautious interpretation. Because of the essential dipolar nature of the Earth's main field, the anomalies are not always directly above the sources. The position and character of a magnetic anomaly caused by a body of given geometry depends on its magnetization direction, which varies with latitude (Fig. 6.8 c-f). Thus a positive anomaly can be seen, if the source is at the pole (here the main field is vertical); a negative anomaly is encountered, if it is at the equator (here the field is horizontal) (Fig. 6.8 c-e). This problem can be overcome by either reducing the anomaly to the pole (Fig. 6.8 f), which deliberately aligns the anomalies with the sources, or by calculating the magnetization distribution. The latter is mostly adopted because it directly parameterizes the crustal characteristics. The transformation makes the anomalies overlie the sources, making it possible to correlate the magnetic anomalies over gravity and geological information (Fig. 6.11).

VI. Correctness of Anomaly Maps: Forward Modelling

Realizing the utility of magnetic field anomaly maps in numerical modelling of ground and aeromagnetic data, it is useful to examine the physical reality of

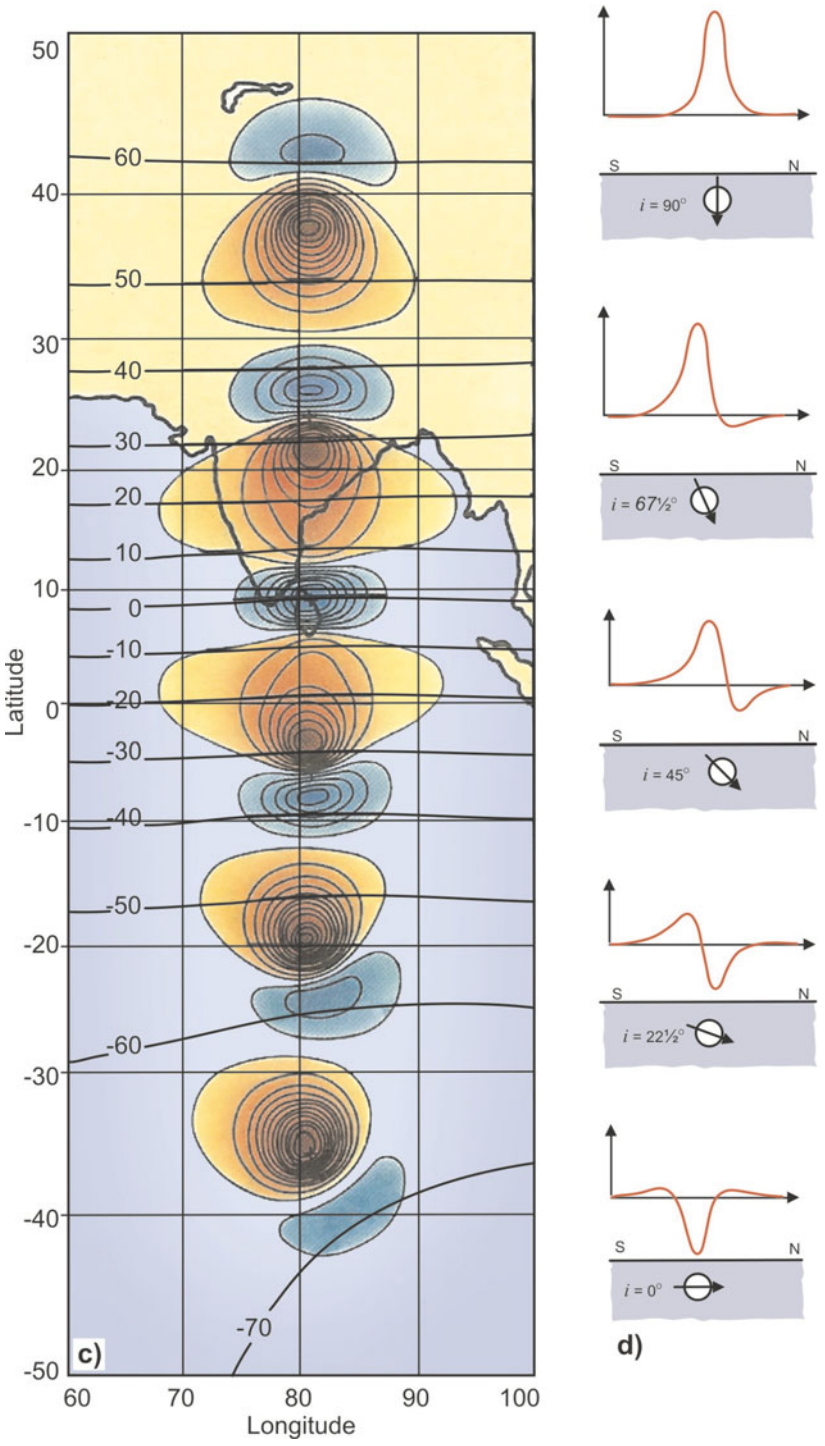
50
40
30
20
10
0
-10
-20
-30
-40
-50
Latitude
60
70
80
90
100
Longitude
60
50
40
30
20
10
0
-10
-20
-30
-40
-50
-60
-70
c)
S
N
i = 90°
i = 67½°
i = 45°
i = 22½°
i = 0°
d)

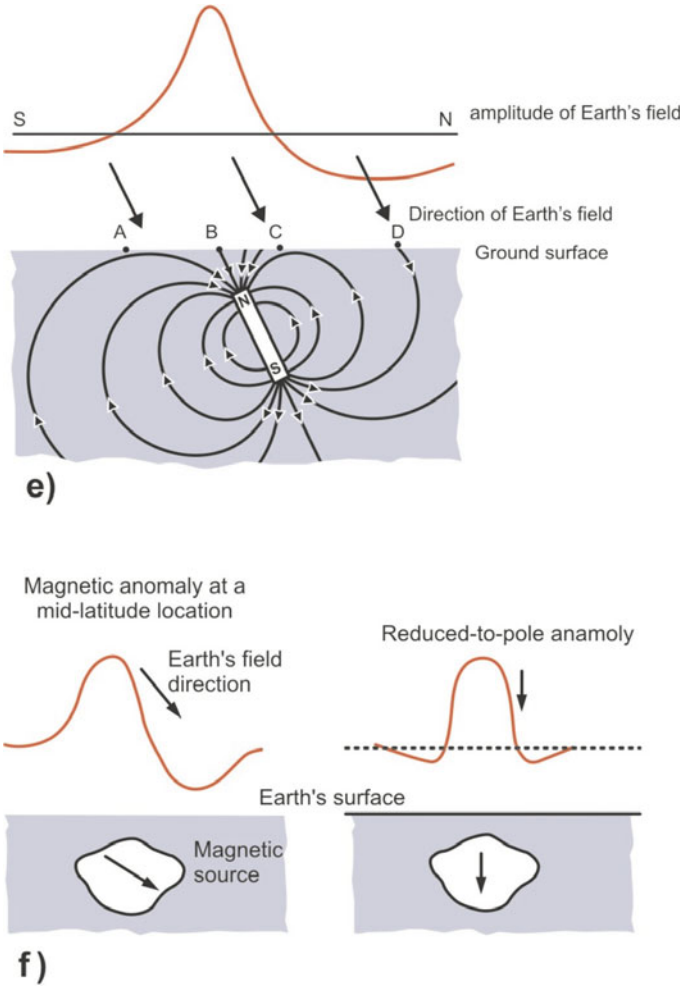

Figure 6.8. (c) The magnetic anomaly produced by a magnet of given dimensions (a point source marked by a + moving latitudinally), which always has two poles, one positive (red) and the other negative (blue), depends on the magnetic direction within the body. The main field is dipolar and its inclination is a function of latitude. The bold lines represent inclination of the main field. Note the position and shape of the poles of the magnetic anomaly produced by a point source depend on the latitude of the source (courtesy: Achache et al., 1988), (d) The variation of magnetic anomaly with (magnetic) latitude. I = inclination. The magnetized body is a sphere with all the magnetization induced, (e) The magnetic anomaly profile across buried ore body situated at a magnetic latitude of 60°N, in which magnetization is entirely induced. The magnetization in the body is dipping in the same direction as the EMF, at ~60°. The magnetic field measured at point A to D is a combination of the Earth's field (black) and the field induced in the body (red), and (f) Skewness of a magnetic anomaly due to a uniform arbitrarily magnetized source below the Earth's surface in an obliquely oriented EMF (left) and its reduced-to-pole expression in the vertical magnetization and vertical field condition (right).

the isolated crustal component. The forward model assumes: (1) the source field of the anomaly to lie within the crust, (2) only induced magnetization exists, and (3) the susceptibility is constant over the whole region represented by the dipole. Since there is little information on susceptibility and its variation with depth for the Indian region, a mean value of 0.0025 emu/cc (0.031 SI) is used for the model. For computation of the anomalies, the total region is divided into dipoles of 4° by 4° size with their depth of magnetization extending to the Moho discontinuity. This being the usual crustal thickness, is derived from the Bouguer gravity anomaly (Δg) maps using the relation $T = 32.0 - 0.08\Delta g$. By using this formula, the calculated values of crustal thickness are given in Fig. 6.9. As Bouguer gravity anomaly maps are not available in the deep sea region, thin oceanic crust of ~5 km is assumed.

With this information, the anomaly in total field (B_{an}) is calculated at Magsat 420 km height in spherical co-ordinates using the equivalent point source (EPS) distribution of magnetic dipoles. Evaluation of the anomaly is done numerically using the Gauss-Legendre quadrature integration method. The salient features of the calculated anomalies (Fig. 6.10b) show good agreement with observed Magsat anomalies (Fig. 6.10a). In particular, the zero contour line across central India and negative anomalies to its north of the observed map are well reproduced in the computed map. However, to the south of the zero line,

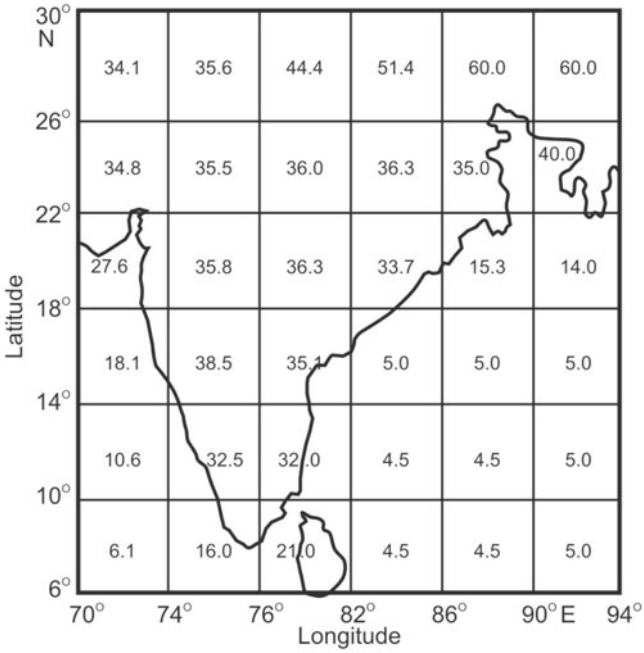

Figure 6.9. Average crustal depth values in 4° by 4° grid of the Indian region. Crustal depths have been derived from the Bouguer gravity anomaly maps (Rajaram and Singh, 1986).

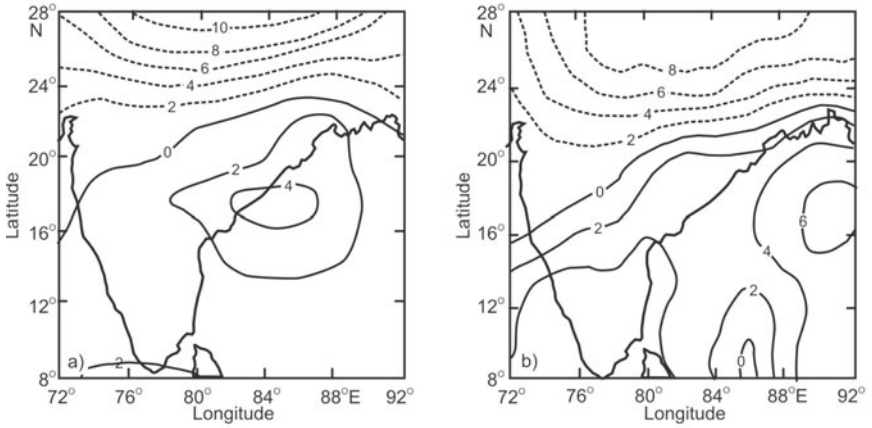

Figure 6.10. (a) Scalar magnetic anomaly map deduced from the MAGSAT data. (b) Scalar magnetic anomaly map deduced from spherical Earth model. The anomalies are contoured at 2 nT interval (Rajaram and Singh, 1986).

particularly over the Bay of Bengal, the agreement is not good because of the nonavailability of a good estimate of the crustal thickness. It is established that the crustal component of satellite data is accurately isolated. The details of anomaly features are then used to find lithological structures through inversion techniques.

VII. Ridge Regression in Inversion of Low Latitude Magnetic Anomalies: Crustal Magnetization Map

The approach adopted is to calculate moments of a set of dipoles over the surface of the Earth in such a way that they collectively reproduce the observed anomaly at satellite height in the sense of least squares. Magnetization being totally induced, dipoles are considered magnetized in the direction of the main field at their point of location. The moment, being directly dependent on the product of layer thickness and susceptibility, forms a useful parameter, and reflects well the depth of Curie isotherm. The inversion technique differs from the forward model calculation in the sense that dipoles of 2° by 2° size provide finer details of the crustal structure. First the gross feature of the anomaly is tested, and through inversion, the finer details of the Magsat measurements are used.

The ridge regression technique is used to stabilize EPS inversion over the low latitude equatorial regions. Anomalies averaged over 1° by 1° blocks form the input data, and the calculated moments are for dipoles representing magnetization of 2° by 2° crustal blocks. The whole region between –8°S and 38°N latitude, and 60° and 100°E longitude is treated as one 46° × 40° block. The magnetization of the crust derived by inverting the anomaly in Z-field is given in Fig. 6.11. The resultant crustal magnetization maps facilitated tectonic

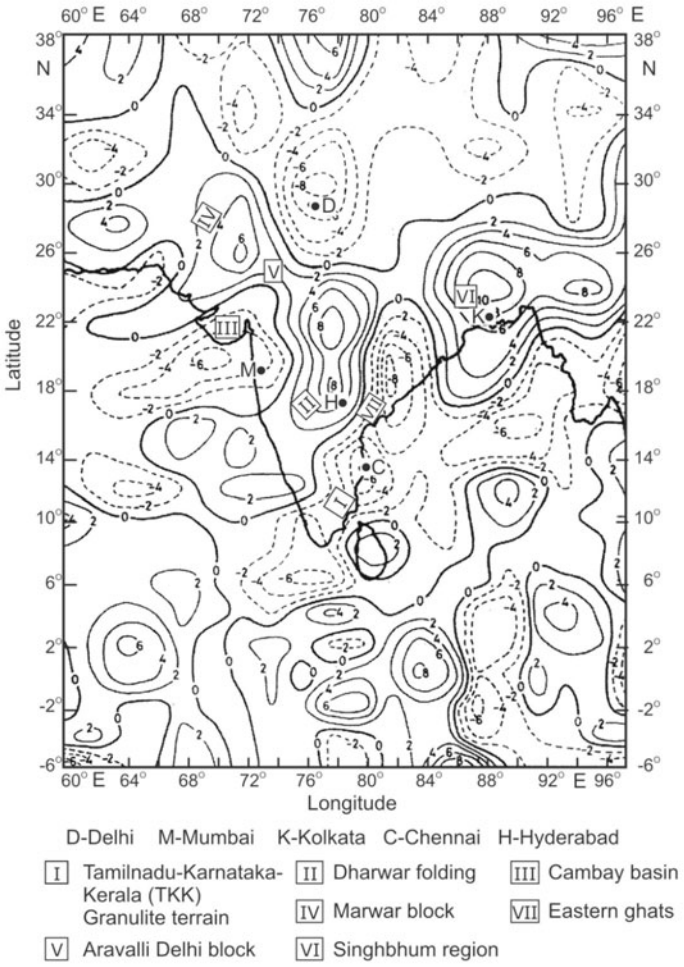

Figure 6.11. Lithospheric magnetic anomaly cannot be directly interpreted in terms of the geological properties of the crust. To circumvent this, anomalies are inverted using a ridge regression technique to calculate magnetization values. Magnetic moment (10^{14} Am^2) distribution of 2° by 2° blocks calculated by inverting anomalies in the vertical component of the magnetic field (Z) observed at MAGSAT height (contour interval $2\times10^{14}Am^2$). The magnetic moment is proportional to the product thickness of the crust and susceptibility of its material. In representation, a positive moment means a thick crust and a negative moment a thin crust (Basavaiah and Singh, 1997).

analyses of magnetic susceptibility variations within the lithosphere; mostly due to magnetization of the lower crust.

VIII. Geological Interpretation of Magnetization Maps

The magnetization map displays only relative magnetization levels that are correlated with the thickness and magnetic content of crust and depth of Curie

isotherm (Fig. 6.11). In this concept, negative magnetization represents a thin crust, crust containing weakly magnetic material, or a high subsurface temperature. On the other hand, for areas of positive magnetization, the geophysical situation is just reverse, i.e., thick crust, low temperature and high susceptibility. Therefore, the highs and lows on the magnetization map (Fig. 6.11) signify lateral variations in the magnetic crust. An overall correlation is noticed between magnetization and broad tectonic elements of the region, starting from I to VII.

The high values over four stable Precambrian blocks of the Indian landmass, namely Dharwar (II), Aravalli-Delhi (V), Marwar Craton (IV) and Singhbhum (VI) do conform to the high susceptibility of lower crust, since reflection seismic studies in several parts of the world have found the crustal mass underneath shield areas to be composed of alternating layers of mafic and ultramafic material. On the other hand, relatively low magnetization values are observed over eastern ghats, Kerala-Tamilnadu-Karnataka (KTK) granulite terrain, Panvel flexure and petroliferous Cambay basin. The low magnetization in KTK granulite correlates well with granites and some retrograded metamorphic rocks exposed in the region, while the low over a rift-type Cambay basin indicates a high heat flow. Likewise, over the Himalayas and Tibet plateau the low magnetization may have arisen from thermal state of the region. Seismic and gravity studies have inferred the crust to be thick beneath the Himalayas and Tibet plateau. The physical evidence that the triple junction of the western coast is characterized by low magnetization supports the presence of a small scale convection generated by hot spot activity. This heat transport has played an important role in the generation of hydrocarbon deposits found in Bombay High and also those expected in the Cauvery basin.

The magnetization pattern also correlates well with known variations in crustal thickness as estimated by gravity, seismic and heat flow data. Typical values for thickness of the crust from south to north are 35 to 40 km under the peninsula, 30 to 35 km under Indo-Gangetic plains and 60 to 80 km under the Himalayas and Tibetan plateau. Magnetization is negative under Indo-Gangetic plain, where the crust is thin, and positive on both sides where the crust is thick. Assuming that the oceanic crust is very much thinner than the continental crust, it is expected the former to have less degree of magnetization. Such a drop in magnetization, as one proceeds from continental realm to oceanic is clearly seen around the peninsula and Sri Lanka island (Fig. 6.11), where the magnetization changes from a positive to negative value.

In general, negative values are seen over the oceanic regions and features prominently over IOL (a structure which still remains to be fully understood). As expected, positive magnetization values are observed over Laccadives-Chagos and 90°E ridges. A special trait of interest is the transition from continental to oceanic crust and is seen to be sharp on the east coast, and gradual along the west. Positive magnetization contours (continental crust) extend into the northern portion of the Bay of Bengal. The fact that these patterns are seen

at satellite heights indicates their deep-seated origin and modelling may provide some unique information on the tectonic framework of the subsurface structures.

IX. Tectonic-anomaly between Magnetization and Residual Gravity

To constrain source characteristics of tectonic boundaries, and determination of their depths, satellite magnetic and gravity data are jointly analyzed in conjunction with geologic and other geophysical datasets of seismic, heat flow and petrophysical properties. This is done to understand the relationship between large-scale features and broad general patterns in the magnetization and residual gravity data. The joint analysis featured high gravity and low magnetization anomaly found across the eastern ghats can be modelled in terms of crustal thinning (as analogous to high heat flow). The SW and NE trending magnetic low contours over the Arabian Sea seem to centre near Mumbai—a region associated with local gravity high and also basic and ultrabasic dykes. Other known associated geological features with this axis of inverse correspondence between magnetic low and gravity high are the Konkan coast, hot springs, the Cambay rift and the Panvel flexure. Basic and ultrabasic post-Deccan trap volcanism, occurrence of mercury, carbonates and high heat flows that characterize this region suggest it to be a marginal aulacogen.

The other highlight is the occurrence of inverse correspondence between high gravity and low magnetization over petroliferous basins like the Assam oil field, Bombay High and Cauvery basin. This is related to a shallow Curie depth, consistent with high heat flow values, and a thin crust of gravity high. A comparison with the heat flow map of the region depicts zones with heat flow ~70 mWm^{-2} are areas of low magnetization with the exception of the central Indian region. An inverse relationship in the two anomalies over the Himalayas is due to higher thermal gradients that average beneath these high mountain ranges. Therefore, inverse correspondence between residual gravity and magnetization (Figs 6.5 and 6.11) can possibly be used to infer heat flow values. Nevertheless, with the availability of heat flow map for the country, Magsat results and gravity maps can be used more effectively.

The western region of India and the Rajasthan shield is associated with magnetic as well as gravity 'high'. Magnetically this region has similarity to the southern, rather than northern shield. The 90°E ridge in the Bay of Bengal is associated with a NS trending magnetic and gravity high, flanked by lows to the east and west. The IOL south of Sri Lanka finds an expression as localized closures.

The low magnetization (Fig. 6.11) and low mass distribution (Fig. 6.12) are consistent with the trans-Himalayan conductor and the Palk Strait conductor (Figs 6.32 and 6.33) identified by EM induction methods. This correspondence between the two suggests that both these conductors are associated with either high heat flow or low magnetic susceptibility and density. The anomalous

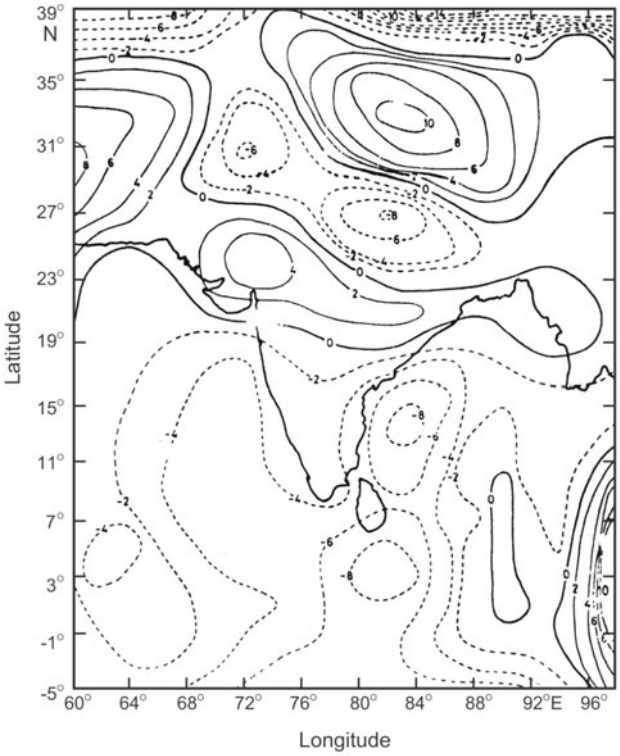

Figure 6.12. Anomalous mass distribution of 2° by 2° blocks calculated through inversion of satellite gravity anomalies at 400 km height (given in Fig. 6.1a) taking the location of equivalent point sources to be at a depth of 200 km. Contour interval 2×10^{19} g. Note two highly conducting regions in the Palk Strait and trans Himalayan area (Fig. 6.32) depict low mass distribution from satellite gravity data (Basavaiah, 1993).

character of the lithosphere immediately south of India has low magnetization anomaly, which reflects thin magnetic crust related to the rise of the Curie isotherm.

6.4 AIR-BORNE MAGNETIC SURVEYS

Magnetic surveys are carried out over several spatial scales and elevations. Aeromagnetic surveys are the most common component of reconnaissance appraisals conducted to estimate depth of the basement, or equivalently the thickness of the sedimentary basins. With an advent of aircraft-mounted magnetometer system developed mainly for submarine detection during World War II by Muffly in 1946, the areal magnetic coverage has expanded rapidly. Surface and subsurface information are gained in a relatively cheap way through aeromagnetic surveys, which also provide uniform coverage of inaccessible areas.

I. Survey Objectives

Aeromagnetic surveys are done for a variety of reasons, primarily for geological and structural mapping, mineral and oil exploration, environmental and ground water investigations. Most surveys are flown to aid in surface geologic mapping, where the magnetic effects of geologic bodies and structures are detected even in areas where rock outcrop is scarce or absent, and bed rock is covered by water, ice, sand or vegetation. Broad correlations are made between rock type and magnetic properties, but the relationships are complicated often by temperature, pressure and chemical changes. Nevertheless, the combined ground and aeromagnetic maps with available geologic information are effective for meaningful geological insights. Certain kinds of ore bodies may produce magnetic anomalies that are desirable targets for mineral exploration. Hydrocarbon deposits are not directly detectable by aeromagnetic surveys, but magnetic data can be used to locate areas that provide favourable conditions for oil/gas production and accumulation. Similarly, mapping magnetic signatures of faults and features within water-bearing sedimentary rocks provide valuable constraints on the geometry of acquifers and framework of groundwater systems.

The first aeromagnetic survey for geological properties was carried out in 1945 in Alaska and by the end of 1940s, it had a global sweep. Parts of India too have been aeromagnetically surveyed. These results are published in the form of total intensity contour maps in degree sheet format without incorporating corrections due to main field variations of the Earth, which can be acquired from GSI.

II. Quality Control

The magnetic effects of different heading directions and aircraft manoeuvres are first measured during a calibration flight in the absence of magnetic anomalies, and then subtracted in real-time during survey operation as magnetic anomalies are recorded. During survey operation, the recorded aircraft attitude is used to apply an appropriate correction to each reading of the magnetometer. The following tests are carried out periodically to demonstrate the success of compensation.

The 'clover-leaf' test for magnetic heading effect: The 'clover-leaf' test is designed to demonstrate that the aircraft and system have no significant 'heading effect', i.e. that the same magnetic field value is recorded at a given location in x and y, regardless of the direction in which the location is overflown (once corrections for temporal variations of the magnetic field are applied). A visible point on the ground in an area of few

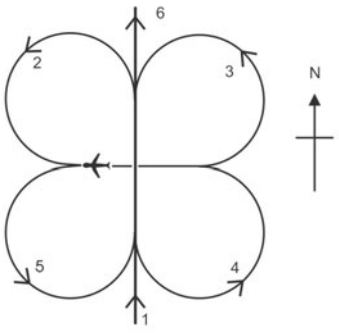

magnetic anomalies is chosen and overflown at survey altitude in, say, a northerly direction. The aircraft then turns and flies over the same point again in an easterly direction, then in a southerly direction, a westerly direction and finally in a northerly direction again to check for any diurnal variation since the first overflight.

Noise level monitoring: Noise experienced while recording a magnetometer profile can be divided into discontinuous and continuous noise. The former causes spikes to appear on the profile, which may be attributed to a plethora of sources, internal and external to the aircraft. These include lightning, DC trains and trams, power lines, radio transmission, electrical switching and so forth. Such effects usually demand manual elimination—or non-linear filtering—during data reduction. The continuous effects are largely eliminated by the compensation system in a modern installation, but there will be detectable residuals, which still set the limit to the sensitivity of the system.

Lag test for correcting the position (herringbone effect): The differing positions of magnetometer (or other) sensor within the aircraft and possible electronic delays in recording values are checked by overflying a magnetic object such as a bridge twice, the second time in the direction opposite to the first. The displacement between the two anomalies relative to the source is twice the shift that must be applied to bring magnetic and positional information into registration. A lag of 0.1 to 0.2 sec—equivalent to about 10 m on the ground—is not uncommon. Since survey lines are often flown alternately in opposite direction, i.e. after completion of flying one line E to W, the aircraft turns around and flies the next line W to E. Failure to correct adequately for lag can result in values being shifted systematically, e.g. E on lines flown E-W and W on lines flown W-E. This is one possible cause of the so-called 'herringbone' effect seen on contour maps of surveys, which are not reduced correctly. However, in modern surveys such effects are more often due to incomplete levelling of the flight lines.

III. Aeromagnetic Survey Operations and Processes

Usually oil exploration and regional surveys are flown at a constant elevation in order to provide a constant datum for the basement depth estimates. Mineral surveys are carried out with a constant ground clearance. The planning of survey operations consists of choice of magnetometer, aircraft, navigational aids, proper scales for base maps, and flight parameters such as flight line direction, spacing and flight elevation.

Magnetometers: Compared to the magnetometers used in the 1940s, the resolution and accuracy of recent magnetic field measurements have increased significantly (Chapter 4). The early fluxgate magnetometers had resolutions of ~1 nT, noise envelopes of 2 nT and suffered from appreciable drift of ~10 nT/hr. The fluxgate magnetometer can also be used as gradiometer, and it is therefore most sensitive to shallow magnetic sources. Proton precision

magnetometers have followed fluxgate magnetometers with a resolution of 0.1 nT, noise envelope of 1 nT and minimal drift. These are superseded by the cesium vapour magnetometers, which have a resolution of 0.001 nT and a noise envelope of 0.005 nT.

Single magnetometer aircraft configurations simply produce measurements of the magnetic field intensity in the direction of the EMF. By adding extra sensors, various other quantities can be measured. With increased sensitivity, three component systems at the wing-tips and tail are increasingly being used.

Aircraft motion, noise, attitude sensors: Magnetic noise caused by the survey aircraft arises from permanent and induced magnetization effects and from the flow of electrical currents. The permanent magnetization of the aircraft results in a heading error. Induced magnetizations occur due to the motion of the aircraft in the EMF. These effects are partially reduced by mounting the magnetometer either on a boom attached to the aircraft's tail or in a towed 'bird' attached by a cable. One serious disadvantage with the towed bird installation is that the motion of the bird in the EMF causes noise on the magnetometer record, and there is virtually no satisfactory way of compensating for the motion of the bird. A rigid extension of the airframe—usually in the form known as a stinger—solves many of these problems, but necessitates closer attention to the sources of magnetic effects on board the aircraft. The permanent magnetic field of the aircraft at the magnetometer sensor is compensated (backed-off) by passing appropriate DC currents through each of three orthogonal coils in the vicinity of the sensor. The induced component was offset by mounting pieces of highly permeable material close to the sensor in a position (found by trial-and-error) such that their magnetic effect is always equal and opposite to that of the engines. The eddy-current effects are similarly mimicked, but in opposite sign by coils of wire placed close to the sensor. Recently, active magnetic compensators have been developed to address these problems 'on-line' during survey flight. Once the survey is started, the aircraft's noise level is assessed repeatedly to ensure that the same level of data quality is maintained.

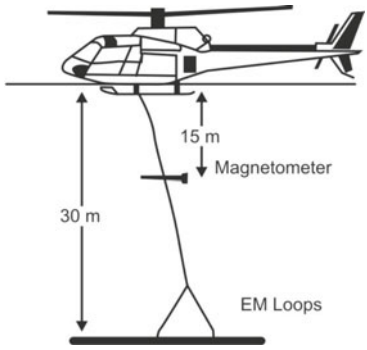

The choice of aircraft is a matter of economics and balancing costs against performance. The most common aircraft types include single-engine cessnas, twin-engine aircrafts, and larger model Dakotas.

Navigation, positioning: No matter what accuracy is achieved in the magnetic field measurements, the value of the final survey data is dependent on exact location of measurement points. Traditional methods of navigation rely largely on visual tracking using aerial photographs. The actual location of the flight

path is recovered manually by comparing these photographs with images from onboard video cameras. However, in areas of poor photographical features, navigational aids like Doppler or ANA (aircraft navigation using atomic standards) become necessary. These techniques are superseded by the introduction of GPS in 1990s. GPS relies on the information sent from an array of satellites, whose locations are known precisely. Signals from a number of satellites are used to triangulate the position of the receiver in the aircraft, so that its position is known for navigational purposes and to locate the magnetic field measurements. GPS brings a number of important benefits to aerial surveying. Firstly, the coordinates of the survey aircraft (horizontal and vertical) are provided on a continuous basis. This not only improves the quality of survey navigation and reduces its cost, it also eliminates to a large degree the tedious and error-prone manual steps inherent in flight path recovery from film or video. Secondly, GPS provides a reusable positioning system. Surveys flown at different times in the same area may be correlated in position, making it easy to repeat survey lines or to fly infill lines. Current surveys generally use real-time differential GPS navigation where the raw positional information is corrected as the data is being collected. Altimeter keeps track of the altitude.

Temporal effects: Monitoring of the EMF is an essential component of aeromagnetic surveys. The time-varying effects due to micropulsations, magnetic storms and diurnal variations are removed through base-station subtraction, tie-line levelling and microlevelling (decorrugation). One or more base station magnetometers are used to track changes in the field during survey operations. The smoothly changing diurnal variation is removed from the data using tie-line levelling. Simply subtracting this variation from the measured data is not sufficient, since diurnal changes may vary significantly over the survey area. Nonetheless, the recorded diurnal is used as a guide in the levelling process. Tie-line levelling is based on the differences in the measured field at the intersection of flight lines and tie-lines that run perpendicular to the flight lines. If the distance and time taken to fly between these intersection points is small enough, then it can be assumed that the diurnal varies approximately linearly and can be corrected for.

Micro-levelling (de-corrugation): Creating a grid is still less than satisfactory in that some line-related noise remains evident. This effect is described as corrugations and the standard procedure for its removal as de-corrugation or micro-levelling. The micro-levelling procedure used to remove line-related noise has become standard in recent years. It is essentially a filtering process, whose wavelength in the across-line direction is equal to twice the line spacing and in the along-line direction to the spacing between the tie-lines. The need for micro-levelling arises from the imperfections in the polynomials applied to hang the flight line data on the tie-lines. Micro-levelling is applied to gridded data and the adjustments made to improve the grid are then feed back as a correction to the original profile data so that, when next gridded, line-related noise will not be evident. Adjustments made in micro-levelling need to confine

to a few nT. The assumption in micro-levelling is that the near-DC component of each profile resembles that of its neighbour, i.e. that the 'regional' field varies only smoothly from line to line across the whole survey area. The danger is that genuine geological features can also follow flight lines and micro-levelling can remove these.

Example, aeromagnetic survey operations, data acquisition: Aeromagnetic surveys over the peninsular shield were conducted in distinct epoch and altitude ranges (Fig. 6.13). The flight lines, which are parallel lines flown in a regular pattern of equally spaced, are N25°E - S25°W, where the flight altitude is 7000 ft, and for the rest of the region, the flight lines are N-S. The line spacing for all these blocks was maintained at 4 km, except for the 'drape' survey over Cuddapah basin (altitude 500 ft) covered under 'operation hard rock', where the line spacing varied from 500 m to 1 km. It thus becomes inevitable to reduce data to a common barometric altitude to obtain an overall idea of magnetic response of the geological terrain in general.

IV. Data Display and Interpretation

The final product is a set of levelled flight line data that are interpolated onto a regular grid of magnetic field intensity values covering the survey region. These values can be displayed in a variety of ways, the most common being a colour map, where the magnetic field values based on their magnitude are assigned a specific colour. Similarly the values can be represented as a simple line contour map. Both kinds of representation can be used in a qualitative fashion to divide

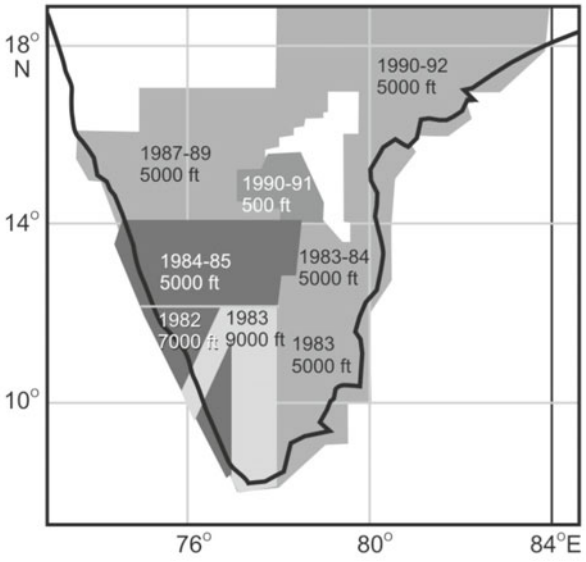

Figure 6.13. Sketch map depicting epoch and altitudes of aeromagnetic survey undertaken. Note different flight altitudes are indicated in different colours (Rajaram and Anand, 2003).

the survey area into sub-regions of high and low magnetizations. Since the data are available digitally, it is straightforward to use computer-based algorithms to modify and enhance the magnetic field image for the specific purpose of the survey. Transformation and filtering allow certain attributes of the data to be enhanced, such as the effects due to magnetic sources at shallow or deep levels, or occurring along a specified strike direction. More sophisticated methods may estimate the depths, locations, attitudes, and magnetic properties of magnetic sources.

Example, aeromagnetic anomaly map preparation: The GSI catalogue published in 1995 has details about the collection of aeromagnetic data. There, however, exists a data gap, as degree sheets are not available over a part of the Cuddapah basin, hence ground magnetic data collected over this basin at 10 km interval has been incorporated. The acquired degree sheet maps were machine digitized along contours. The observed digital aeromagnetic data for each block are corrected to remove the main field contribution using the 1980 and 1985 IGRF models interpolating appropriate date and altitude of observation. The data were then regrided at 2 km interval. IGRF removed data in different blocks are at different elevations, therefore all are continued to the same elevation of 5000 ft above msl and merged. The colour-shaded image of aeromagnetic crustal anomaly map, thus prepared is presented in Fig. 6.14. The red colour represents high and blue low values.

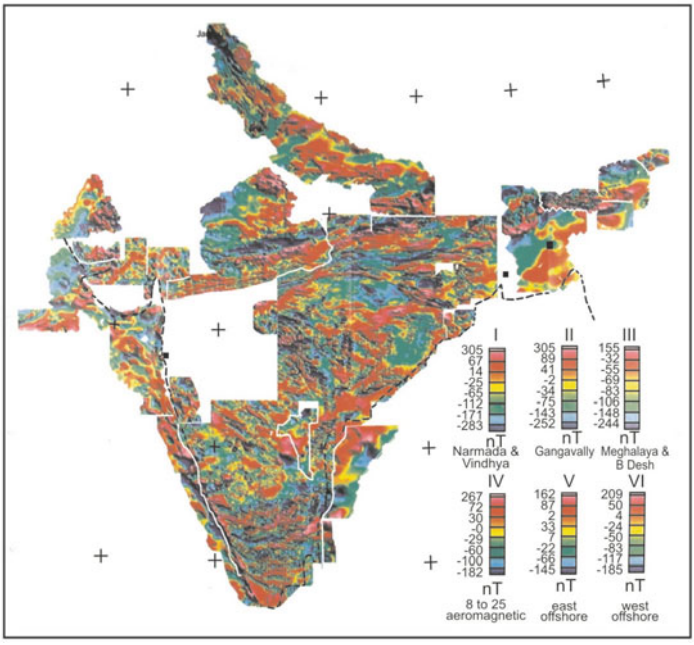

Figure 6.14. Composite aeroborne total intensity anomaly map. The aeromagnetic anomalies are used to understand tectonic elements and regional magnetic characteristics of the Indian peninsula showing a thin exhumed southern granulite crust with its lithological and mineralogical changes at ~22 km (Rajaram et al., 2006).

V. Geological Correlations of Crustal Magnetic Anomaly

The map (Fig. 6.14) clearly shows tectonic elements and regional characteristics of the peninsula. Superposed on it are short wavelength anomalies near surface features. A very striking element of the map is that north of 13°N, coinciding almost with the line of change of amphibolite to granulite facies, the trend of anomalies change from NNW-SSE in the north to essentially E-W in the south. The region between the line of change of facies and the Palghat-Cauvery shear zone exhibits east-west trending alternate high and low values. This striking contrast in gradients across the Moyar-Bhavani shear system is indicative of a change in magnetic sources.

Based on magnetic anomaly pattern (Fig. 6.14), the image map can be broadly classified into two distinct blocks, viz. block I covering area between 13° and 18°N latitude and block II between 8° and 12°N with a transition region between 12° and 13°N. Block I includes the Dharwar craton and block II comprises southern granulite terrain (SGT) and northern granulite block. Block I is heterogeneous and characterized by sparsely distributed broad anomalies, besides isolated 2D linear anomalies. A well defined 3D feature is much less common. In contrast, block II is fairly homogeneous and is characterized by a generally high density of anomaly distribution. This block is dominated by 2D linear anomalies trending mainly ENE-WSW to E-W and contains a localized 3D feature. Dense anomaly signature along the west coast between 8° and 14°N latitude represents post-Gondwana rifts and Cretaceous-Eocene magmatic activity.

The investigated area being in low latitude region, the inclination of the inducing main field increases the complexity of anomalies and makes the interpretation difficult. The analytic signal of total field reduces the magnetic data to anomalies whose maxima mark the edges of the magnetized bodies, thus helping in identifying the magnetic source distribution. The analytic signal map is represented in Fig. 6.15. The peaks (sources) of analytic signal within the Dharwar region represent intrusives/localized iron ore bodies. At 13°N parallel, the maxima align themselves along E-W direction parallel to the orthopyroxene isograd. The zone between Moyar-Bhavani-Salem-Attur faults and the Achankovil shear zone is characterized by many maxima representing extensive magnetic sources related to charnockites. Thus the analytic signal can be used to define change in grades of metamorphism. In fact, subsurface charnockites, and those in inaccessible regions like forests can be mapped using the analytic signal map. The west coast fault is also clearly visible. Surprisingly, no signature of khondalite belt is evident in this picture though they show clear highs in aeromagnetic anomaly map. This is because low gradients prevail over the khondalite belt in the aeromagnetic map, which has a lower susceptibility compared with charnockites.

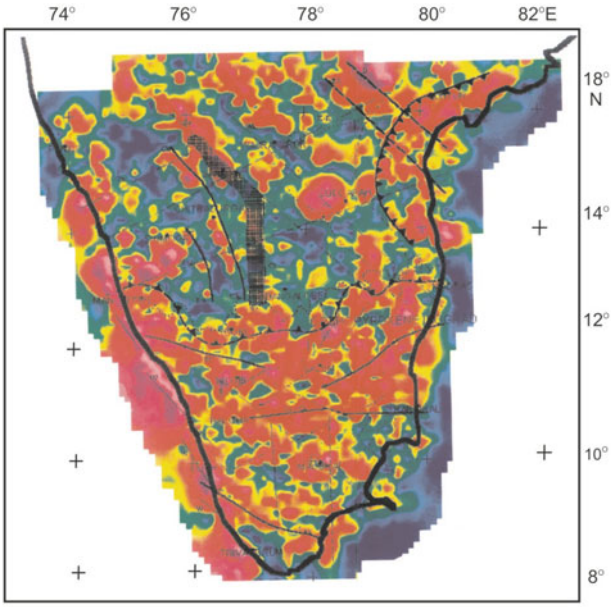

Figure 6.15. Analytic signal map of the aeromagnetic anomaly. Red colour represents magnetic sources (highs). Analytic structural trends, lineaments and faults identified are demarcated. Magnetic sources (highs) in the region south of 13°N are mainly charnockitic and that above 13°N are iron ore bodies of schist belts (Rajaram and Anand, 2003).

VI. Aeromagnetic Interpretation

The sources of magnetic anomalies over peninsular India are charnockites, intrusives, iron ore and trap flows. In the Dharwar craton, the NW-SE trends are deeper, older and are cut by several younger NE-SW shallow trends, the junction of which yields diamond-bearing kimberlite pipes. Chitradurga schist belt forms the dividing line between eastern and western Dharwar. The analytical signal map also reveals changes in metamorphic grades.

Magnetic crust below the high-grade terrain of SGT and all along the east coast is thin. Below the thin exhumed crust of SGT, there is a lithological/mineralogical change at ~22 km depth also seen as velocity change in deep seismic sounding (DSS) studies. The inverted magnetic data gave a crustal model along the existing Palani-Kolatur DSS profile. The model suggests that alteration of charnockites into hornblende-biotite-gneiss is more towards the north than south, wherein the process of retrogression is high but the exhumation of charnockites is more between Cauvery fault and Salem-Attur fault. Aeromagnetic anomalies on the east coast continue and merge gently with marine magnetic anomalies till the ocean continent boundary, but the west coast fault abruptly terminates the aeromagnetic anomalies towards the western offshore.

6.5 NATIONAL GROUND MAGNETIC SURVEYS

I. Data Acquisition and Total Field Anomaly Map

Aeromagnetic data in general and satellite surveys in particular regionalize the surface and subsurface geological characteristics, whose exact location is decoded by supplementing with ground survey data. Study of continental anomalies from a national magnetic anomaly map is being carried out extensively in USA. For such a study in India, SOI prepared total field anomaly map (Fig. 6.17) based on ground measurements at ~800 field and repeat stations, whose distribution is shown in Fig. 6.16.

II. Data Reduction and Processing

Based on these data, an analytical field representation is developed through a sixth degree polynomial as a function of latitude and longitude. This covers spatial variation of the field with wavelengths as short as 1000 km. The field values at stations corresponding to above model are subtracted from the observed field values, and residual values are used to compile the magnetic anomaly (Fig. 6.17), which can be considered free from anomalies >1000 km. The shortest wavelengths are ~80 km controlled by inter-station spacing.

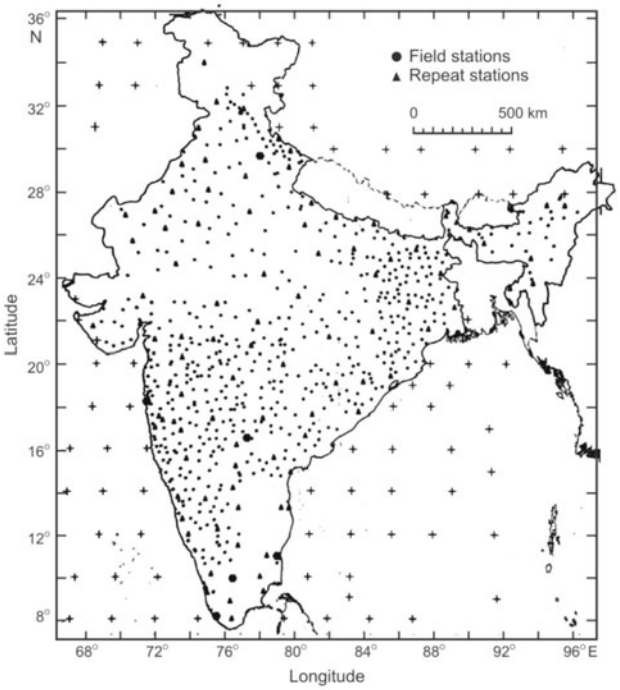

Figure 6.16. Location map of ~800 field and repeat stations installed by the Survey of India in order to collect the ground magnetic data used in the preparation of regional isomagnetic charts over the Indian region.

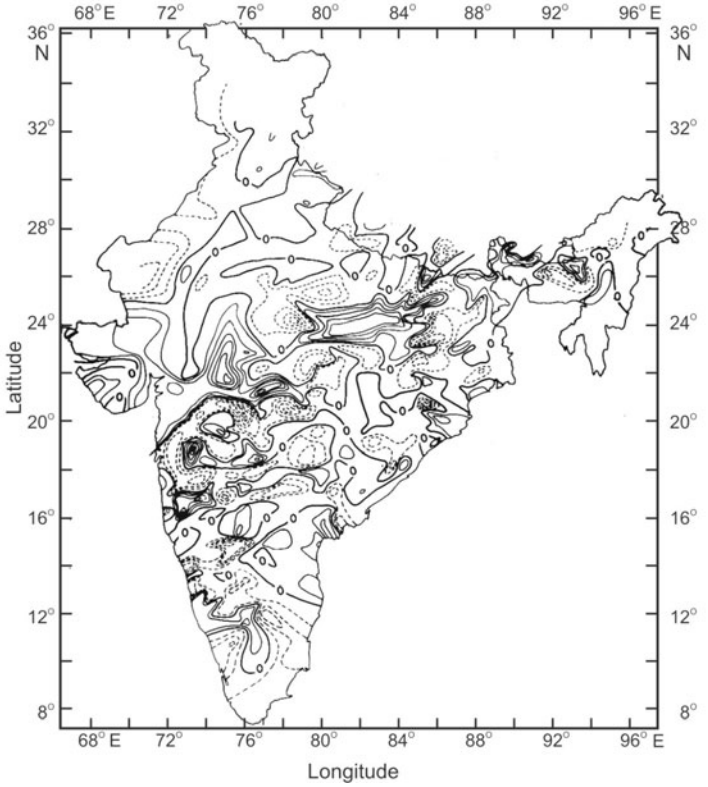

Figure 6.17. Residual total intensity anomaly map prepared after removing regional anomalies represented by a sixth degree polynomial model from the observed field values at stations in Fig. 6.16. These residual anomalies are considered to be free from anomalies of wavelengths >1000 km. The anomaly patterns are used to understand the crustal structure by comparing with an anomaly in total field as seen from the Magsat heights of 420 km. Contour interval 100 nT (courtesy: Survey of India).

III. Qualitative Interpretation of Anomaly Trends: Tectonic Features

The most conspicuous feature of total magnetic intensity anomaly map (Fig. 6.17) is the presence of a number of parallel to subparallel E-NE trending zones over central India that stretch right from west to east coasts. These anomalies correspond well with the Narmada-Sone lineament (NSL). NSL forms the boundary between the Vindhyans to the north and the Gondwanas to south and is known to be a prominent rift structure from gravity and seismic observations. To the north, anomalies are aligned in N-E direction corresponding to Aravalli mountain ranges. These mountain ranges represent rejuvenated uplifted block mountains resulting from tectonic activation of Indian shield. The whole of southern peninsula and Deccan trap region are characterized by small scale, large number of positive and negative anomalies, though Deccan

has blanketed the pre-existing topography over a considerable area. However, the presence of structures such as basins, rift valleys, fissure zones and dykes have been conjectured with scanty information from geophysical surveys. It would be interesting to examine whether the zones of positive anomalies characterize the fissure zones along which large lava eruption has taken place. The negative anomalies correspond to presence of pre-trappean sediments, primarily Mesozoic, which are also indicated from seismic surveys.

IV. Tectonic Correlations between Magsat and Ground Anomalies

In satellite anomaly maps due to natural filtering, many of the local features disappear because of which large scale regional features get sufficiently enhanced. When Magsat total field anomaly (Fig. 6.8b) is compared with ground data (Fig. 6.17), it is found that the ground anomalies cannot be distinctly separated in geological provinces. The conspicuous Magsat anomaly over the Himalayas is indecipherable in ground data. The general trend in Magsat data has a positive and negative anomaly over the southern and northern regions respectively, separated by a zero anomaly coinciding with NSL. The demarcation of NSL is not so clear in ground data. Perhaps, strong features of local extent mask the presence of this lineament. Other applications extend the existing analysis capability for knowledge of the conductivity of the upper mantle useful for inferring temperature, structural and compositional variations.

6.6 GROUND MAGNETIC SURVEYS

The magnetometer readings made at each observation point on ground surface represent a combination of main field, its temporal variation due to ionospheric current system and the relevant anomalous component due to lateral variations in magnetic parameters of the crust, mostly in the outer shell measuring 18 to 25 km thickness. Watchful evaluation and removal of extraneous contributions are essential to the attainment of a satisfactory picture of magnetic anomalies of small relief. Careful attention to various corrections to magnetometer reading corrections forms an important aspect in the application to oil prospecting in view of weak anomalies than to the exploration for iron ores, igneous intrusions, etc. where the anomalies are stronger. Table 6.1 shows different stages of magnetic data reduction in calculating crustal magnetic anomalies.

I. Plan of Conducting Ground Magnetic Surveys

The exact manner of conducting survey depends upon the purpose of the survey, the type of host region, the ease of transportation, and the type of anomalies expected. Regional surveys involve large areal extent (thousands of sq km) and can be for mineral or oil exploration. In contrast, detail surveys for minerals usually cover only a few km. Regional surveys are primarily intended to serve

Table 6.1 Typical example of reducing magnetometer data

Sl. No.	*time-F*	*obs-F*	*time-Z*	*obs-Z*	*H*	*Z*	*IGRF-F*	*ext.H*	*ext.Z*	*IGRF(F+ext)*	*Final-F*
1	8.45	40578	8.47	8478	2.5	4.1	40403	38109	18519	40027	551
2	8.55	40536	8.57	8546	2.6	4	40401	38111	18517	40024	512
3	9.05	40517	9.07	8426	2.6	3.9	40400	38111	18515	40024	494
4	9.12	40432	9.14	8332	2.8	3.8	40399	38114	18513	40020	411
5	9.18	40574	9.20	8525	2.9	3.6	40398	38116	18510	40020	555
6	9.25	40540	9.27	8440	3.1	3.4	40397	38119	18506	40017	523
7	9.35	40537	9.37	8373	3.2	3.2	40396	38121	18502	40016	521
8	9.42	40514	9.44	8343	3.4	3.1	40394	38124	18500	40012	502
9	9.48	40486	9.50	8336	3.6	3.1	40392	38128	18500	40007	479
10	9.55	40531	9.57	8466	3.8	3.1	40391	38131	18500	40003	529

the purpose of reconnaissance, to identify favourable ore environments or to understand geological or tectonic framework of a region. It helps to delineate major lithographic units favourable for specific type of mineralization or fault-fracture pattern of a region as a prelude to detailed work. Magnetic surveys for oil exploration over large sedimentary basins are primarily intended to know the thickness of sediments and the configuration of the underlying basement in order to locate structural oil traps. Regional surveys can be carried out on a regular grid pattern at 2 to 3 km interval or stations can be set up on all available roads and tracks so that an average station density of 2 to 3 km is achieved. 1:5000 scale maps are adequate for such a survey.

Detailed surveys for minerals are usually carried out on regular grid. The profiles are laid at right angles to the geological strike. A baseline along the strike of the body is fixed and profiles are set across the baseline. If L is strike length and w the width of the geological body, a profile interval of L/4 or L/5 and station interval of w/10 are adequate.

II. Surveyed Areas and Frontier Sedimentary Basins

The eastern continental margin of India (ECMI) has several sedimentary basins, which evolved following the dismemberment of Gondwanaland in Mesozoic (245 to 65 Ma) and formed between late Jurassic (200 to 130 Ma) and Miocene (23 to 5 Ma) as a result of southwesterly drainage associated with northward anticlockwise drift of India from southern latitudes to its present position. These basins were intracratonic, pull-apart type during their initial stage of formation, but after the break-up, became pericratonic. The intracratonic basin occurs on continental crust, either in the interior or at the crustal margins of old continental plates. They are caused by divergence and tension within the continental block and more often by subsidence along reactivated primordial faults. The pericratonic rift basins, on the other hand, form by subsidence of rifted trailing edges along extensional faults. Their basin axes are usually parallel to continental/oceanic crust boundary and sediments overlap into the oceanic crust. The common feature of east coast basins is subsidence along down-to-basement faults. The sedimentary fill, ranging in age from Jurassic to Pliocene, includes deltaic transitional marine sediments, carbonates, clastics, etc. In order to shed light on the evolution of ECMI and hence to reconstruct the configuration of Gondwanaland, knowledge of the structure, tectonics and sedimentation history of these sedimentary basins is very vital.

Ground magnetic survey was carried out over Deccan trap (Maharashtra), Cambay and Kutch (Gujarat), Khandwa (Madhya Pradesh), Mahanadi (Orissa), schist belts of Chitradurga-Holenarsipur (Karnataka), Krishna-Godavari (Andhra Pradesh), and the Proterozoic Cuddapah-Palar (spanning Andhra Pradesh and Tamilnadu) (Fig. 6.18). These surveys were carried out with point readings maintaining an average station interval from 5 to 10 km on a grid using indigenous PPMs (Chapter 4).

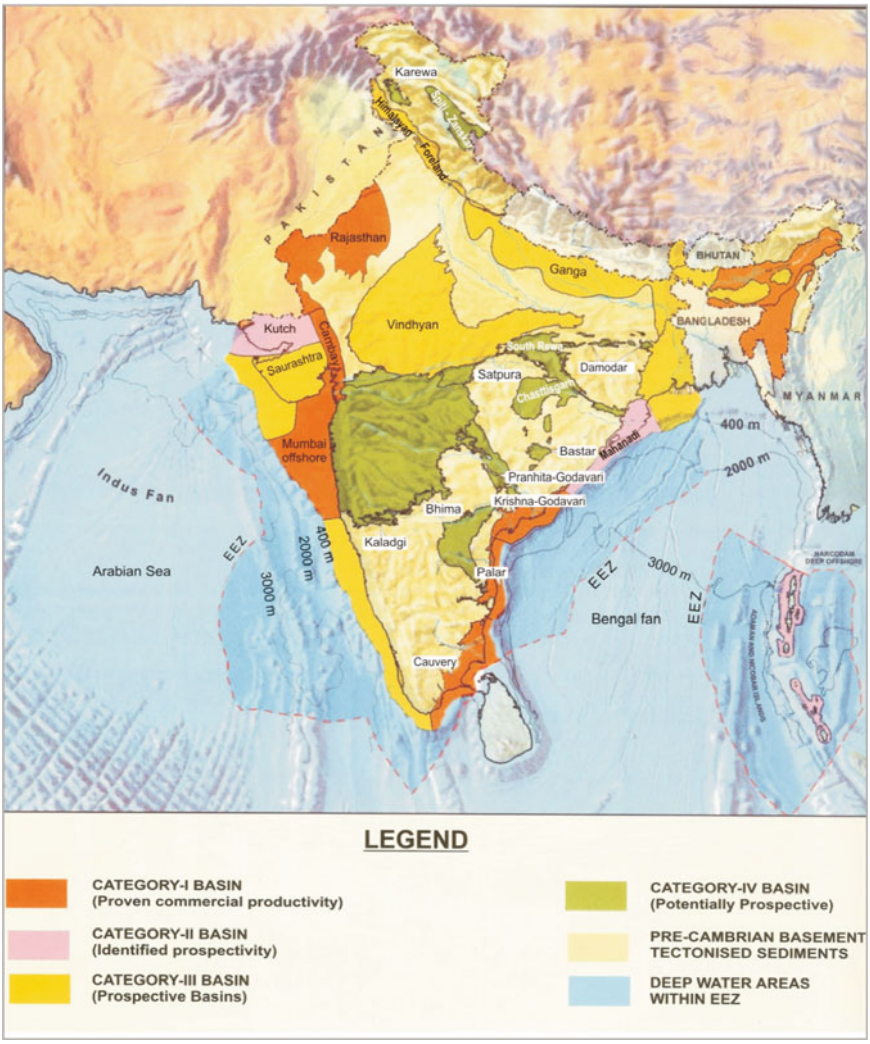

Figure 6.18. Generalized map of various sedimentary basins, which are categorized according to their hydrocarbon bearing potential (Biswas et al., 1993). These form the potential regions for carrying out ground magnetic surveys to understand the relationship between their magnetic characteristics and hydrocarbon bearing potential.

III. Reduction of Ground Magnetic Observations

To isolate crustal anomaly, spatial and time variations occurring in EMF over the period of surveying area are determined, and removed from the raw measurements. The EMF, however, varies rather uniformly over large distances of hundreds of km, and is thus easily predictable using IGRF. This, together with contributions from external current systems when subtracted from the observed field (obs-F in Table 6.1), leaves behind the magnetic anomaly.

(i) Diurnal corrections: These corrections are very important since the magnitude of diurnal variations of EMF is from 10 to 100 nT. There are three methods used for making diurnal correction: **(1) Observatory measurement:** Magnetic observatories make continuous records of magnetic measurements. Data are procured from the closest MO and corrections effected. But it has two roadblocks: (i) the data may not be available immediately, and (ii) the surveyed area may not be in the vicinity of observatory. **(2) Repeat observations:** Repeated observations at the same point during the course of the day can check for constancy of magnetic intensity. Any inconsistency in the readings will give out magnetic variation for the day. However, the daily variation curves show readings at an interval of even 2 hr can miss details of the daily variation of as large as 10 nT. Therefore, this method is inadequate, wherein a precision of a few nT is desired. **(3) Continuous recording:** In this method, an auxiliary base instrument is used, which records continuous curve of the daily variation at the base station. This curve is used for corrections, which is considered safe to effect corrections in field station curves within a perimeter of 80 km.

(ii) Normal corrections: This correction is made to remove normal variation of magnetic intensity over the Earth's surface. The magnetic field is determined from magnetic charts, since it cannot be represented mathematically in terms of the geographical coordinates; its direction, distance, and absolute value are also not normally known at the base. The corrections are made by drawing contours of normal variations at a convenient interval of 10 nT. For example, the N-S and E-W gradient can be evaluated from the isomagnetic maps published at five-year intervals by the world data centre. Knowledge of the NS and EW distance of the field station from primary base helps remove the normal variation (with proper sign) from the observed data. For example, for Indian latitudes, say ~20°N, the normal field gradient of the order of 5 to 6 nT/km along NS and ~1 nT/km along EW direction exists for 1985 epoch.

IGRF coefficients of a fixed epoch are used to calculate the response of main field at each observation point (IGRF-F). For quantifying period of external field variations of the survey area, data recorded at a nearby magnetic observatory are used. In Table 6.1, values of H and Z represent digitized data from magnetograms corresponding to the date and time of the recording done at field, while the ext.H and ext.Z represent horizontal and vertical magnetic field components, obtained by adding the baseline values after multiplying H and Z with their scale values. The baseline and scale values are supplied by the observatories along with the magnetograms. Ext.F is obtained by squaring and adding ext.H and ext.Z and taking the square root. The value of ext.F thus obtained is summed with IGRF value and deducted from the observed total field value to gain the final anomaly (final-F), which is further plotted against location co-ordinates. The total field anomaly map (F) thus prepared for different basins is shown in Figs 6.19, 6.20, 6.23 and 6.28 for Cambay, Mahanadi, Krishna-Godavari, and Cauvery basins, respectively.

IV. Transformation and Interpretation of Magnetic Anomalies

The varying amplitudes and wavelengths of the total field come from magnetic sources at different depths. To know certain characteristics of sources, anomaly maps are subjected to various transformations. Transformation and filtering allow certain attributes of the data to be enhanced such as the effects due to magnetic sources at shallow or deeper levels or those occurring along a specified strike direction. To resolve shallow sources, downward continuation and second vertical derivative transformations are done. Upward continuation and horizontal gradient of pseudogravity (HGPG) transformations are performed to isolate deeper sources. **(i) Magnetic field analytical continuation:** The continuation techniques transform mathematically the magnetic anomalies on to a plane either above or below the plane of observation. In the upward continuation, i.e. to a plane above the level of observation, the regional features are preserved at the cost of shallow sources and in the downward continuation, i.e. to a level below the level of observations, the shallower sources are enhanced and regionals suppressed. **(ii) Derivative technique:** In the magnetic data processing, derivative is generally used to denote the first or higher vertical derivatives of magnetic anomalies. These are used to enhance the anomalies of shallower sources. When the influence of overlapping sources or regional features is predominant, derivatives help to resolve the shallower sources better than the original field. Computation of even second, fourth, sixth derivatives, etc. is much easier in the space domain than the odd derivatives. Several procedures are in vogue now for the preparation of second derivative maps. **(iii) Reduction to the pole:** The magnetic anomaly observed over a particular source is dependent on its location and orientation. Usually, the magnetic anomalies constitute a pair of negative and positive peaks located on either side of the source. Instead of dipolar anomalies, a technique known as 'reduction to pole' centres the anomalies over the respective sources (Fig. 6.8f). This procedure does not create any confusion with respect to dipolar anomalies. Reduction to pole maps are generally used for quantitative interpretation, and for direct comparison of gravity and magnetic maps. **(iv) Apparent susceptibility mapping:** This is a data processing technique that converts a total field magnetic map to an apparent susceptibility map. This method involves such operations as downward continuation and reduction to pole; all conducted in the frequency domain. It has advantages such as overlapping of anomalies being reduced, areas of uniform susceptibility appear relatively flat, and level differences appear between units with different magnetic properties and contacts between rock types, are demarcated clearly. The application of the various techniques is discussed below.

1. Cambay basin: The anomaly trend is controlled by faults within the basin (Fig. 6.19) and outside on the NE; it depicts the Aravalli trend. The anomaly map also shows margin faults, ENE-WSW trending NSL, major faults and geological features. Also the expected residual gravity values are higher inside than outside the basin, while magnetic anomalies are low over the graben.

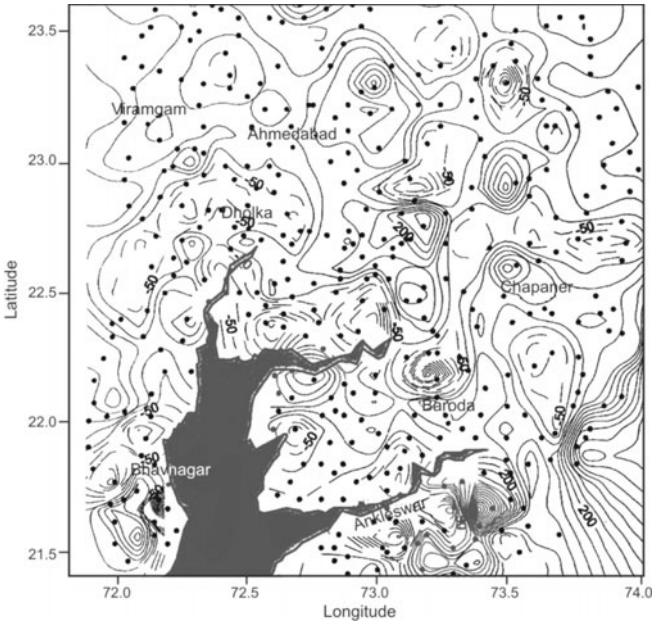

Figure 6.19. The ground magnetic data collected at ~5 km over petroliferrous Cambay basin. Data are used to prepare its total field anomaly map. Note the correlation between magnetic anomalies and tectonic structures in its basin evolution. Regions of high heat flow reveal negative magnetic anomalies and positive gravity anomalies indicating a thin crust beneath them.

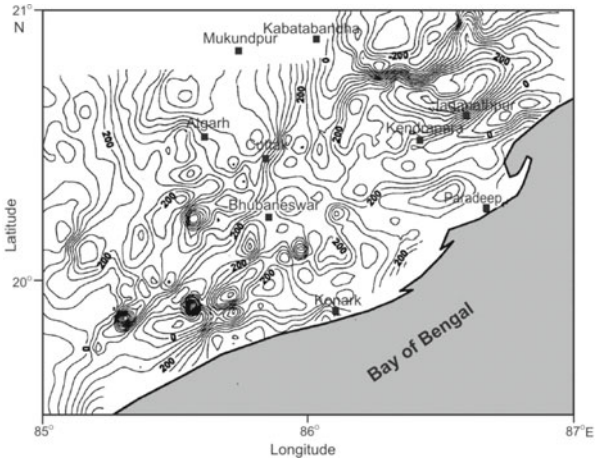

Figure 6.20. The correlation between total field anomalies and tectonic structures in the Mahanadi basin. Contour interval is 40 nT (Anand et al., 2002).

This is in line with the satellite gravity and magnetic anomaly interpretation of their inverse correspondence depicting high heat flow, resulting into this proven petroliferous basin.

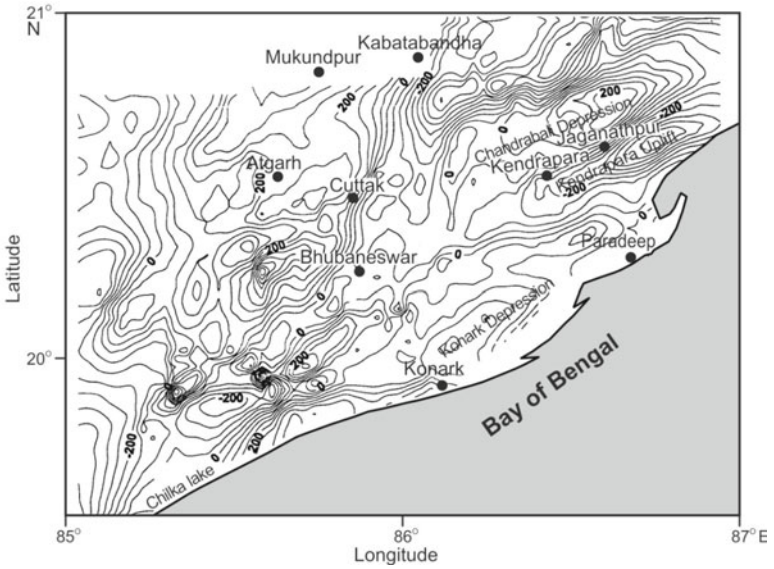

Figure 6.21. Second vertical derivative map of Mahanadi basin showing NE-SW to E-W trends associated with shallow features. Contour interval is of 50 nT/sq km (Anand et al., 2002).

2. Mahanadi basin: Ground magnetic surveys were conducted at 5 km interval over Mahanadi basin covering an area of 21,000 sq km. The total field anomaly map (Fig. 6.20) shows a combination of NE-SW, E-W and NW-SE trends.

Second vertical derivative map (Fig. 6.21) has enhanced the shallow NE-SW to ENE-WSW source trends, which are in conformity with eastern ghats rock exposures on the western side as well as the trend of the ridges and depressions within the basin. The thick band contours running NE-SW from north of Chilka lake to south of Kabatabandha, are the basin margin fault, which limits the basin to the west. This fault was not delineated by gravity studies. A geological contact is found further west.

The anomaly map continued to 10 km above msl reveals deeper features having NW-SE trends (Fig. 6.22). The observed NE-SW and E-W trends in second vertical derivative and downward continuation are related to shallow ridges and depressions of the coastal basin. However, the deeper features evidenced from upward continuation show NW-SE trends (Fig. 6.22), possibly associated with extension of Mahanadi graben under the coastal basin. The shallow trends of NE-SW to E-W seem to be superposed on deeper NW-SE ones formed prior to the breakup of Gondwanaland. Thus, this delta has two structural units, wherein the shallower one is associated with breakup of Gondwanaland and the deeper with formation of intracratonic Mahanadi graben.

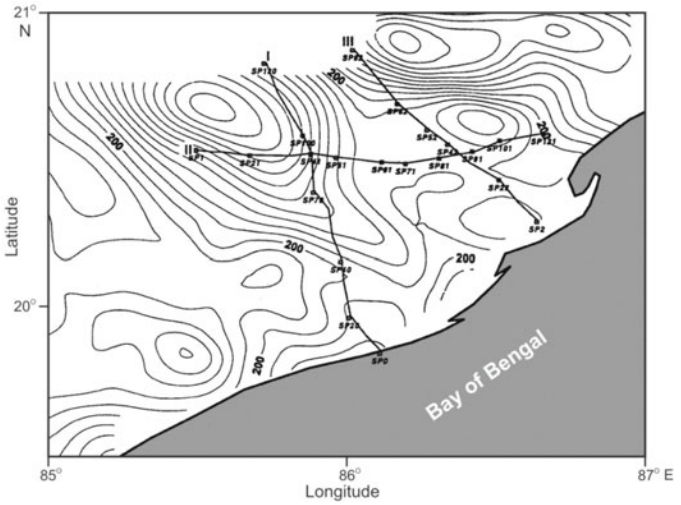

Figure 6.22. Anomaly map of Mahanadi basin continued upward to 10 km above msl, showing NW-SE trend of the deeper features. Locations of I, II and III are DSS profiles (Anand et al., 2002).

3. Krishna-Godavari basin: The prominent trends (Fig. 6.23) are in the NE-SW direction in accordance with subsurface ridges and depressions in this basin. The elongated negative anomaly initially runs NE-SW and later turns ENE-WSW aligning with Baptala, Tanuku and Kaza ridges. Some secondary NW-SE trends are terminated at the NE-SW ends. One such trend passes right on to the south of Rajamundry (RAJ) forming the eastern boundary fault of Chintalapudi sub-basin.

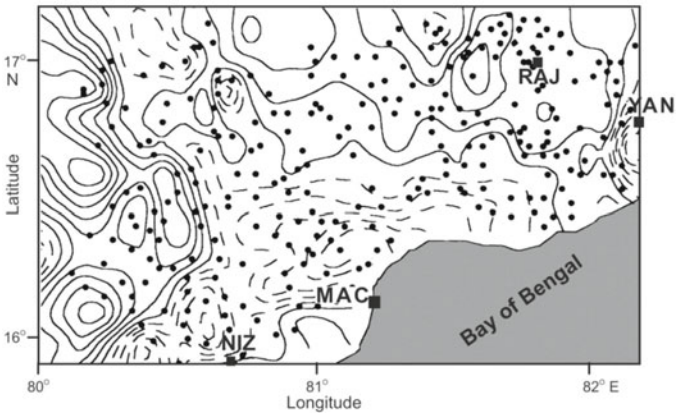

Figure 6.23. Map of total field anomaly over Krishna-Godavari basin prepared from the ground data. Data are interpreted in terms of its basement configuration and estimating the total thickness of sediments. Solid lines represent highs and dashed lines low. Contour interval 40 nT. NIZ: Nizamapatnam, MAC: Macchlipatnam, RAJ: Rajamundry (Rajaram et al., 2000).

Similarly, in the NW portion of the map, another NW-SE trend is found to match with Chintalapudi cross (CCS) trend. Several close anomalies south of CCS are associated with eastern ghats and charnockites.

West of Rajamundry (Fig. 6.23), the closed anomaly pattern is due to the basaltic exposures. The coastal basin has lower values, whereas the Archaean exposures of eastern ghats have relatively higher values. Like Mahanadi, NE-SW trends in KG basin are shallower and superposed on deeper N-S trends related to extension of Godavari graben.

The second vertical derivative map (Fig. 6.24) shows a combination of N-S, NNE-SSW and NE-SW trends. Towards the western side, trends of N-S to NNE-SSW are seen; the N-S to NNE-SSW trend is associated with eastern ghats and NE-SW trends reflect the KG basin. The ridges and depressions cannot be distinctly demarcated probably due to a large station spacing of ~10 km in comparison with the width of the structures.

Figure 6.25 shows the anomaly map continued down to 2 km from msl, which shows a combination of NE-SW and N-S/NNE-SSW shallow trends associated with coastal basin and eastern ghats, respectively.

Figure 6.26 presents 6 km upward continuation from msl. As the level of continuation increases, the NW-SE trends become more prominent. The most conspicuous feature of this map is the appearance of several NW-SE trends at the expense of dominant NE-SW trends, implying limited extent of KG basin, while sources related to NW-SE trends are at larger depth.

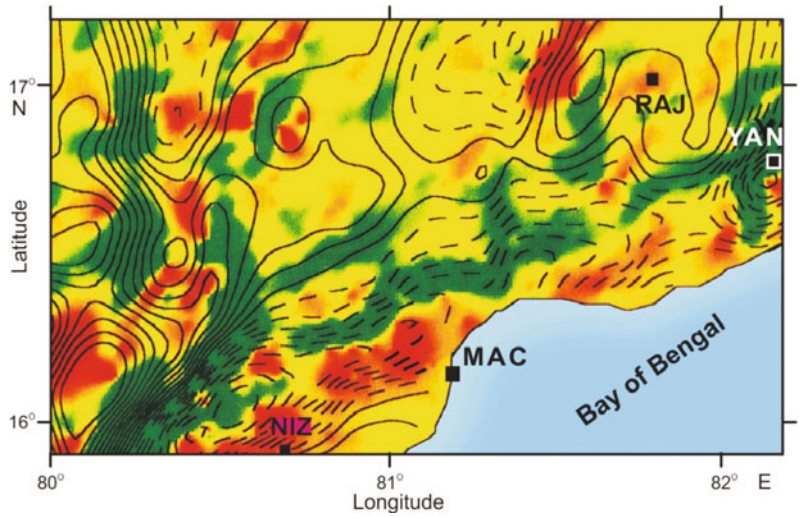

Figure 6.24. Second vertical derivative anomaly map of the ground total magnetic field superposed on the shaded relief map of the Krishna-Godavari basin to isolate the NE-SW trends (red depicts maximum reflectance decreasing to green). Contour interval is of 30 nT; solid lines represent high values and dashed lines low values (Rajaram et al., 2000).

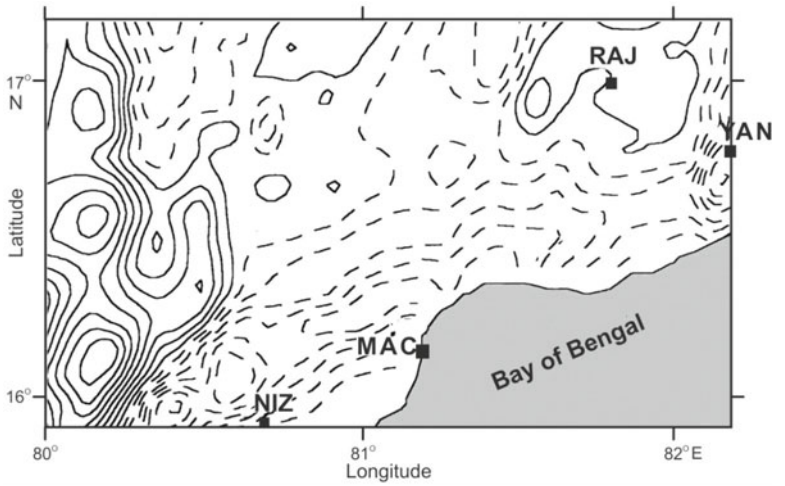

Figure 6.25. Anomaly map of the Krishna-Godavari basin continued downward to 2 km. Contour interval 200 nT (Rajaram et al., 2000).

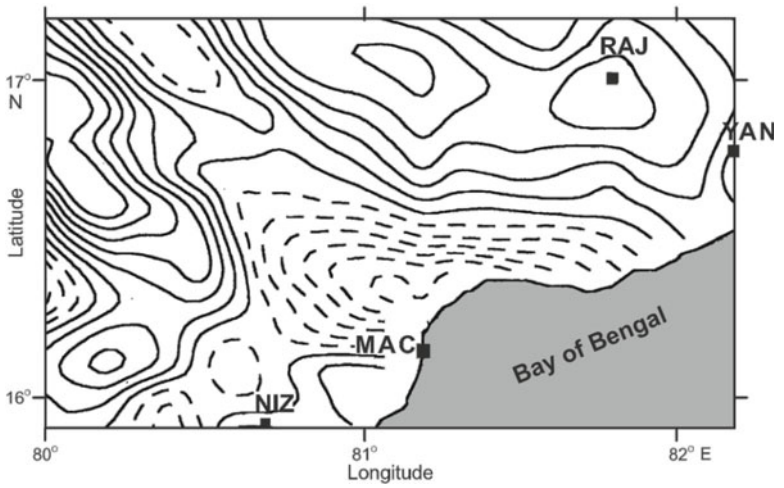

Figure 6.26. Anomaly map of Krishna-Godavari basin continued upward to 6 km. Contour interval 10 nT (Rajaram et al., 2000).

The total field magnetic anomaly is converted into gravity anomaly by replacing magnetization distributions with identical density distributions. This is the pseudogravity anomaly and is measured in pseudo mgal. The steepest horizontal gradient of gravity anomaly or of a pseudogravity anomaly caused by a tabular body tends to overlie the edge of the body. It amplifies the long wavelength components. This characteristic of pseudogravity anomalies is used to locate abrupt lateral changes in magnetization. The horizontal gradient tends to have a maxima located over the edges of pseudogravity sources, hence

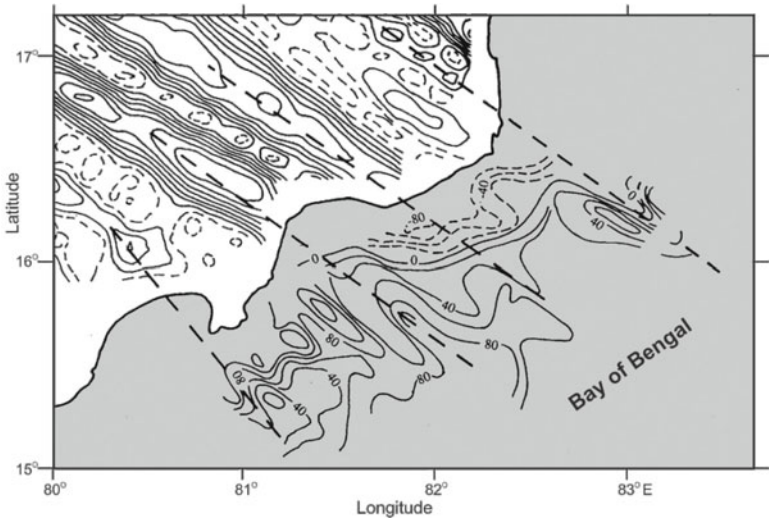

Figure 6.27. Composite HGPG map of ground F data (contour interval 0.5 mgal; solid lines represent highs and dashed lines low; all the values are positive) and the marine magnetic total field anomaly map over the KG basin and its offshore region. The continuation of the NW-SE trends into the offshore is marked on the figure as dashed lines (Rajaram et al., 2000).

horizontal gradient pseudogravity (HGPG) transformation is carried out. The composite HGPG anomaly map of ground data and the marine magnetic anomalies (Fig. 6.27) shows clear and direct continuation of onshore NW-SE trends.

The magnetic data reveal deeper features associated with Dharwar and Bastar cratons prior to the rifting of India from Gondwanaland. The superposed horst and graben structures are formed as a result of rifting and drifting of India from Gondwanaland. The deeper features and horst/graben structures belong to two different tectonic events. NE-SW trends associated with the coastal basin and N-S to NNE-SSW trends of the eastern ghats indicate shallower sources.

4. Cauvery basin: NW-SE anomalies are seen to dominate within the Cauvery basin (Fig. 6.28), which are constrained within the eastern ghats folding. Anomaly trends also show mixed high NW-SE, NE-SW and E-W anomalies over the charnockites. Regions of marine transgression also depict high anomalies. Interestingly, the Ariyalur-Pondicherry (AP) depression is associated with a NE-SW high on ground and aeromagnetic anomaly maps, while the gravity anomaly map shows a low over this depression. The gravity low is due to large sediment thickness of ~5 km, while the magnetic high is due to charnockite basement. The high associated with the AP depression extends offshore in NE-SW direction right up to the ocean-continent boundary.

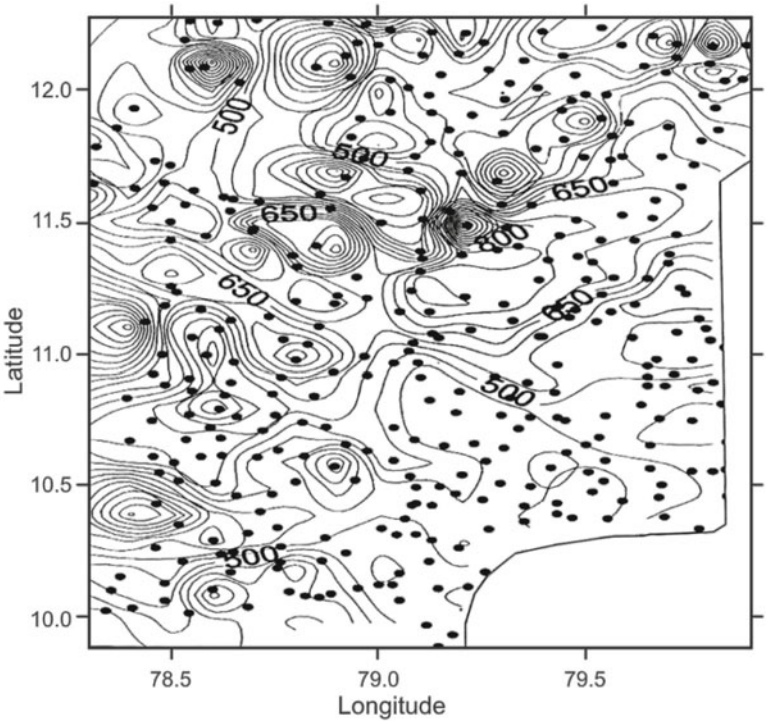

Figure 6.28. Total field anomaly map of the Cauvery basin. The anomaly trends are used to understand the influence of eastern ghat orogeny on its basin evolution and characteristics of ocean-continent boundary.

6.7 ELECTROMAGNETIC (EM) INDUCTION METHODS

Subsurface images of the electrical conductivity can be gained from two methods. The first is electrical technique, in which a constant electrical current is applied to the Earth. The second is EM induction, in which electrical currents are induced to flow in the Earth by a time varying external field. GeoEM induction maps the Earth's surface through to the mantle, where it delineates conductivity structures to improve upon the prevalent understanding of tectonic processes. These studies are carried out on local and regional scale of a few km to hundreds of km to get both lateral and depth extensions of the conductor. Local scale studies include active fault zones or volcanoes, while regional studies include investigations of subduction zones, orogenic belts, seafloor measurements, and mantle hot spots. EM induction studies are used to construct models of electrical conductivity variation in 1D, 2D or 3Ds.

EM induction methods are broadly categorized by the type of source field. If the source of the externally varying field is sufficiently distant from the location of measurement, the source is approximately plane wave, and is said to be 1D (varying in only one direction). On the other hand, if the source and

measurement are close, then it is 3D (varying in all spatial dimensions). This latter category can be further subdivided into techniques, (i) that use a continuously varying controlled source field, usually in the form of a sine wave, known as frequency domain EM, and (ii) those that require a source that abruptly switches on and off as a square wave, known as time domain EM or transient EM induction. Deep Earth conductivity is being traditionally demarcated either by geomagnetic depth sounding (GDS), or magnetotelluric (MT) methods. These two methods do not have any measurement limit, since they use the dynamic part of EMF temporal variations, unlike the static magnetic anomalies that can probe only up to Curie isotherm (~20 to 40 km). The data generated through these methods extend the existing knowledge on conductivity patterns, useful in inferring temperature, structural and compositional variations from the crust down to the lower mantle (~1500 km).

In gravity or magnetic fields, the anomalies are small perturbations over the normal field, but in transient variations they can be greater than the normal part by a few orders of magnitude. The causative process is the large electrical conductivity contrast of 13 orders of magnitude (e.g. dry crystalline rocks have conductivities $<10^{-6}$ S/m, while ores have conductivities exceeding 10^{6} S/m). Electrical conductivity is a sensitive parameter for saline fluids, carbon grain-boundary films, conducting minerals, high heat flow and partial melts (molten rocks or aqueous solutions). This parameter is extensively used in GDS, OBM and MT for mapping geoelectrical structures.

6.8 BASIC METHOD OF EM INDUCTION

A time-varying magnetic field induces currents in a neighbouring conducting medium in accordance with Faraday's law. An oscillating externally magnetic field of the wave generates electric currents in the Earth through EM induction, and the signal propagation becomes diffusive, resulting in signal attenuation with depth (skin depth). The induction process is governed by Maxwell's equations (Appendix 6.1). The factors that control the strength of induced currents are: conductivity distribution of the Earth's interior, and variation in time and space of the external field.

I. Earth's Natural EM Field

The source of natural currents flowing inside the Earth is definitely located outside of it. Periodic and transient EMF fluctuations are correlated with time varying solar emissions, which have a great influence on the ionospheric currents. The telluric currents are thought to be induced in the Earth by currents flowing partly in ionosphere and magnetosphere.

The currents are produced through complex interaction of EM radiation and particle flux radiated from the Sun with the EMF. The incoming EM radiation interacts with gases in the upper atmosphere producing distinct ionized layers at 40 to 400 km. These layers move across the EMF due to thermal

gravitational action of the Sun producing varying currents in the ionosphere. These variations depend on the Earth's position with respect to the Sun, hence have a periodicity of 24 hrs, which is the periodicity of Earth's rotation. The currents in the magnetosphere are due to complex interaction of solar wind, interplanetary field and EMF. These currents are situated around $4R_E$ to 10 R_E (Chapter 3). Below a frequency of 1 Hz, most of the signals originate in the magnetosphere as periodic external fields including magnetic storms, substorms and micropulsations. These signals are normally incident on the Earth's surface. Above a frequency of 1 Hz, the majority of EM signals flash out through lightning activity.

The inductive mechanism is an EM field propagated between the ionosphere and the Earth surface somewhat in the manner of a guided wave between parallel conducting plates. That is to say, it proceeds by bouncing back and forth between these boundaries, and hence has a large vertical component. At large distances from the source, this is a plane wave of variable frequency (10^{-5} Hz to audio range). Obviously, these MT fields can penetrate the Earth's surface to produce the telluric currents.

II. Principle of EM Method and Relations between Primary and Secondary Fields

If an EM field is produced on Earth's surface, currents flow in the subsurface conductors in accordance with EM induction laws. The natural electric field associated with these currents inside the Earth is of the order 10 mV/km. The 'primary' currents in the induction process are electric currents, which flow external to the Earth and change with time. As the solid Earth conducts electricity, 'secondary' currents (which are out-of-phase and of same frequencies with the primary current) are induced. In general, the resultant field recorded at the Earth's surface differs from the primary field in intensity, phase and direction, revealing the presence of subsurface conductors. In many instances, the primary fields are uniform and spatially uncorrelated from one induction event to the next; but the spatial patterns occurring systematically reflect spatial patterns in the secondary fields due to conductivity structures.

III. Determination of Nature of Conductivity (High/Low) of EM Anomalies

The EM field shifts in phase on encountering a relatively good conductor. In fact, the conductor becomes the source of a secondary field, which differs in phase from the primary field, while having the same frequency. In commonly used EM field method, the in-phase and out-of-phase components are measured. If the secondary field is 90° out-of-phase with the primary field, the subsurface conductor is a bad one. On the other hand, if the out-of-phase secondary field is 180° with the primary field, it is a very good conductor.

IV. EM Depth Sounding

It is used to study the variation of conductivity with depth. EM depth soundings are carried out either by change of frequency or change of transmitter to receiver (T-R) separation. Measurements may be in frequency or time domain. The sounding depth of any EM method depends on the frequency (time period) contents of the induced fields, and subsurface conductivity (skin depth). The EM signal diffuses to a distance into the Earth, defined as the skin depth, δ, in metres by $\delta = 503/\sqrt{\sigma f}$, where σ is the conductivity (S/m) and f is the frequency (Hz). The skin depth is inversely related to the frequency, and thus high frequency signals probe the shallow subsurface, while low frequency fields penetrate a much wider induction space and depth into the Earth. Depth persistence of the conductor or conductive overburden can be resolved by the use of two frequencies.

If the anomalous conductor is indicated by more than one T-R separation, it is assumed that the conductor persists with depth. If the same anomalies are indicated on the adjoining traverses (y-direction), the body persists along the strike direction also.

V. Advantages of EM Sounding Method

The major advantage of EM induction methods of GDS, MT and OBM is that the frequency can be varied to obtain different profiles for different frequencies. Such EM profiles then help in locating the target more clearly. Another advantage is that it requires no ground contact, and can successfully be used in sandy areas. Also, EM soundings have operational convenience even in highly resistive surface areas, where DC resistivity surveys are not feasible. In noisy environments, active EM methods like transient EM, and controlled source EM can be a good choice, but the sounding depth of these methods is restricted to the first few metres, but in favourable conditions perhaps a few km. For the really deep targets, one can only rely on natural source MT.

VI. EM Data Interpretation

If the Earth had ideal spherical symmetry, and its properties (including electrical conductivity) varied with the depth only, the observational analysis for structure determination is straightforward and is termed 1D. But for a 2D situation, the conductivity varies with two spatial parameters such as depth and one horizontal direction; while in a 3D situation the conductivity may vary in all directions.

Developments in modelling of EM induction data are closely parallel to those in other subsurface geophysical imaging techniques such as seismology. The forward problem of EM induction involves solution of Maxwell's equations in the electrically conducting Earth, excited by appropriate external sources. Inverse modelling of EM data reverses this process, using data generally observed on the surface to image conductivity variations within the Earth. For natural source methods such as GDS and MT, the frequency-dependent response

of the Earth to large-scale sources is determined by statistical estimation of transfer functions (especially local ratios of field components) from EM time series data.

Initial inverse modelling efforts were focussed on 1D interpretation, wherein data from one site are inverted to obtain information about the local conductivity-depth profile. Later 2D inversion methods were developed for profiles of data across a dominant geoelectric strike. Finally, as more powerful computational resources became available, methods for full 3D inversions evolved.

6.9 GEOMAGNETIC DEPTH SOUNDING (GDS)

The technique of detecting inhomogeneities in the subsurface conductivity with GDS has its origin in the pioneering works of Schuster in 1908 and Chapman in 1919, which was a popular natural source EM method between 1950 and 1980. The book by Rokityansky in 1982 covers all aspects of the GDS, while a detailed account of theory is given by Weaver in 1994. With the advent of more powerful computing facilities, MT took over from GDS, which was then somewhat ignored.

6.10 METHODOLOGY, OBJECTIVES OF GDS TECHNIQUE

I. GDS Survey Instruments

These instruments are different from MT since they employ only the magnetic, and not the electric field to investigate subsurface electrical conductivity distribution through an array of three-component magnetometers. Magnetic observatories provide the requisite periodicity data to map depths running into hundreds of km. But, because of their poor distribution, only the smoother fields can be defined adequately. In GDS profiles or arrays, three-component Gough-Reitzel or fluxgate magnetometers are left in position for periods of one to several months, during which time they record geomagnetic variations such as storms, bays, pulsations and the normal daily variation. These variations contain the external and internal parts. By mapping the patterns of induced currents, and using suitable analysis of the magnetic variations, theoretical models of the subsurface electrical conductivity structure are inferred. GDS is also known by the term magnetovariational (MV) method, since it uses the ever changing magnetic variations.

II. Sounding the Earth Using Natural Geomagnetic Variations

A slowly varying magnetic field inside a uniform conductor (conductivity σ and relative magnetic permeability μ) satisfies the induction equation: $\nabla^2 E = \mu\mu_0\sigma\delta B/\delta t$, the time varying field induces eddy currents in the conductor,

which flow so as to exclude the field from the deeper parts. The amplitude of a spatially uniform field of frequency ω falls to 1/*e* of the surface value at the 'skin depth': $Z_0 = (2/\omega\mu\mu_0\sigma)^{1/2}$. This expression provides a rough guide to the 'sounding depth', which might be expected of a particular frequency. The basis of sounding method is to measure the Earth response at a range of frequencies and/or source wavelengths.

6.11 ACQUISITION, ANALYSIS AND PRESENTATION OF GDS DATA

I. GDS Data Acquisition

The method involves collecting simultaneous records of N-S (X), E-W (Y), and vertical (Z) components of naturally time-varying geomagnetic field from a 2D array of magnetometers deployed in a regular grid pattern. The observed variations over the surface of the Earth have contributions from external currents as well as from induced currents. Over an infinitely conducting horizontally layered surface, the field due to spatially uniform external varying field and its induced counterpart interact with each other in such a way that they nullify the vertical component Z and enhance the horizontal components H or D of the observed field to an extent that it becomes twice the value due to external field only. Under this condition, if one observes Z over the surface of the Earth, it can be indicative of lateral heterogeneities of conductivity near the observation site.

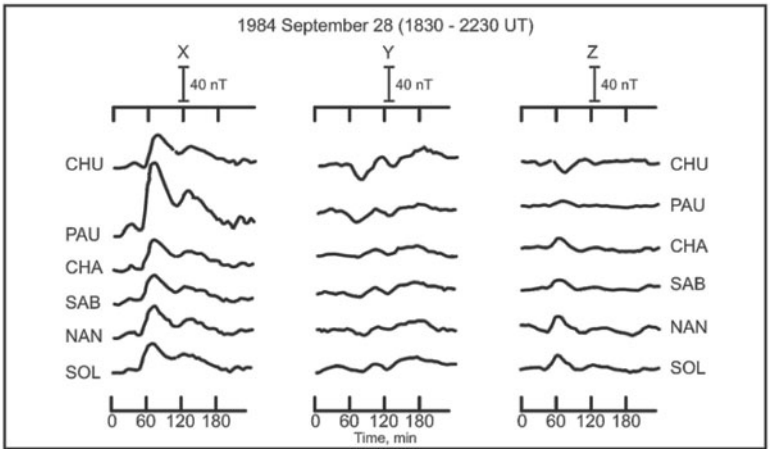

Figure 6.29. Stacked profile of substorm recorded on 28 September 1984 at some of the lesser Himalayas array stations. Note a marked enhancement of X and highly suppressed Z variation at PAU. But the two stations on its two sides show opposite Z variations, indicating the presence of a conducting zone beneath PAU.

II. Stack Plots

In the first instance, a sample stack plot of variations in the three components of the field is prepared by taking data recorded through an array of magnetometers from a disturbed period. An example of such a plot is given in Fig. 6.29 taken from array records of 28 September 1984. A reversal in sign of Z is seen between CHU (Chaukutia) and CHA (Champawat). The conductor is located between these two stations underneath PAU (Pauri). Therefore, the observed features of associated X, Y and Z variations are used to locate subsurface conductive zones. However, the observed variation over a site is due to combined response of different subsurface conductive layers. To achieve the proper estimates of contribution of each layer to the observed phenomena, data processing techniques given in section 6.12 are used.

6.12 DATA PROCESSING TECHNIQUES

The determination of the vertical variation of conductivity has two steps: (1) measurement of the response or transfer function, which links the input (external part of the magnetic field) to the output (internal part created by induced currents), and (2) inversion of the response for the conductivity, detecting conductivity from the response and its associated errors. For arriving at proper estimates of dimension, conductivity, depth and direction (strike) of the causative body, one or more of the Fourier transform maps, transfer functions, Parkinson's vectors, etc. are used.

I. Fourier Transform Maps

GDS data gathered in time domain are converted to frequency domain to map fields at selected periods. The spectral peaks of amplitude and phase exhibit EM response of structures in a particular depth range. It thus enables to isolate the response of layers of interest, and study their behaviour separately over the array area.

II. Transfer Functions

Transfer functions are more quantitative and frequency dependent. For calculating transfer functions, five or more events of almost same duration and with different intensity and polarization are selected to arrive at Fourier transforms, after removing the linear trend. Tables 6.2a,b and Appendix 6.2 present the procedural steps followed in processing the raw data to compute transfer functions.

III. Parkinson's Induction Vectors

The first task in interpretation is to determine the spatial pattern of conductivity without actually modelling the response. If there are a number of irregularly

Table 6.2a Information from time series raw data

Event date	*Period range, sec*	*X-Variations, nT*	*Y-Variations, nT*	*Z-Variations, nT*
1 April 2004	1-512	(-30) – (20)	(15) – (-12)	(-10) – (20)
30 March 2005	1-512	(-40) – (40)	(25) – (-15)	(22) – (17)

Table 6.2b Data in frequency domain after determination of transfer functions

Period, sec	*A*	*B*	*C*	*D*
256	(0.868, -0.016)	(0.033, 0.015)	(0.100, 0.060)	(0.796, -0.097)
90	(0.891, 0.037)	(0.051, 0.024)	(0.159, 0.017)	(0.708, 0.039)
60	(0.911, 0.042)	(0.067, 0.018)	(0.163, -0.019)	(0.708, 0.039)
40	(0.928, 0.039)	(0.077, 0.001)	(0.145, -0.055)	(0.708, 0.039)
30	(0.937, 0.035)	(0.076, -0.016)	(0.121, -0.017)	(0.708, 0.039)

distributed magnetometers, then induction arrows are plotted. Parkinson showed in 1964 that geomagnetic variation in the amplitude of Z-component mainly depends on the direction of horizontal field. The Z-response is maxima for a particular direction of horizontal field. Near a conductivity contrast, Parkinson vectors always point towards the zone of high conductivity.

IV. Complex Demodulation

Variation of field component with time represents gross response from subsurface layers. Complex demodulation method was introduced by Banks in 1976, which combines the time and frequency domain analysis. It provides variation with time of both amplitude and phase of selected frequency for the time duration of the event. Additionally, this procedure provides an accurate method for estimating the transfer function from a single storm's stretch of data, which has different directions of polarization.

V. Hypothetical Event Analysis

This method was developed as an analytical tool in the absence of simultaneous records from recording stations over a surveyed area. For each station, an estimate of A and B is made, and then the analysis proceeds to estimate the Z-response for hypothetical uniform source fields for selected direction of polarization. Contour plots and pseudo-sections of anomalous vertical fields estimated from the hypothetical event analysis on transfer functions are essential to characterize the orientation and dimensionality of electrical conductive structures of the region.

VI. Thin Sheet Modelling and Island Effect

The electromagnetic induction effects due to highly conducting sedimentary basins, seawater of variable depth (continent-coast interface, island effect) are

solved by assuming that these conductivity anomalies are confined to a thin layer. In such cases, mathematical model used comprises an infinitesimally thin sheet of varying surface conductivity materials. It is known as thin sheet because thickness of this sheet is negligible as compared to the skin depth of underlying layer. This condition ensures that electrical properties of the materials in the thin sheet itself are electrically linked to substratum so that at the period of interest, horizontal electric field remains constant over the thin sheet.

A number of records are generally analyzed to cover wide range of frequency bands, and different polarizations of incident waves. Electromagnetic impedance of ratio of vertical magnetic variation and most correlated horizontal component is estimated to gain transfer functions. The transfer functions are frequency dependent, and they provide induction arrows, and its variant hypothetical event analysis and Z/H pseudosections for various source field polarizations. All these data analyses methods are based on the fact that a time varying magnetic field tries to avoid a conductor.

6.13 GDS FIELD SURVEYS

Magnetic array studies provided valuable initial information on the conductivity structure of the crust and upper mantle all over the globe, especially in North

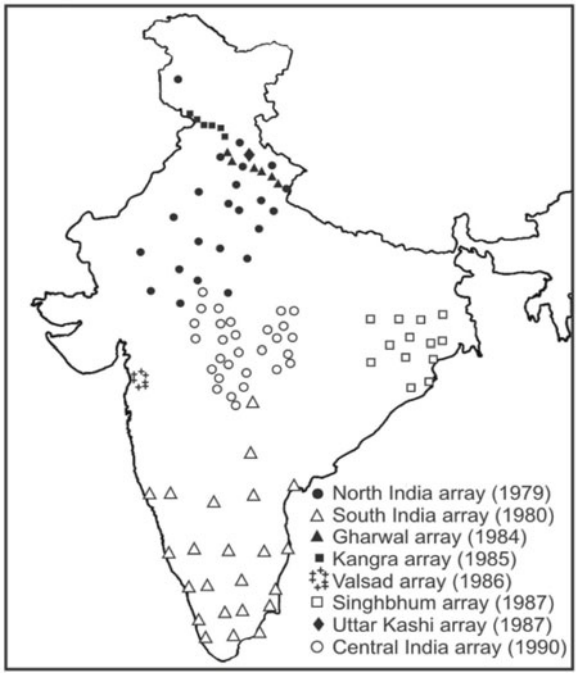

Figure 6.30. Location map of some arrays of magnetometer operated to understand the subsurface electrical conductivity of the Earth. The map shows where and over what periods these arrays operated.

America, Africa, Australia, and Europe. India, too, is not lagging behind in these studies. With the inception of two equatorial geomagnetic observatories at Annamalainagar and Trivandrum in the 1970s/1980s, an exciting era of induction studies was initiated. To account for anomalous behaviour in observed Z variations at these observatories, the phenomena of induced current perturbations was invoked. So, they were started in 1979 in India after which areas such as Garhwal, Kangra, Valsad, Singhbhum, Uttarkashi, central India and Ladakh-Leh regions were surveyed under different array campaigns. Figure 6.30 shows the station locations and some of the regions covered by these arrays.

6.14 MAGNETIC VARIATION MAPPING EXAMPLES

Large magnetometer arrays employed in different tectonic regimes imaged deeper structures of the crust and upper mantle. The observed conductivity anomalies have different causes and variable regional extents, which are presented below in the form of case studies.

I. Conductive Bodies below the Himalayas

A 'trans Himalayan conductor (THC)', running from the NE Indian shield to the foothills of the Himalaya was deciphered. The position of this conductor coincides with a localized high seismicity zone (Figs 6.32 and 6.58). This

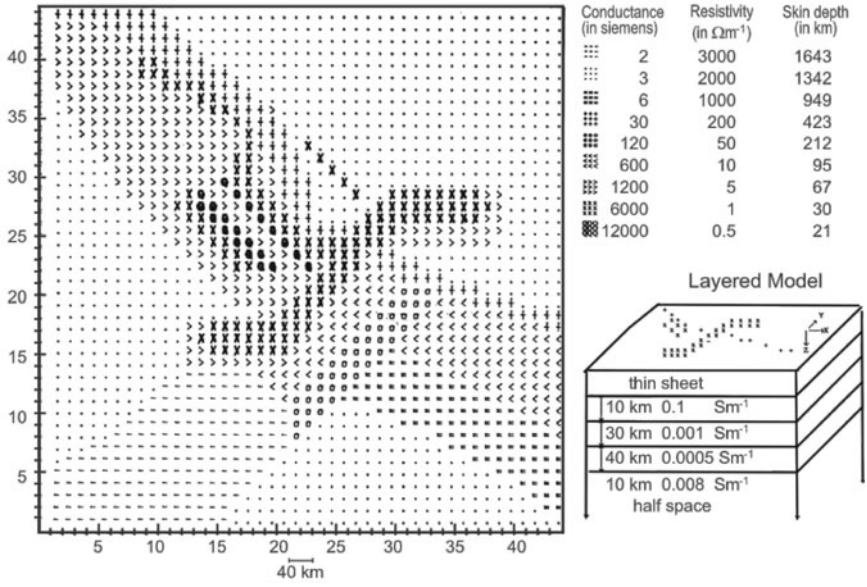

Figure 6.31. 3D view of the conductance map. The integral sign high conductance zone signifies eastward and westward extension of the THC. Also, note the furrowed type conducting zones paralleling the trend of Himalayan collision zone.

conductor is modelled as a 45 km wide, 85 km high protuberance from the asthenosphere into the lithosphere (Fig. 6.31). A resistivity of 2 ohm-m and background resistivity of 10^4 ohm-m were used in the modelling. Also, 'Garhwal Lesser Himalaya conductivity anomaly' was established along the Uttarkashi region (Figs 6.30-6.32). This mapped conductive zone in the epicentral track of 1991 Uttarkashi earthquake is viewed as a shallow but extended fracture zone above an obducted crustal block. Movement in the fracture zone to readjust compressive forces explains the correlation of this conductive zone with Garhwal Lesser Himalayan seismic belt and with recent Uttarkashi earthquake.

II. Conductance and Seismicity in Central and Western Parts of India

A plutonic body delineated near Valsad in south Gujarat is embedded in the upwarped asthenosphere along the western continental margin (Figs 6.32 and

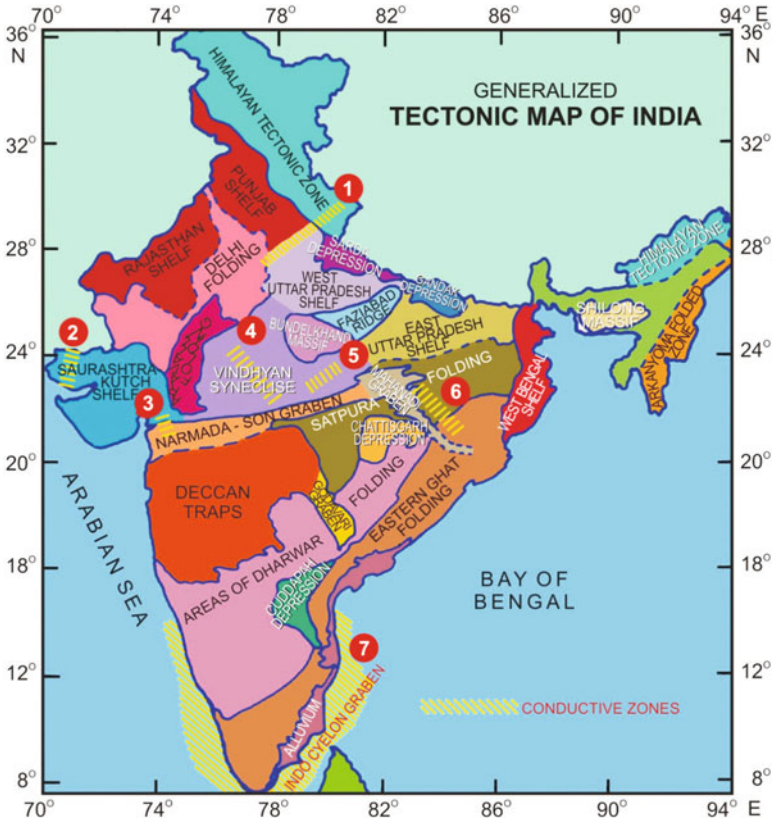

Figure 6.32. Generalized tectonic map of India and the different conductivity structures identified through GDS, MT and long-period MT probes. The numbers on the map are the following conductive structures: 1 - Trans Himalaya, 2 - Bhuj, 3 - Valsad, 4 & 5 - Central India, 6 - Singhbhum, 7 - South Indian offshore conductivity anomaly.

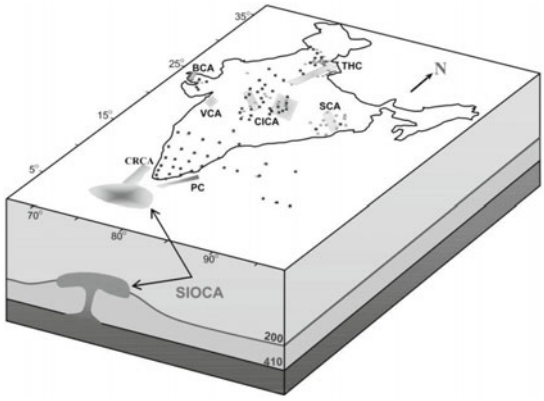

Figure 6.33. A composite map of different conductivity structures. THC - Trans Himalayan Conductor, BCA - Bhuj Conductivity Anomaly, VCA - Valsad Conductivity Anomaly, CICA - Central India Conductivity Anomaly, SCA - Singhbhum Conductivity Anomaly and PC - Palk-Strait Conductor. (Arora and Subba Rao, 2002).

6.33). This region has been experiencing earthquake swarms in recent years. Studies in seismically active Bhuj region point to the concentration of induced currents in thick sedimentary columns. The high conductance prevalent in western part of Kutch region, NW of Lodai is related to half graben formed due to the uplifted Wagad upland (Figs 6.32 and 6.33). An arcuate-shaped conductor at mid-crustal depth is also found beneath the Satpura ranges. This conductor coincides with Mandla gravity high. A geothermal anomaly is also observed in this area.

The Godavari graben is mapped up to the southern limit of NSL beyond which it is shrouded under the thick cover of Deccan traps (Figs 6.32 and 6.33). Electrical characteristics of the Bengal basin marginal fault and also the E-W trending conductor bordering the Singhbhum craton are well established (Figs 6.32 and 6.33). In Singhbhum region, a linear trend of conductivity anomaly extending in E-W direction is located to the north of Ranchi and Bokaro lying at greater depths. Its source is the Gondwana grabens of Damodar valley (Figs 6.32 and 6.33).

III. South Indian Offshore Conductivity Anomaly

The south Indian offshore conductivity anomaly (SIOCA) is associated with relics of the Marion plume outburst. The conductivity anomaly beneath Palk Strait is due to thermal interaction, when the Indian lithosphere passed over the Marion plume. However, the conductivity anomaly observed beneath Comorin ridge and a rift structure encountered along the west coast margin of India appear to be related to Reunion hotspot activity (Figs 6.32, 6.33 and 6.34).

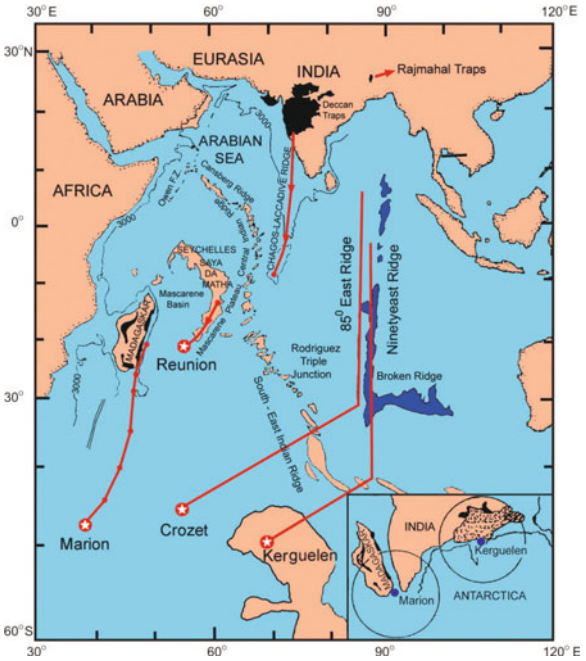

Figure 6.34. Locations of different hotspots (white stars) and volcanic ridges formed during the transit of the Indian plate over them. Inset: Areas affected by the outburst of Marion plume that led to the separation of Madagascar from India (Arora et al., 2003).

IV. Determining Electrical Conductivity from MO Data

The MOs spread over the globe collect time-series data of magnetic and electric fields. This data can be inverted to gain a profile of electrical conductivity with depth. For example, crustal conductors are modelled following finite difference and thin sheet approximation (3D modelling), providing important geoelectrical parameters of lithosphere. This MV data are important to study conductivity heterogeneities residing in the deep interior of 1000 km. Theoretical model on electrical conductivity structure of the upper mantle (~50 to 1200 km) is

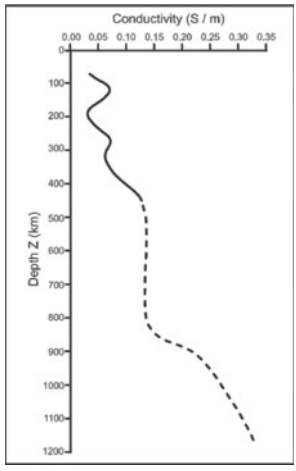

Figure 6.35. Conductivity distribution pattern with depth derived from continuous strings of geomagnetic field components recorded at Indo-Soviet chain of MOs (Chandrasekhar and Arora,1992).

developed using the continuous strings of geomagnetic field components recorded at Indo-Soviet chain of MOs. This model reveals alternate increase and decrease in the conductivity up to ~500 km from where it does not change up to ~900 km, beyond which a steady increase is seen (Fig. 6.35).

6.15 OCEAN BOTTOM MAGNETOMETER STUDIES

The ocean floor, with pressures of up to 600 atm (60 MPa), temperatures ~3°C and no possibility of radio contact with instrumentation, presents a particularly harsh environment for carrying out magnetic and electrical measurements. Furthermore, sea water is corrosive and a conductive fluid. However, with the availability of reliable underwater technology, electrical conductivity studies of the ocean bottom have now become a routine affair. This is done through ocean bottom magnetometers (OBMs), which are similar to GDS fluxgate units. They can enhance understanding the surface and subsurface structures of the ocean in conjunction with land-based geoelectrical studies. OBMs sit on the floor and measure the attenuation of magnetic field components between sea surface and seafloor. As magnetic field variations are difficult to measure on sea surface, nearest land station is taken as a reference station. OBM data are found to have increasing applications on seafloors to study mid-oceanic ridges, plate margins, subduction zones, hot spot trails and others.

6.16 OBM FIELD EXAMPLES

OBM arrays were set at Mariana trench back-arc spreading centre, Barren Island in Andaman Sea, 85° ridge, 90°E ridge in the Bay of Bengal, and off the coast of Cochin in the Arabian Sea. The latest trend in marine surveys is to gain improved depth resolution through MT methods using ocean bottom electrometers (OBE).

I. Conductivity (Resistivity) below Arabian Sea and Bay of Bengal

A long conductive structure aligned in a N-S direction at a depth of ~12 km below the Arabian seafloor was identified ~100 km off Cochin. The oceanic crust and upper mantle underlying the Bay of Bengal is more resistive than the crust and mantle below the Andaman arc region, because the Bay of Bengal crust is older than the Andaman arc region. The OBM results reiterated the subduction of Indian plate beneath the Burmese plate, providing a breakthrough for understanding mantle dynamics related to plate subduction (Fig. 6.36).

II. Barren Island Volcanism

Two different conductivity zones in depth ranges of 17-27 km and 80-100 km mapped beneath the Barren Island in Andaman Sea saw eruption of a volcano

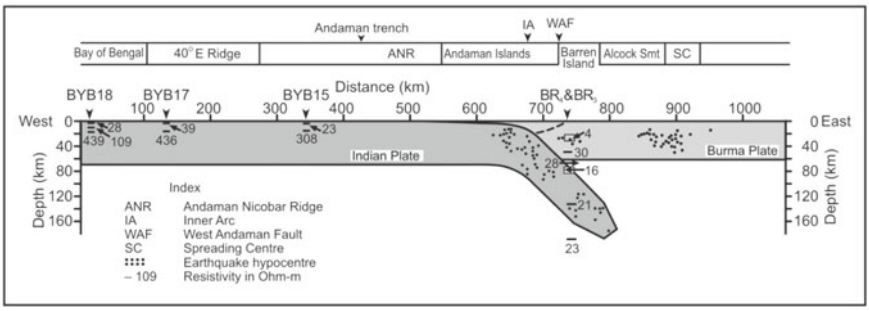

Figure 6.36. Map showing the subduction of Indian plate beneath the Burmese plate along with the resistivity values obtained from OBM array studies (Subba Rao et al., 2000).

in March 1991 (Fig. 6.36). Furthermore, the Andaman Sea experiment showed the spreading ridge significantly perturbs the regional current flow. A subsurface conductive channel is proposed between the mouth of the Irrawaddy River and Coco Island. No evidence of conductive plume or plug is noticed beneath the Narcondam or Barren Islands.

6.17 MAGNETOTELLURIC SURVEYS

Natural EM signals are used in magnetotellurics (MT) to image subsurface electrical structures. It is now routinely used in both commercial exploration and pure research. Its commercial applications include exploration for minerals, hydrocarbons and geothermal resources. Researchers use MT to study the continental subsurface structures and dynamics of plate boundaries. Most continents consist of Archaean cratons, which are enclosed by Proterozoic and Phanerozoic geotectonic belts and suture zones. Many of the old structures are covered today by huge sedimentary basins, whose position and structure can be unravelled through this method.

Excepting seismic method, greater depths of exploration are not attainable by other techniques. Hence, MT holds promise for deep exploration, forming an alternative to seismic in oil exploration and basement studies. Additionally, the method can be valuable for reconnaissance, especially in sedimentary areas, where highly insulating formations like salt, anhydrite and evaporite beds are involved. This is because the EM waves penetrate large depths, if the ground is highly insulating. Specifically, the Deccan volcanics provide an ideal geological setting for exploiting MT method. Here, the entire Precambrian formation is covered by Deccan basalts, and is thus not available for scrutiny through conventional geological methods. The basaltic cover forms a high velocity zone and a large number of reflections generated by these rocks make the seismic interpretation difficult. Hence, MT methods are useful in this terrain. Recently, the scope of MT studies has been extended to

map lithosphere-asthenosphere boundary by introducing long-period MT instruments called LMT measurements. These instruments measure very low frequencies ($1–10^{-4}$ Hz), and are used for imaging the lower crust and upper mantle.

Determination of Earth's conductivity by measuring the geomagnetic field and telluric currents was suggested by Taikhonov in USSR and Cagniard in France. Cagniard showed that if magnetic and electric fields comprising a plane EM wave travelling into Earth are measured, the resistivity of the Earth can be computed. Later on, considerable studies were carried out by Vanyan and other Soviet investigators regarding depth soundings by natural and artificially induced electromagnetic fields. Keller furnished English translation of these papers in 1967 which also gives an interesting historic account of the developments in this field.

6.18 METHODOLOGY, DATA ACQUISITION AND TIME SERIES PROCESSING

I. Basic Method of MT and Time Series Data Processing

MT method involves simultaneous measurement and analyses of five components of naturally existing EM fields of the Earth constituting two orthogonal electrical and three orthogonal magnetic fields. In this method, oscillations of the electrical and magnetic fields are recorded normally in two or three frequency bands in the range of 10^{-4} to 10 Hz. Though Earth's natural EM fields contain a wide spectrum of frequencies originating from different causes, frequencies <1 Hz originating from interaction between EMF and flow of plasma of the Sun (solar wind) are of interest to MT. Hence frequencies higher than a few Hz originating mainly due to sources of meteorological and man-made power lines are not considered.

II. MT Data Collection and Penetration Depth

An example of recorded time series (variation of field amplitude with time) of the five electrical and magnetic field components is shown in Fig. 6.37. The total recording for a MT sounding is ~5 to 7 hrs. MT time series data are processed to yield frequency domain estimates of apparent resistivity and phase. Modern processing schemes compute fast Fourier transform of subsections of the time series. In MT data collection, time series data are recorded simultaneously at several locations to allow for the removal of noise at the measurement location through the remote reference method.

In MT, the skin depth δ (km) for a period T (hrs) in a half-space of conductivity σ (S/m) is calculated using the same formula as given in GDS section, i.e. $\delta = \sim 30.2 \times (T/\sigma)^{1/2}$. The better the conduction and higher the frequency are, the smaller is the skin depth or penetration depth.

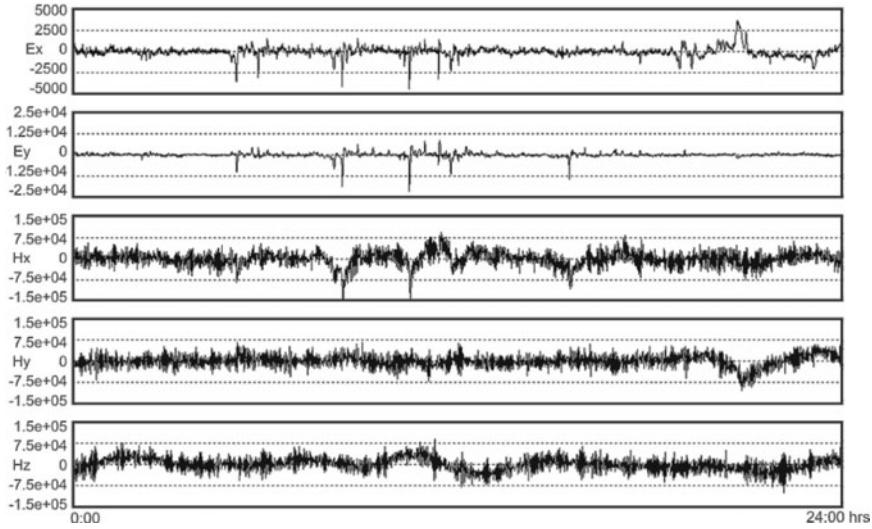

Figure 6.37. The measured time series of the five components (Ex, Ey, Hx, Hy and Hz) at a MT sounding site.

III. Instrumentation and Field Technique

MT soundings measure tangential components of both the electrical and magnetic fields on the ground surface so as to determine their ratio as a function of frequency. A typical field set-up of MT data acquisition is shown in Fig. 6.38 which basically consists of the following components: (i) two electric sensors that are normally two pairs of grounded non-polarizing electrodes connected to suitable amplifiers for measuring electric components Ex and Ey, (ii) three highly sensitive magnetic sensors for measuring the three magnetic components Hx, Hy, and Hz. The magnetic sensors are normally induction coil type or more recently super conductivity magnetometers (Chapter 4). Highly resistive fluxgate type magnetometers can also be utilized when low frequencies are of main interest, (iii) suitable post amplifier units for five field components, Ex, Ey, Hx, Hy and Hz, (iv) digital data acquisition system for recording and analyzing the data by computer, and (v) a five-channel analog strip chart record for monitoring the field data.

Presently, there is a clear tendency for a large number of recording instruments to operate simultaneously, and with much denser site spacing. Another development has taken place in 3D MT wherein instruments are distributed over an area or aligned in a grid instead of simply following profiles.

IV. Basic Theory

For developing the basic theory for MT method, an isotropic Earth of a plane surface and plane EM waves are assumed near the site of measurement. A homogeneous isotropic Earth has no real significance in exploration geophysics,

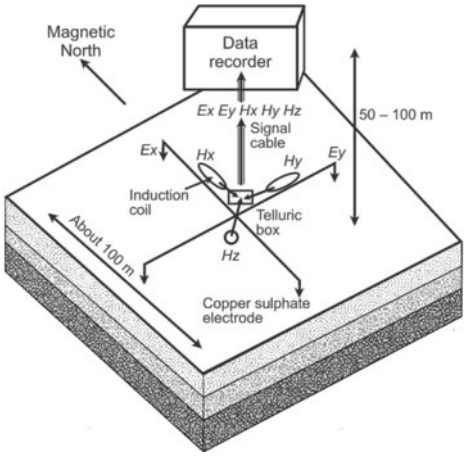

Figure 6.38. A pictorial representation of the field set-up for MT sounding. (http://science.jrank.org/article_images/science.jrank.org/ magnetotelluric-prospecting.1.jpg).

but the response of such a model can be utilized to define an apparent resistivity. Since the theory is concerned with EM fields, any material medium can be described by the three physical parameters, viz. electrical conductivity (σ), magnetic permeability (μ) and dielectric constant (ε). Starting from the Maxwell's EM equations (Appendix 6.1), it can be shown that impedance is a characteristic of the electric properties of the medium of propagation and the frequency of the EM field. The impedance is calculated by taking the ratio of the amplitudes of electric field and the associated orthogonal magnetic field (E_X/H_Y or E_Y/H_X) for a given frequency. The subscript X and Y denote the direction of the measurements. The frequency provides an extra dimension to the measured ratios, which permits deduction of the frequency variations of the apparent resistivity similar to that obtained at various electrode separations in DC resistivity method. By determining the impedance elements at various discrete frequencies, the conductivity of the Earth as a function of depth is obtained. Appendix 6.2 reports calculation of elements of a 2×2 impedance tensor Z.

In MT analysis, initially four impedance values of ZXX, ZXY, ZYX and ZYY are determined from the measured electrical and magnetic field components. In the case of a horizontally stratified Earth model, both ZXX and ZYY are equal to zero and ZXY = – ZYX. When a structure is present, such as fault, both ZXX and ZYY are nonzero. In this case the impedances in various directions are mathematically determined by rotating the coordinates of the measured impedances. When one of the rotation axes becomes parallel to the strike direction, the quantity Z'XX + Z'YY will become minimum, while the quantity Z'XY + Z'YX will become maximum (here Z'XX, etc. are the

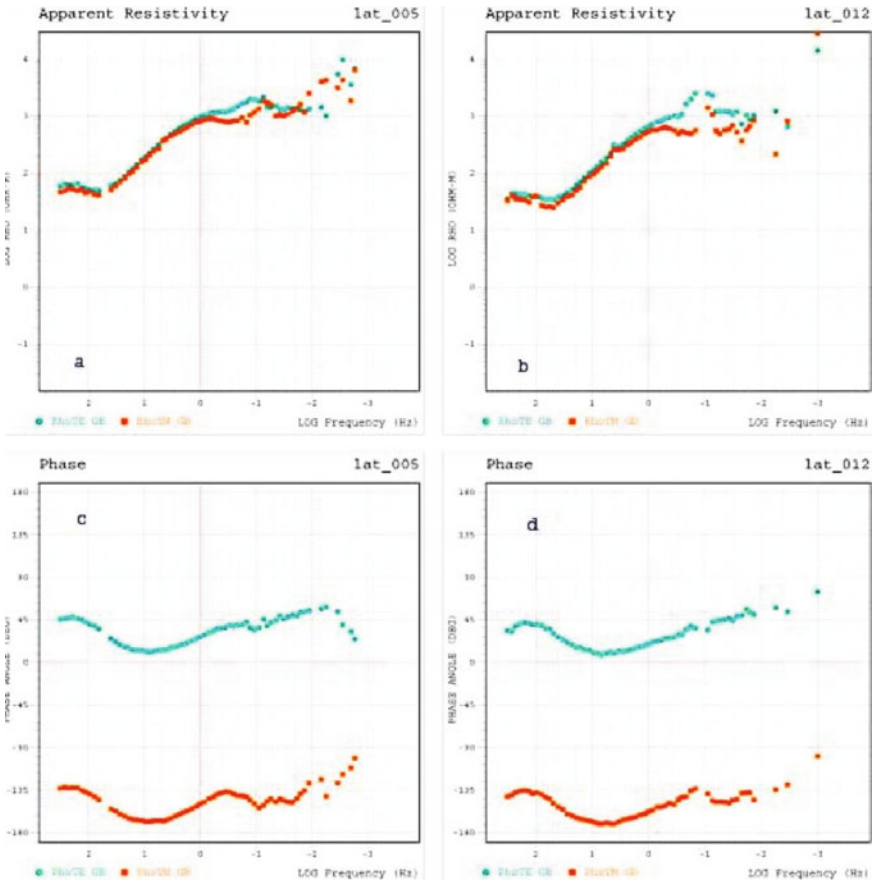

Figure 6.39a-d. An example of MT sounding curves of the apparent resistivity (and phase) vs. frequency.

rotated impedance values). This property of the tensor impedance is utilized to determine the values of Z'XY and Z'YX—known as principal impedances. One of the principal impedance elements is either parallel (transverse electric, TE or E-polarization) or perpendicular (transverse magnetic, TM or H-polarization) to the strike of the structure or formation. The rotated data, with respect to the strike direction, are used to calculate the apparent resistivities (ρ_a) in the principal directions, i.e. parallel and perpendicular to the strike from

$$\rho_a(T) = 0.2\ T\ |Z'|^2$$

where T is the time period and Z' is the subsurface impedance of the stratified Earth either in TE or TM mode. After calculating the apparent resistivities, the data are presented as MT sounding curves by plotting apparent resistivity values versus time period and apparent resistivity versus phase. Examples of frequency

versus resistivity, and frequency versus phase curves at a site in two different directions (both for raw and rotated data) are shown in Figs. 6.39a-d.

V. MT Data Interpretation

Based on various Earth response functions obtained from processed data like skew, tipper, induction arrows and polar diagrams, the data are analyzed for dimensionality (1D/2D/3D) and directionality of the subsurface conductors. Before modelling or inverting MT data, it is vital to understand its dimensionality. Tensor decomposition is a common approach and determines well the measured MT impedance data fit to a 2D geoelectric model and gives an estimate of the geoelectric strike direction. Once the dimensionality is understood, and distortion for static shifts addressed, MT can be forward modelled or inverted in 1D, 2D or 3D to recover a model of subsurface electrical conductivity. Thus, analysis of MT signals yields apparent resistivity, and phase as a function of frequency. The interpretation involves deducing subsurface geometry from quantitatively interpreting true resistivities, depths of geoelectric layers and postulating the possible geological structures. The basic technique of MT interpretation involves comparing field results with those obtained from computed models.

6.19 PRINCIPLE OF MT METHOD AND ITS UTILITY

The MT method involves a comparison of the amplitudes and phases of the electric and magnetic fields associated with the telluric currents. It can be shown that the surface electric and magnetic fields E and H respectively are horizontal and orthogonal. Their amplitudes are related by

$$\rho = 0.2\, T\, |E/H|^2$$

where ρ is in ohm-m, E in mV/km and H in nT. Their phases differ by $\pi/4$, H lagging behind E. If, then, E and H are measured at a definite frequency, the first indication of the non-homogeneity of the Earth is that the phase difference θ will not be $\pi/4$. Secondly, ρ calculated from measurements at different frequencies is the same. However, apparent resistivity ρ_a can always be defined by the above equation. On determining ρ_a and θ as functions of frequency by actual measurements, MT sounding curve analogous to electrical resistivity sounding curve is obtained.

GDS and MT are considered to be two complementary geophysical methods. The former has a better lateral (horizontal) resolution, while the latter has a better vertical resolution. For some years now, MT measurements have added substantial information to that gleaned from GDS observations. For example, MT soundings conducted along the foothills of Kumaon Himalayas have not only confirmed the presence of the trans-Himalayan conductor (Figs 6.32 and 6.33) postulated by GDS, but also provided support to earlier estimates

of its depth and lateral extent. The effectiveness of MT data to provide constraints on the tectonic configuration under study increases on synthesizing its information with gravity, seismic wave velocity and heat flow data.

While the theoretical aspects of MT method are dealt with exhaustively, there are scanty publications on practical applications from the subcontinent. Now however more and more scientists and organizations are planning to put this technique to enhance its practical use. Furthermore, efforts are on to compile all the available 'Indian' EM data generated so far to derive a comprehensive electrical conductance model to demarcate thermally favourable zones of hydrocarbon deposits and to provide a better insight into the seismic pattern of the region.

A few more EM induction methodologies are: (i) audio-frequency magnetic field (AFMAG) or audio-frequency MT (AMT) based on measurement of natural magnetic field originating in thunder storms at frequency 100–500 Hz. The method is said to be useful to explore large deep seated conductive zones, faults, shear zones, and water bearing fissures of appreciable extent and (ii) very low frequency EM method (VLFEM) which utilizes EM fields in the range 15–25 Hz radiated by powerful radio stations meant for military communications.

6.20 APPLICATIONS OF MT IN GEOPHYSICAL PROSPECTING

In geophysical prospecting, MT is used in a very large frequency range, which corresponds to a depth interval from the surface to some hundred kms. The aim of the exploration varies according to depth. The method is widely used in Russia, and has been developed further in USA, Canada, and Germany. In India, MT studies were initiated in 1984 with the procurement of a conventional band (4 to 4096 sec) MT system; presently the Indian geoscientists are working with three wide band (300 to 0.002 Hz) MT systems.

Analysis of the MT signals yields the apparent resistivities, phases and various other parameters as a function of frequency. These data are interpreted into a geoelectric section of the subsurface from which inferences are drawn regarding the geoelectrical structures. The main applications of the MT method are in the evaluation of large sedimentary basin and Earth deep interior. It is a complement and often as alternative to seismic method. The results presented here come from MT measurements made on various geological and tectonic settings, such as the Deccan traps, Vindhyan and Siwalik sedimentary regions, Precambrian crust of Rajasthan and Dharwar, the Himalayas, etc. These campaigns (Fig. 6.40) yielded some major findings, not amenable for studies with other techniques.

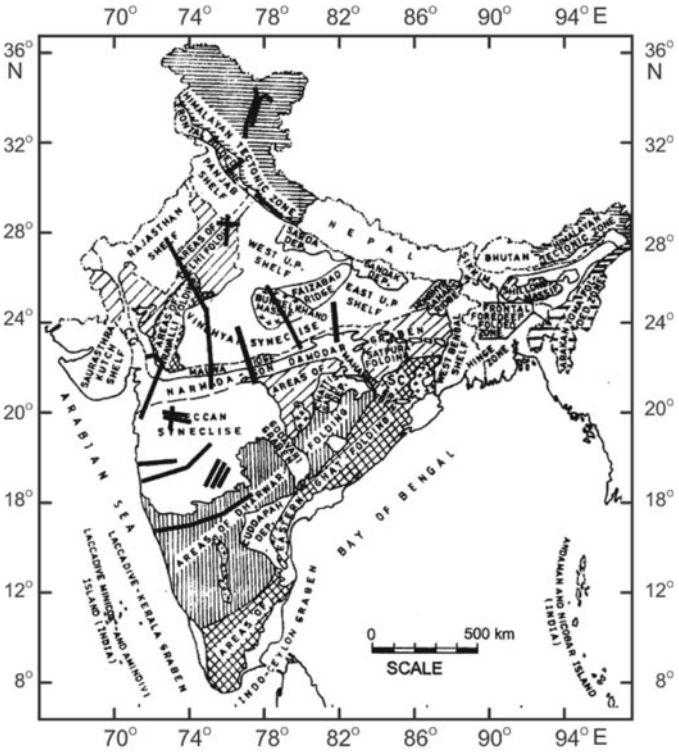

Figure 6.40. Geological map of India showing locations of the MT profiles over the period 1984-2003 (Gokarn, 2003).

I. Geoelectrical Structure below the Dharwar Craton

From studies on granite-greenstone formations over Dharwar craton, a shallow and deep sections (Figs 6.41 and 6.42) of the geoelectric structure are inferred that constitute a high resistive (2000 ohm-m) upper crust and a deep crustal conductor (DCC) between the depths of 5 and 25 km. Variations in Bouguer gravity are attributed to the undulations of DCC. From joint analysis of MT and seismic data, an anticline is delineated in the region of Closepet granite. However, the Closepet granite, which is assumed to be a major crustal divide, has only a weak signature in the geoelectric cross-section.

II. Electrical Conductivity Image from Seismic Regions of West and Central India

A conducting fluid filled ductile layer is identified in the depth range of 10 to 17 km in the earthquake-affected region of Bhuj. It is conjectured that this ductile layer prevented accumulation of stress within this section of crust, leading to earthquake hypocentres being concentrated either in the brittle upper crust above or in the lower crust below this conducting layer. Indications are obtained regarding the prevalence of compressional tectonics regime prior to

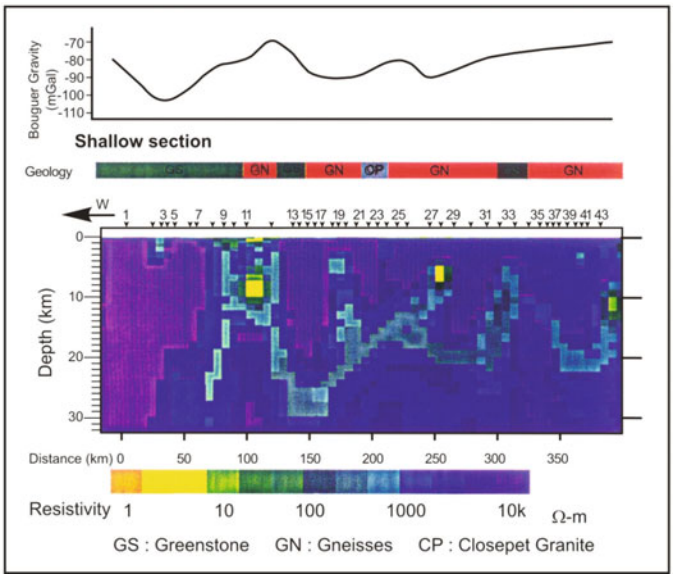

Figure 6.41. Shallow crustal structure in the Goa-Raichur region. Also shown are the Bouguer gravity variations along the MT sounding profile. The geology along the profile is also shown on the top of the crustal section (Gokarn, 2003).

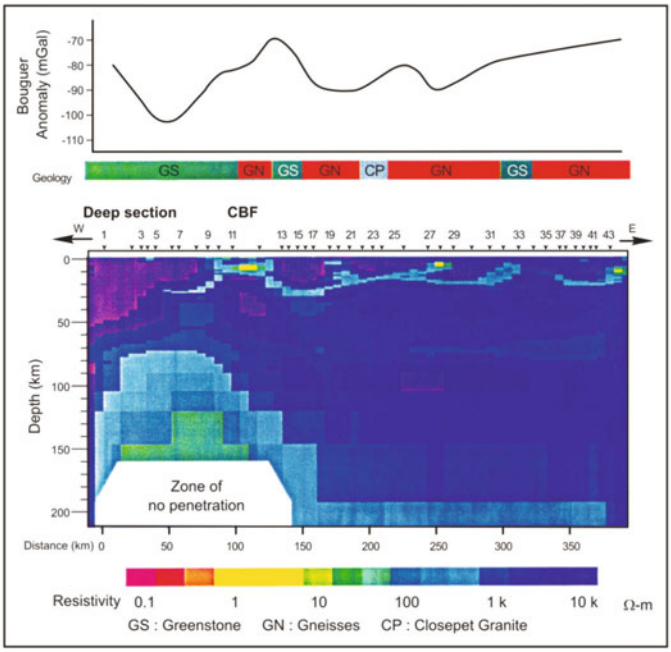

Figure 6.42. Deep section of the geoelectric model over the Goa-Raichur profile. The important geological units along the survey profile and the Bouguer gravity along the profile are shown on the top (Gokarn, 2003).

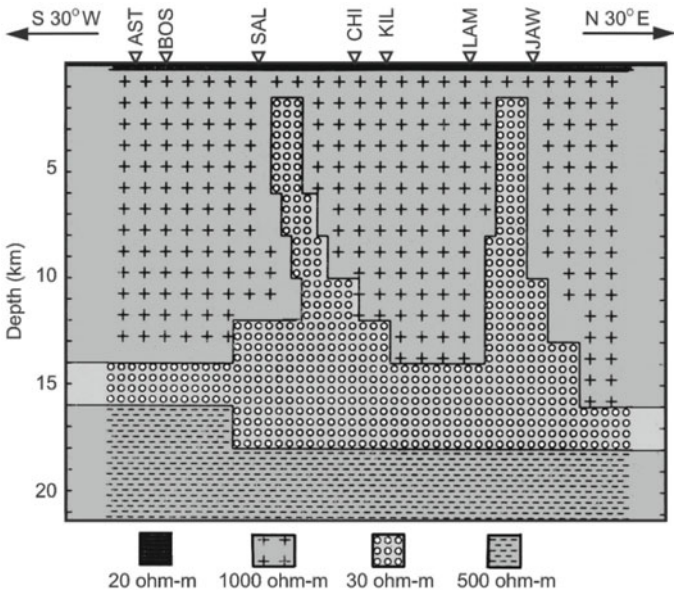

Figure 6.43. MT data were collected at seven stations along a linear profile of ~100 km across a part of Kurduvadi rift. 1D analysis revealed a four-layered conductive structure in the region surveyed. AST -Astha, BOS - Bosga, SAL- Salegaon, CHI - Chincholi, KIL - Killari, LAM - Lamjana and JAW - Jawli (Gokarn et al., 1992).

Deccan volcanism near Nasik, and conversely an extensional tectonic regime around Koyna. At Koyna, existence of a resistive block has been suggested in vicinity of the epicentre of the earthquake that rocked it in 1967. MT has also revealed a mid-crustal conductor across the Kurduvadi rift in Solapur region (Fig. 6.43) at a depth of 15 to 20 km at the Concord discontinuity, allowing interpreting the gravity low in this area to be not due to a rift-type structure but rather due to undulations in the crustal thickness. MT campaigns have delineated NW-SE trending high conductivity (100 ohm-m) structure at a depth of 60 km below the Panvel flexure (Fig. 6.44). This flexure extends to south and goes beneath the Dharwar craton and has been attributed to the passage of Indian plate over the Reunion hot spot (Fig. 6.34)

A lower crustal intrusive body that rises from below Jabalpur to shallow depths of ~2.4 km is dentified. This study is important in terms of understanding the cause of recent earthquake that occurred on 22 May 1997 with a magnitude of 6.0 on the Richter scale. The epicentre of this earthquake is located 20 km SE of Jabalpur. Furthermore, MT studies have yielded a strong lateral resistivity contrast (Fig. 6.45) near the great boundary fault along the Kota-Kekri profile and also similar formations in the Katangi-Jabalpur region separating the Precambrian upper and lower Vindhyan sediments on the north and the Deccan basalts on the south as well as other regions south of Mandla. A 10 km thick conductive layer of oceanic crust is also identified along a 400 km long profile in the NW Rajasthan shield area.

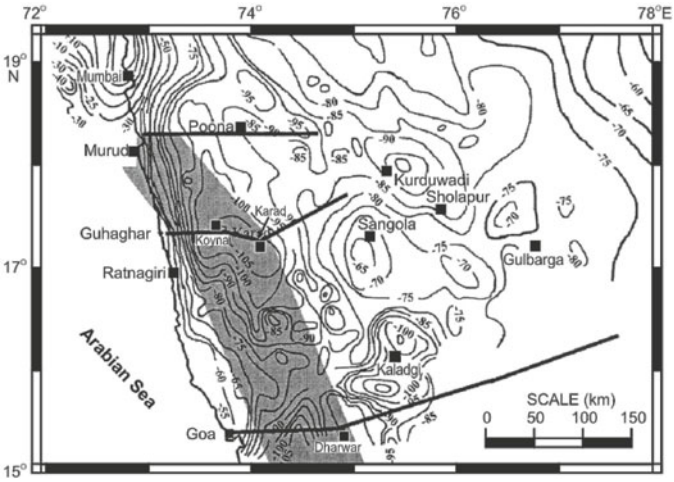

Figure 6.44. The Deccan trap volcanic region is experiencing mild to severe seismicity, necessitating its investigation at several closely-spaced sites in this region. The low resistivity feature in the lithospheric mantle is the shaded portion, superimposed over the Bouguer gravity map of the Deccan volcanic province and the northern part of the Dharwar craton.

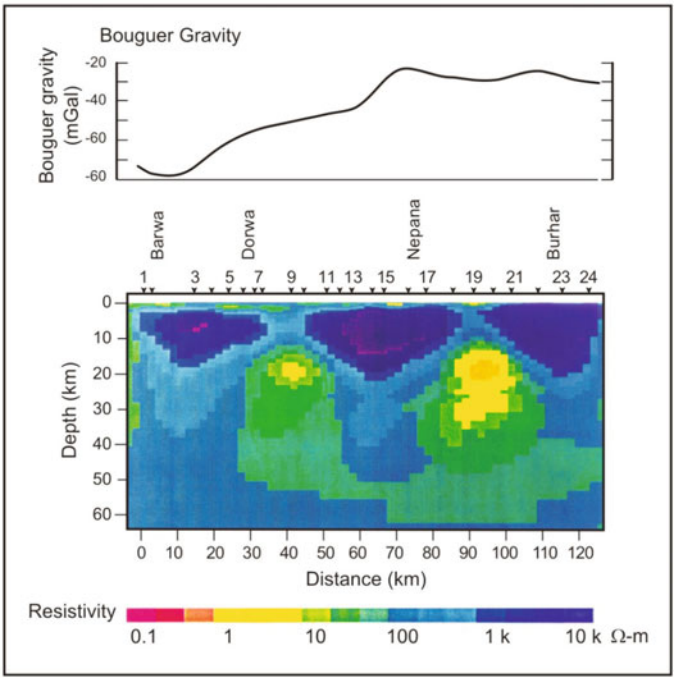

Figure 6.45. Deep geoelectric structure in the Satpura region. The Bouguer gravity variation is shown on the top of this figure (Gokarn, 2003).

III. Electrical Image of Siwalik Sediments

Thickness of Siwalik sediments is ascertained over 150 km long profile in the Mohand-Ramnagar region. This geoelectric structure is predominantly four

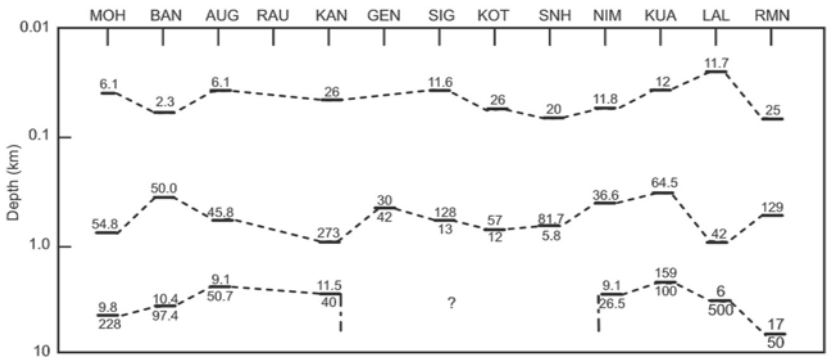

Figure 6.46. MT data were collected at 13 stations along a ~100 km long linear profile in the Mohand-Ramnagar region. 1D analysis showed a four-layered geoelectric cross-section at different sites. Note the break in the delineation of resistive basement between stations GEN and SNH, broadly coinciding with the width of the THC identified by GDS. MOH - Mohand, BAN - Bandarjudh, AUG - Aurangabad, RAU - Rauli, KAN - Kangri, GEN - Gendikhata, SIG - Siggadi, KOT - Kotdwar, SNH - Sanch, NIM - Nimgot, KUA - Kuakhera, LAL - Laldhang and RMN - Ramnagar (Gupta et al., 1994).

layered (Fig. 6.46) and is explained by presence of three layers of sediment overlying the resistive basement. The top layer (50 m thick) is due to the alluvial and post-Siwalik sediments deposited over a more resistive upper Siwalik layer with a thickness of 700-1000 m. The third layer is ~3 to 4 km thick and is believed to be of middle and lower Siwaliks. The resistive basement is delineated below the middle and lower Siwaliks at depths of 5 to 8 km from the surface.

IV. Transects along the Himalayan Collision Belt

In NW Himalaya, MT deep sounding studies are carried out to obtain information on the position and structure of deep crustal blocks over the Himalayan collision belt under the HimProbe project, as part of deep continental studies. Two high resistive blocks of Ladakh and Chushul batholiths (Figs 6.47 and 6.48) with a depth extent of 12 km are delineated to the north of Indus Tsangpo suture (ITS) zone. A vertical low resistivity zone (500 ohm-m) demarcates the Ladakh and Chushul batholiths.

The use of MT as a tool for geoexploration is on the rise because of its many advantages: a number of national and international groups are using this technique to explore various geological and tectonic settings, not amenable with other techniques. In fact, Indian scientists have already ventured into the Himalayan collision belt, where topographic effects are rather strong. Recently, MT studies were conducted in the syntaxial belt of NE Himalayan region and

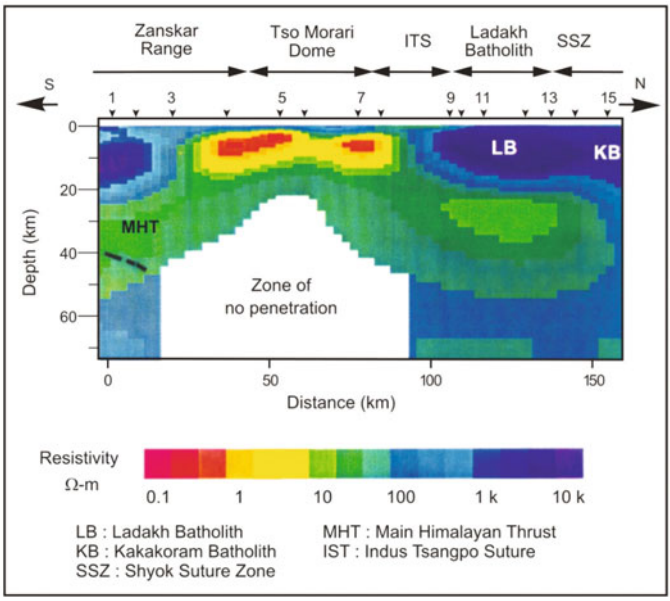

Figure 6.47. Geoelectric structure over the Bara la Cha la Panamic profile. The major structural features are marked on the top part of the figure (Gokarn, 2003).

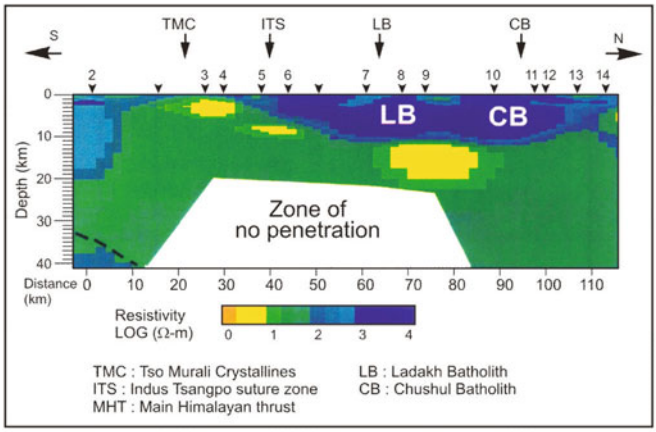

Figure 6.48. Geoelectric structure over the Pang-Phobrang profile. The major structural blocks are marked on the top of the figure (Gokarn, 2003).

also in Andaman Nicobar islands. Also a major thrust is needed towards understanding the complex nature of crust below the Vindhyan sediments and a complex pattern of rift valleys prevalent in the basement below the Deccan basalts. Precambrian tectonics and crustal evolutionary processes will also be carried out by MT technique.

6.21 EARTHQUAKES: CAUSATIVES AND MEASUREMENTS

Earthquakes are the outward manifestation of Earth's internal dynamism and occur where tectonic deformations are active, i.e. mainly along the boundaries of mobile crustal blocks, where portions of the crust are either scraped or generated or destroyed. They also occur, when fluvial migrations leave behind a hollow.

All the current hypotheses acknowledge that when stress exceeds the material strength of crustal rocks, a fracture occurs across the weak planes releasing large amount of accumulated strain energy. The release can be in almost one go or in successive stages through the violent breaking of rocks. This energy travels through Earth in the form of vibrations called seismic waves consisting of P (primary), S (secondary/shear/transverse) and surface (Love/ Rayleigh) waves (for their characteristic features, refer to Chapter 2). Seismic waves move out from the focus (the place where the rupture begins) of the earthquake in all directions. The intensity and position of earthquakes, seismicity (frequency of earthquakes) of an area, type of fault in the rocks and the velocity of the waves (mainly P (Vp) and S (Vs) waves) in different rocks, reveal different properties of the Earth (Chapter 2). Surprisingly, people on the surface feel tremors, but those in caves in the same area do not. This is because ground motions on the surface are induced by Rayleigh waves, which are seldom felt below 65 m depth. The great 1934 Bihar earthquake brought disaster to coal mines due to wrenching along fault planes. Thus, caves and mines are wholly not immune to earthquakes. It is generally accepted, ground motion decreases with depth during an earthquake.

Changes in crustal stress are seen to precede as well as occur simultaneously with earthquakes. Magnetic properties of crustal rocks are sensitive to stress and this leads to the possibility of monitoring it using magnetic measurements. Local changes in geomagnetic field due to any kind of tectonic activity are termed 'tectonomagnetism' and the study which specifically relates to earthquakes is called 'seismomagnetics'. Location of faults and their extent is deciphered on sharp magnetization and resistivity contrasts in subsurface layers. The prediction is done through analyzing changes in the intensity of magnetization and resistivity that follows an earthquake cycle.

Seismic activity prevalent across the Indian subcontinent is attributed to underthrusting of Indian plate below the Eurasian plate, although convergence is considered as not the sole process responsible for its seismicity. Seismic studies were earlier concentrated in Himalayas to the exclusion of the stable peninsular shield, which is also regularly shaken by violent Earth tremors at Koyna, Latur, Jabalpur and Bhuj. According to plate tectonics, seismic energy dissipates only along the plate boundaries. Since neotectonic movements are leading to catastrophic earthquakes in the peninsular region, installation of wide band sensitive seismographs (instrument recording ground motion) in a

closer grid within critical areas (Fig. 6.60) is being made a priority. Also, integrated geological and geophysical investigations are carried out to supplement seismic studies. This will help in carrying out large scale structural and deformational studies as well as mapping the stress accumulation and release phenomenon (Fig. 6.49) occurring in the Indian plate.

Seismic deformation: A fault rupturing causes two types of deformations (strain)— static and dynamic. Static deformation, unlike dynamic, is permanent displacement of ground due to a rupture event. The earthquake cycle progresses from a fault that is not under stress to a stressed one, as tectonic motions driving the fault slowly proceed to split during an earthquake and form a newly relaxed but deformed state fault (Fig. 6.49)

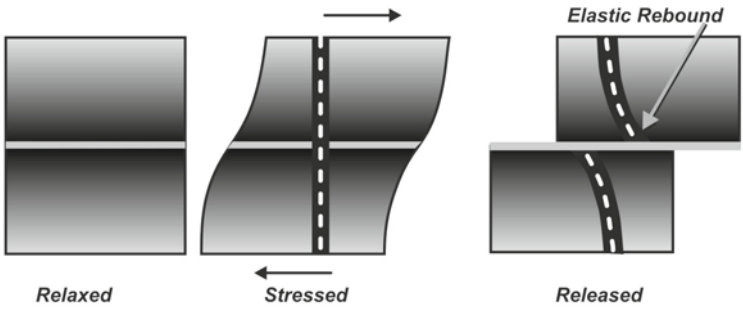

Figure 6.49. Simplified schematic representation of a fault rupture.

Richter Magnitude

The magnitude (M) of an earthquake, represented by Richter scale (RS), is a measure of the amplitude of the largest seismic wave recorded at the time of an earthquake and the amount of energy released. It calculates the strength of an earthquake from seismograph data. The dynamic and transient seismic waves released by any earthquake propagate throughout the globe, and are recorded by sensitive detectors. Nuclear test-ban treaties, in effect, rely on the ability to sense underground nuclear explosions equivalent to an earthquake of magnitude 3.5 (M3.5) on Richter scale.

In early twentieth century, earthquake intensity was measured on a 12-point scale devised by Guiseppe Mercalli. This scale was later modified and called the modified Mercalli (MM) scale. In 1935, Charles Richter, after analyzing data of earthquakes in southern California, proposed an alternative scale, where each point corresponded to 10 times the intensity or 30 times the energy. The MM scale with 12-divisions of intensity is based on the amount of damage caused to various types of structures. The RS has 8-divisions of magnitude, and allows making more uniform comparison of quakes world over. In this scale, the amplitude of the surface waves is measured on a standard instrument called the Wood-Anderson type seismograph.

Under Richter scale, earthquakes M<3 are called microquakes, which are not even felt by people living in the area and are detected only by sensitive seismographs. Earthquakes of M4 can be detected globally and stack up to thousands everyday. Up to M5 are moderate quakes, while M7 are major, and those of M8 or more are the great quakes. The Richter scale has no upper limit (it is open ended), but the largest known quakes fall in magnitude range of 9.0 to 9.5. Earthquakes with M9 and higher, are not possible on RS because rocks are not sufficiently strong to store energy without breaking at higher stress.

Though Richter proposed the 'logarithmic' scale (where the difference between the values of successive points keep increasing), others too have contributed to its refinement. Gutenberg proposed an alternate method in which he used 'body waves', unlike the 'surface waves' utilized by Richter. Actually, the difference in the reported magnitude of earthquake (by different agencies, institutions and countries) arises due to different measurement methods used. For example, the US, Japanese and many other countries use 'surface' waves (M_s mode) for large earthquakes, while it is a common practice to make use of 'body' waves (m_b mode) at large (teleseismic) distances. Thus, magnitudes differ when the method of calculation alters. Magnitudes calculated in the 'local' mode (M_L) are quite different than those calculated in the M_s mode or the M_w mode (moment magnitude). Apart from different methods of measurement, there are also different units in circulation like 'intensity', 'magnitude' and 'energy'. There are several relationships connecting different types of seismic magnitudes. Few of them are well calibrated and therefore universally standardized based on which it is possible to convert one type of magnitude into the other depending on the requirement. A generalized expression for determining magnitude is given by the following empirical equation:

$$M = \log (A/T) + xf(\Delta, h) + y$$

where A is maximum amplitude of a wave in microns, T – wave period in seconds, Δ – distance from the point of measurement of signal amplitude at observing station to the epicentre, in degrees of an arc of meridian (great circle arc), h – focal depth in kilometers, x and y – constants determined empirically and f is the function obtained through study of empirical and theoretical results.

The magnitude scale patterned after the RS is logarithmic and measures the energy (E) released by earthquakes in ergs. Its relation with the magnitude of earthquakes is expressed by the formula: $\log E = 12.24 + 1.44\ M$ for M>5. The use of the scale is explained in Table 6.3 that compares magnitude to the seismic energy yield released in terms of TNT explosive equivalent. For example, the M8.4 Bihar earthquake of 1934 is calculated to have released 2.04×10^{25} ergs of energy, while 1952 Assam quake of M8.7 released an energy equivalent to ~6,000 times that of the atom bomb dropped over Hiroshima. For every unit of increase in magnitude on the RS, there is roughly a 30 fold increase in the energy released by an earthquake. For instance, an M2 earthquake releases 30 times more energy than an M1 earthquake. On the same scale, the

Table 6.3 Richter scale used to compare magnitude with seismic energy yield

Magnitude	*Amount of TNT for energy yield*	*Example (approximate)*
-0.5	6 ounces	Breaking a rock on a lab table
1.0	30 pounds	Large blast at a construction
1.5	320 pounds	-
2.0	1 ton	Large quarry or mine blast
2.5	4.6 tons	-
3.0	29 tons	-
3.5	73 tons	-
4.0	1,000 tons	Small nuclear weapon
4.5	5,100 tons	Average tornado
5.0	32,000 tons	-
5.5	80,000 tons	Little skull mountain
6.0	1 million tons	Double spring flat
6.5	5 million tons	Northridge
7.0	32 million tons	Ryogo-Ken Nanbu
7.5	160 million tons	Landers, California, quake, 1992
8.0	1 billion tons	San Francisco, California, quake, 1992
9.0	5 billion tons	Anchorage, Alaska, quake, 1964
9.5	32 billion tons	Chilean quake, 1960
10.0*	1 trillion tons	San Andreas-type fault circling the Earth
12.0*	160 trillion tons	Fault dividing Earth in half through centre, or Earth's daily receipt of solar energy

* Hypothetical examples

ratio of the energy released between earthquakes of magnitudes M3/M1 is 900 times (30×30).

6.22 MAJOR EARTHQUAKES OF THE WORLD AND INDIA

The earliest earthquake recorded in a catalog occurred in China in 1177 BC, which has description of several dozen large earthquakes from then onwards. Earthquakes in Europe find mention as early as in 580 BC, but the one for which some description is available, occurred in the mid sixteenth century. The earliest known earthquakes occurred in Mexico were in the late fourteenth century and in Peru in 1471. The descriptions of the effects, however, are not well documented for any of these quakes. By seventeenth century, depictions of the effects of earthquakes, exaggerated or distorted, were published around the world (Fig. 6.50).

Earthquake prone areas of the Indian subcontinent: Indian subcontinent is replete with seismic prone areas (Fig. 6.51, Appendix 6.4), the most well known being the Himalayan region, which is a part of worldwide zone of earthquakes running from the Alpine belt through Indonesia, Mynamar, Himalaya (of India,

Date	Place	Magnitude	Deaths	Date	Place	Magnitude	Deaths
① Apr 4, 1905	Kangra, India	8.6	19,000	⑫ Dec 26, 1939	Erzincan, Turkey	7.8	30,000
② Aug 17,1906	Valparalso, Chile	8.2	20,000	⑬ Oct 5, 1948	Ashgabat, Turkey	7.3	110,000
③ Dec 28, 1908	Messina, Italy	7.2	100,000*	⑭ May 31, 1976	Peru	7.9	66,000
④ Jan 13, 1915	Avezzano, Italy	7.5	29,980	⑮ Feb 4, 1976	Guatemala	7.5	23,000
⑤ Dec 16, 1920	Gansu, China	7.8	200,000	⑯ Jul 27, 1988	Tangshan, China	7.5	655,000*
⑥ Sep 1, 1923	Kanto, Japan	7.9	143,000	⑰ Dec 7, 1988	Spitak, Armenia	6.8	25,000
⑦ May 22, 1927	Tsinghai, China	7.9	200,000	⑱ Sep 29, 1993	Latur, India	6.2	9,748
⑧ Dec 25, 1932	Gansu, China	7.6	70,000	⑲ Jan 26, 2001	Gujarat, India	7.7	20,023
⑨ Jan 15, 1934	Bihar, India	8.1	10,700	⑳ Dec 26, 2003	Bam, Iran	6.6	26,200
⑩ May 25, 1935	Quetta, Pakistan	7.5	60,000*	㉑ Dec 26, 2004	Sumatra, Indonesia	9.0	283,106**
⑪ Jan 25, 1939	Chiltan, Chile	8.3	28,000	㉒ Oct 8, 2005	Muzaffarabad (PoK)	7.8	N.A.

How many earthquakes occur worldwide each year? **Estimated* *** Including deaths from Tsunami*

Description	Great	Major	Strong	Moderate	Light	Minor	Very Minor
Magnitude	8 & higher	7 - 7.9	6 - 6.9	5 - 5.9	4 - 4.9	3 -3.9	2 - 2.9
Annual Average	1	17	134	1319	13,000 *(Estimated)*	130,000 *(Estimated)*	1,300,000 *(Estimated)*

Source : The United States Geological Survey

Figure 6.50. Map of the world showing the locations and the time of the known major earthquake occurrences (http://earthquake.usgs.gov/earthquakes/world/historical.php/).

Nepal, Tibet, China), Afghanistan, Iran and Turkey to the Mediterranean Sea. This belt has been the seat of great many earthquakes in the past resulting in massive destruction. Peninsular shield made of Dharwar, Aravalli and Singhbhum protocontinents was considered seismically less hazardous. Yet the disastrous earthquakes at Koyna (1967, M_w= 6.3), Killari (1993, M_w= 6.1), Jabalpur (1999, M_w= 5.8) and Bhuj (2001, M_w= 7.7) disprove this myth. The intra-plate earthquakes, unlike the plate boundary shakings, are less frequent but kill more people. Reservoir induced seismicity (RIS) caused the Koyna quake, but the 1819 Rann of Kutch earthquake (M~8.0) was due to intra-plate events that produced a surface scarp of ~100 km long. During 35 years between 1963 and 1998, Koyna and its adjoining areas have faced 102,715 tremors, of which 79 were above M4.0, and seven were above M5.0. Seismologists

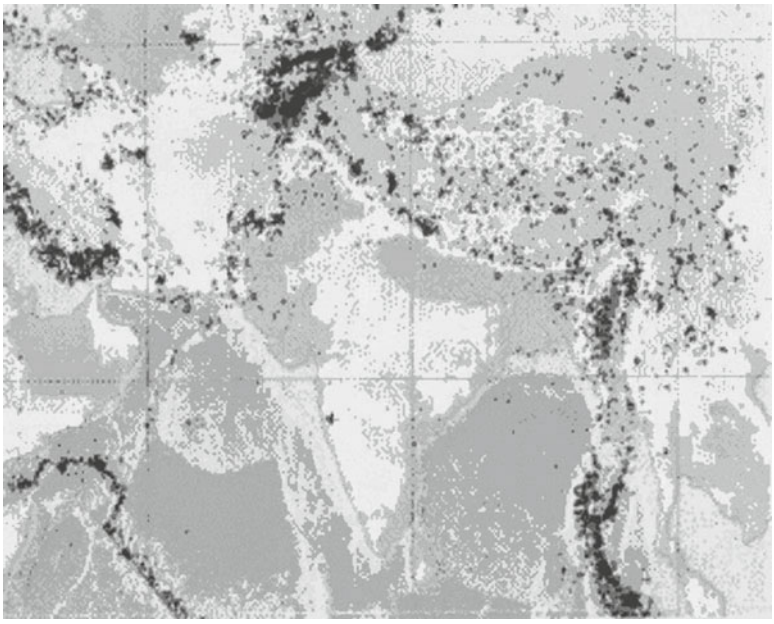

Figure 6.51. Seismotectonism of the Indian subcontinent. Note the seismic prone areas in the subcontinent; the most well known being the Himalayan region, which is a part of worldwide zone of earthquakes running from the Alpine belt through Indonesia, Mynamar, Himalaya (of India, Nepal, Tibet, China), Afghanistan, Iran and Turkey to the Mediterranean Sea (http://www.cessind.org/ earthquakes_inindia.htm#eqindian).

conclude that Killari (Latur, M6.4) type of disasters can occur on discrete faults in regions generally presumed to be aseismic.

Data recorded at Indian and international permanent seismological observatories are analyzed to model the structure and tectonic setting of Indian subcontinent. For example, P and S wave analysis led to estimating seismic velocity structure below the Indian region. Tomographic analysis of tele-seismic P wave residuals over the Deccan trap and adjoining area revealed the existence of 600 km long and 350 km wide NS trending anomalous high-velocity zone (2 to 5% contrast) at a depth over 100 km. Also, focal depth, faulting mechanism and moment tensor estimations are made for several other earthquakes.

6.23 HIMALAYAN TECTONICS AND ITS EFFECT ON PENINSULA

Seismicity in the Himalayan belt is attributed to movements along the main boundary thrust (MBT) and main central thrust (MCT). The MBT is the intracrustal boundary along which the Indian plate is sliding down. In the Himalayan region, seismic activity largely results due to building up tectonic stress from continuous movements along the faults and thrust zones. The

Figure 6.52. Generalized schematic map of major rift zones of Indian subcontinent and their association with seismic activity. The seismicity in peninsular India is found mostly restricted mainly along NE-SW and NNW-SSE trending faults and fractures.

resultant pressure has upwarped the peninsula at many places, and reactivated ancient rifts (Fig. 6.52). The seismicity in peninsular India is found mostly restricted mainly along NE-SW and NNW-SSE trending faults and fractures. The Coimbatore earthquake in 1900 (M6) is attributed to a NNW-SSE fault. The Bhadrachalam earthquake of 1969 (M5.7) is thought to have been caused by movement along a graben fault. The earthquake that shook up Bharuch in 1970 was located at the intersection of the boundary faults of the Narmada and Sabarmati grabens. Movements along faults in a NNE-SSW direction delimiting the Aravalli ridge are considered to have given rise to earthquakes in the Delhi region. 1993 Latur earthquake occurred due to the rubbing together of landmasses on two sides of the 400 km long Kurduvadi rift having 40-60 km width and spreading from SE of Solapur and ending in the north of Pune (Fig. 6.52).

The Himalayan collision zone witnessed four great earthquakes (1897 Assam, 1905 Kangra, 1934 Bihar-Nepal and 1950 Assam) in a span of 53 years. The quantitative seismicity map of the Himalayan terrain shows high seismicity (M5-6) in the Kashmir valley, Doda in Jammu, Spiti, Nepal and Bhutan. Seismicity in the northern part of the Tibetan plateau and adjacent regions is attributed to strike-step movements along E-W trending transcurrent faults. The frequent moderate earthquakes and the infrequent great earthquakes suggest ongoing episodic slippage. These processes also imply future great earthquakes in the unruptured 'gaps' of the Himalayan front, with uncertainties attached to their recurrence interval. Recent destructive earthquakes from India are described below.

I. 1991 - Uttarkashi (Almora) Earthquake

The 1991 moderate Uttarkashi earthquake (M~6.5) attracted a lot of attention due to its proximity to the high Tehri dam in Garhwal Himalaya. The epicentre of the earthquake was found to lie in Almora, but the maximum damage to buildings and human life took place in Uttarkashi and Chamoli. This damage can be attributed to the incohesive condition of soils and the weak structure of buildings. This earthquake occurred because of slippage along the MCT, a major tectonic boundary, which also divides lesser Himalayan terrain in the south from the snow-clad mountains in the north. Some environmentalists fear that the construction of the Tehri dam across the Bhagirathi river may lead to reservoir induced seismicity. The fear is compounded by the fact that the area is normally prone to seismic activity. From the engineering point of view, it is considered that the proposed dam can withstand earthquakes with magnitude up to 7.2.

In 1995, a pair of telluric and resistivity sounding dipoles and PPM were set up at Rohtak and Jhajjer region (Haryana) to monitor the electric and magnetic precursors to earthquakes in parts of Garhwal Himalaya. Three ultra-low frequency (ULF) stations were also installed in 2001-2002 in Uttarkashi region in Garhwal Himalaya.

II. 1999 - Chamoli Earthquake

The Garhwal region was rocked by M6.8 earthquake on 29 March 1999. The main tremor was followed by after-shocks with magnitudes between 4.9 and 2.0. The focus of the earthquake lay at a depth of 30 km. The death toll and injury in and around Chamoli and Rudra Prayag were at least 100 and 300 people, respectively. The earthquake occurred in zone V in the inner Himalayas. Tremors were reported from adjoining Himachal Pradesh, Jammu and Kashmir, Haryana, Rajasthan and Delhi.

III. 1819 - Kutch Earthquake

The 1819 earthquake (M~8.0) at Kutch generated a 100 km long fault scarp, popularly known as Allah Bund, meaning the wall of God. Mapping the scarp morphology, trenching excavations near Allah Bund and developing age constraints are some of the studies in progress.

IV. 1967 - Koyna Reservoir Induced Seismicity

Seismicity associated with Koyna dam is one of the classic examples of reservoir induced seismicity, whose seismotectonics are governed by a large water load. Remarkable correlations are observed between seismicity and water filling cycles of Shivajinagar lake, Koyna. This is attributed to the pore pressure changes induced by the reservoir load, which reduces the strength of the rocks in the vicinity of the dam, leading to fault failure. Globally, Koyna is among

the four well documented RIS cases, where earthquakes in excess of M6.0 have been generated. An earthquake of M6.5, and many aftershocks of M>5, occurred at Koyna on 10 Dec 1967. There is an alternate theory. This earthquake might have resulted from Earth movement over a 10 km stretch long N10°E-S10°W trending fault below the Deccan traps. Because of this, the region is under tensional stress leading to record tremors of different magnitudes. Migration of seismic activity due south of the clustered Koyna events, is reported in recent studies.

V. 1993 - Latur Earthquake

The painful consequences of Killari earthquake felt over ~110 sq km area in the Latur and Osmanabad, Maharashtra are highlighted by the loss of 10,000 lives and several razed villages. The M6.3 Latur earthquake of 30 Sept 1993 is the world's most devastating stable continental region (SCR) earthquake, whose epicentre lies in an aseismic region. After the earthquake, several fractures in the ground are observed (Fig. 6.53), and high concentration of helium over the fractures is also detected. With a shallow focal depth of <10 km, this earthquake is similar to other moderate events in the Australian and Canadian shields. The repeat time of moderate SCR earthquakes is at the order of hundreds and thousands of years. Lack of historical documentation makes their strikes a total and unexpected surprise. Latur event gave a new perspective and urgency to initiate seismic hazard assessment in peninsular India leading to strengthening of seismic networks and upgradation of several existing facilities.

Figure 6.53. The Latur earthquake generated a surface rupture that was traceable for about 2 km. The maximum height of the scarp observed near Killari was about one metre (http://www.cessind.org/ earthquakes_inindia.htm#eqlatur).

VI. 1997 - Jabalpur Earthquake

The M6.0 earthquake of 22 May 1997 at Jabalpur was recorded by newly installed broadband digital stations in the shield region. This earthquake not just caused widespread devastation, but also generated great deal of data helping to understand the response of various types of residential and commercial structures to seismic waves. This offered valuable guideline in the design and construction of earthquake resistant buildings. Later, tectonomagnetic studies were initiated in areas adjoining Jabalpur. Figure 6.54a shows the layout map of ground geomagnetic repeat surveys undertaken using PPM. Repeated yearly surveys of 2003 to 2007 show secular changes in total geomagnetic fields concentrating locally (Fig. 6.54b). It also shows the anomalous geomagnetic field SVs in a range of ±0.06 to ±9.54 nT at separate stations across the profiles. These SV are related to anomalous accumulation of tectonic stresses, and tensions on the fault zones and crustal blocks due to recent geodynamic processes along the NSL.

VII. 2001 - Bhuj Earthquake

The Bhuj earthquake (M~7.7) in Gujarat that occurred on 26 Jan 2001 is historically the most catastrophic, whose epicentre is located 20 km NE of Bhuj (Fig. 6.55a). Seismic data from an aftershock array suggested south dipping thrust with a surface projection at ~23.8°N, near the central Rann of Kutch. Aftershocks were unusually deep (up to 30 km). The earthquake severed the lithosphere leaving ~20,000 people dead and ~200,000 injured. Nearly 400,000 houses were destroyed and twice as much damaged. Although damages of such proportion were astonishing, the occurrence of the event itself was not surprising, considering the geologic and seismic history of the region. The

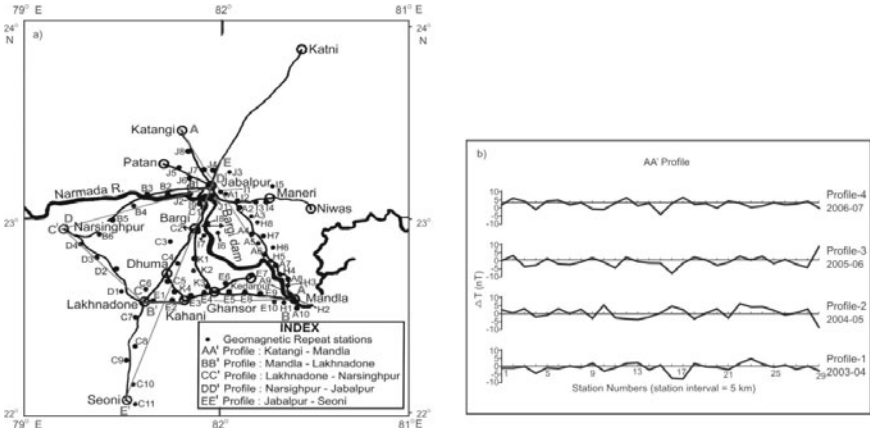

Figure 6.54. (a) Layout map of Jabalpur repeat survey. (b) Secular change of the geomagnetic field T along AA' profile in (a) (Waghmare et al., 2008).

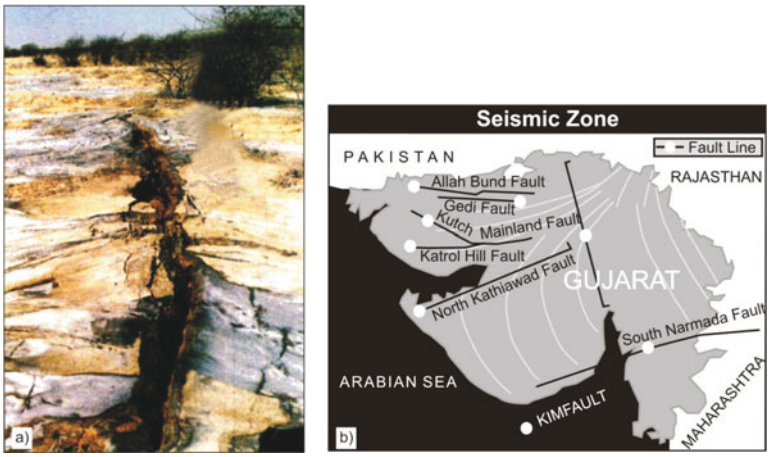

Figure 6.55. (a) The crack at Dhang-Godai village near the epicentre. (b) Simplified criss-cross faults within Gujarat exposing it to seismic activity.

Kutch forms a part of Mesozoic rift system and has been noted for occurrence of large earthquakes since historic times. For example, this area has been experiencing above normal levels of microseismicity throughout the past 200 years, and probably for many more millenia. Damaging earthquakes occurred in 1845, 1846, 1856, 1857, 1869 and 1956 in the same general region as the 1819 and 2001 earthquakes.

After the 2001 major quake, a substantial increase in tremors is seen since Gujarat is located over the south Narmada fault and attributed to its reactivation. Apart from this fault, there are scores of other major fault systems in Gujarat making the region extremely vulnerable to seismic activity (Fig. 6.55b).

6.24 SEISMIC ZONATION MAPS AND SEISMIC HAZARDS

Seismic zonation map (Fig. 6.56) is a guide to the seismic status of the region and its susceptibility to earthquakes. The Bureau of Indian Standards introduced the seismic zoning concept in 1962, and revised it from time to time on the basis of accumulating seismic data. India was earlier divided into five zones with respect to severity of earthquakes, but in the latest version these have been scaled down to just four with zone I getting the axe. Each seismic zone corresponds to a particular 'seismic coefficient' that has to be incorporated in the design of large civil engineering structures. According to the 'seismic gap' theory, the 2400 km long seismic belt of the Himalayas is divided into three major segments (Fig. 6.56b). Future earthquake shocks are likely in the gaps. Unfortunately, the Tehri dam is located on the longest stretch (300 km, between Hardwar and Tanakpur). The validity of the seismic gap theory is questioned, since it is based on circum-Pacific belt, which cannot be applied to the Himalayan terrain. In the circum-Pacific area, continental plates interact with

oceanic plates, but the Himalayan terrain occupies continent-continent collision zone.

Of all the seismic zones, zone V is seismically the most active where earthquakes of M8 or more can occur. In case of shield type earthquakes, historic data are insufficient to plug them in higher zones because their recurrence intervals are much longer than the recorded human history. This gives a false sense of security. Occurrence of the damaging earthquake at Latur, falling in zone I (according to old seismic zonation map) is a typical example of this situation.

However, within a single seismic zone not all structural faults and thrusts, and not even all elements of single fault, are identically active. Furthermore, in the task of preparing seismic zoning map of the region, which lends support to determining the long-term predictability of earthquakes, the structures of the zone in which tectonic stresses cause faults are often not considered. Physical basis of long-range earthquake occurrence patterns cannot be effective without elucidating the deep structures of seismically active regions. Therefore, the emphasis of geophysical research in these regions should be the study of crustal structures to a depth of several tens of km, discrimination of inhomogeneities in terms of structures and physical properties, clarifying their characteristics and distinguishing seismically active areas from relatively inactive ones.

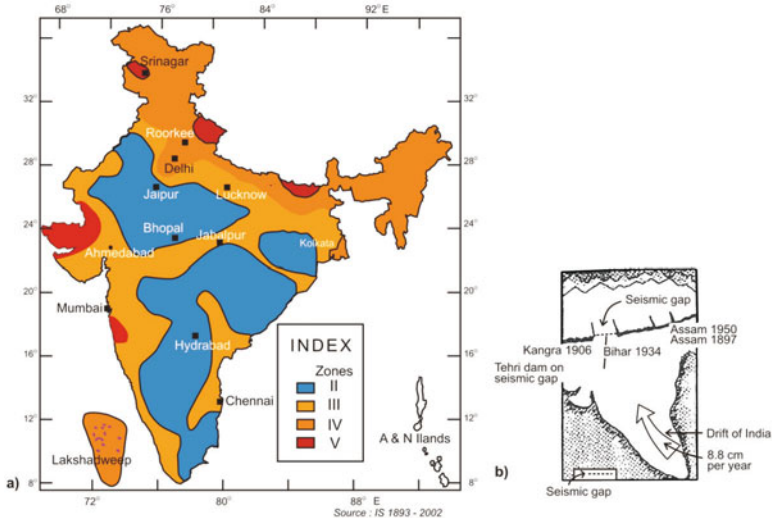

Figure 6.56. (a) Seismic zones of earthquake vulnerability in India at macro-level. Zone II to Zone V show increasing magnitude; Zone V is of the highest seismic intensity, zones IV and III are relatively of moderate damaging intensities for well built structures and dangerous for poor buildings and Zone II is light to minor shaking regions. Within the zones, earthquakes of more or less same intensity may be expected. (b) Himalayan seismic gap.
(http://www.earthscrust.org/earthscrust/science/transects/india.html)

Seismically active areas should intensively be monitored for stress induced changes effected in a host of physical parameters.

6.25 GEOPHYSICAL STUDIES IN SEISMICALLY ACTIVE REGIONS

Lack of geophysical data inhibits understanding into the subsurface linkages of tectonic features with the contemporary seismicity of the region. This necessitates examination of crust from its surficial levels to the lithospheric depths, for which gravity and magnetic (GDS, MT) investigations are recognized as effective tools. Thus, areas rocked by earthquakes are investigated by geological and geophysical (magnetic, GDS and MT) methods for evaluating their long-term seismicity.

GDS and MT can probe the deep interior. They are quick, inexpensive and used as proxy tools to explain spatial-depth distribution of seismicity, identifying zones of strain accumulation, layering, and for constraining tectonic evolution model. These techniques map zones of sharp conductivity contrast associated with fault planes, whose depth and dimension are estimated later on. For example, the noted correlation between mapped structures by GDS, OBM and MT, and high seismicity underlines the role of fluids in current tectonic processes. For instance, consideration of space-time pattern in seismicity in relation with high conductive zone helps infer the nature of electrical conductivity distribution. This can be a sensitive pointer towards the reactivation of subsurface structures that lead to earthquakes. This subsurface structural mapping provides better insight into the seismicity pattern and cycles of stress accumulation and release in the Indian plate. Towards this end, two broadband seismic observatories are established at Rewa and Kolhapur. Few examples from regions in the Himalayas (Nazibabad-Satpuli profile and Trans-Himalayan conductor) and peninsular India are discussed below.

I. Nazibabad-Kotdwar-Satpuli Line

Spatial variation of magnetic field along Nazibabad-Kotdwar-Satpuli in the Himalayas is examined for earthquake precursory signals. Two pronounced anomalies associated with large susceptibility contrasts correlate with Amri thrust and Nayar fault (Fig. 6.57). The magnetic anomalies are explained in terms of intrusion of basic material along the thrust and associated fault plane.

II. Trans-Himalayan Conductor, NW India

GDS experiments over NW India and Garhwal Himalayas discovered a major conductivity structure running across Ganga basin into the foothills of Himalayas following the strike of Aravalli mountain belt of the Indian shield. The overall geometry of this conductivity structure can be approximated as an asymmetric domal upwarp in the middle and lower crust located between Delhi-

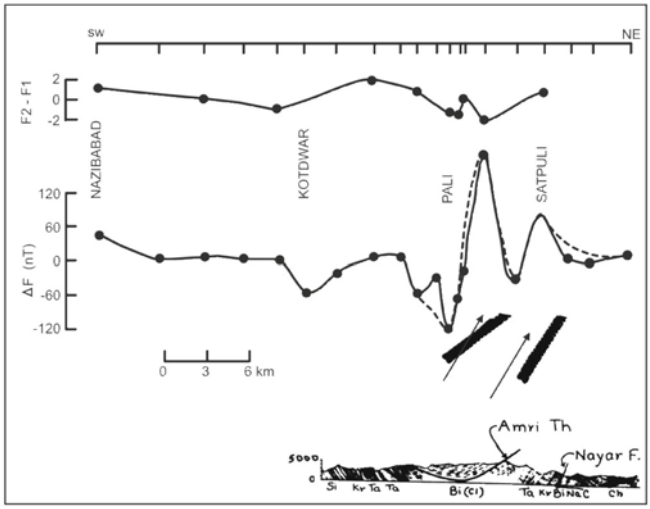

Figure 6.57. Trend-free magnetic anomalies associated with large susceptibility contrasts are shown to correlate with Amri thrust and Nayar fault. Two pronounced anomalies are interpreted in terms of intrusion of magnetic material along Amri thrust and Nayar fault (Singh et al., 1986).

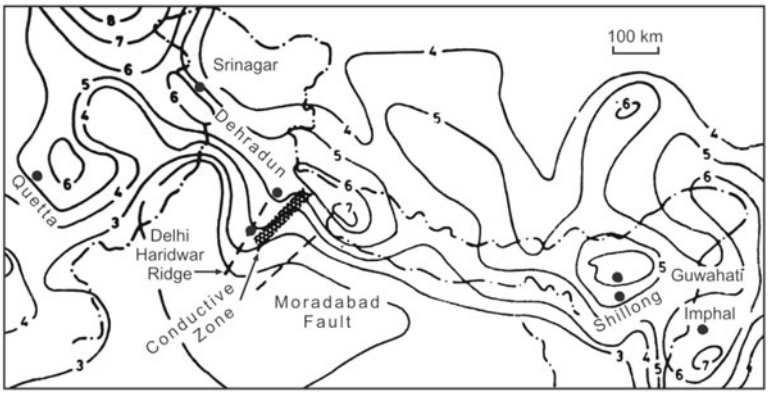

Figure 6.58. Position of trans-Himalayan conductivity structure identified by GDS studies (Arora and Mahashabde, 1987), superimposed on the quantitative seismicity contour map of the Himalayas (Kaila and Narain, 1976).

Hardwar ridge on the NW and Moradabad fault on the SE. The position of the conductive zone is shown in Fig. 6.58, overlain on quantitative seismicity map of the region. A zone of high seismicity characterizes this region, containing the electrical conductivity anomaly. The correlation suggests that this conductivity belt is associated with either present tectonic activity or with ancient tectonic structure, which is now reactivating.

III. Rohtak Region

In the 1960s and 1970s, Delhi and surrounding regions were frequently rocked by earthquakes. The temporary seismic network set up then recorded ~100 shocks of varying magnitudes for ~10 years duration. During Dec 1995, MT data were collected at 18 stations in Bahadurgarh-Jind region covering the epicentral cluster west of Delhi. The results indicate a deep NS trending ~5 km wide conductive feature located below Rohtak and Jind. Microearthquake data indicated deeper microseisms foci in the vicinity of this conductive zone, and the depth of foci to be decreasing away from it. Thus the conductive feature was proposed to be an active fault leading to the earthquakes.

IV. Khandwa-Jabalpur Region

The region surrounding Khandwa has been seismically active, where the earthquake swarms increased between Aug and Sept in 1998. Subsequently, MT surveys were undertaken and data collected at 30 stations along the 250 km long NS trending Burhanpur-Khandwa-Barwaha profile. The results indicated a conductive deep crustal intrusive ~50 km south of Khandwa, which was associated with the EW aligned Malwa ridge. The earthquake epicentres are located on the northern flank of this ridge. MT studies in the Damoh-Jabalpur-Mandla region delineated a similar deep crustal intrusive ~30 km SE of Jabalpur, which is again due to the Malwa ridge. This occurrence along with the enhanced seismic activity in the Khandwa region is indicative of the fact that the north flank of the Malwa ridge is seismically reactivated.

V. Nasik-Dalvat Region

The magnetic (GDS) and deep resistivity (MT) studies conducted in the Nasik-Dalvat region indicated a complex rift pattern in the basement, which is covered by 500 to 700 m thick Deccan volcanics. MT showed a NS aligned rift valley passing through Nasik, extending almost up to Dalvat on the Maharashtra-Gujarat border. Another rift valley was identified perpendicular to the Nasik–Dalvat rift near the village Vani ~30 km north of Nasik. Further investigations are needed to get a detailed picture of the rift pattern in this region.

VI. Koyna Reservoir Region

Spatial behaviour of residual magnetic field around the Koyna reservoir was monitored in four phases between May 1978 and October 1980. Figure 6.59 gives the residual field for three phases of measurements reckoned with respect to the field level of phase I (May 1978). The residual field pattern for phase III (May 1980) is quite different from those obtained during phase II and IV (January 1979 and October 1980). The characteristic pattern of phase III is explained in terms of electrokinetic effect suggesting water diffusion along NS fault running parallel to Koyna river in response to high pressure exerted

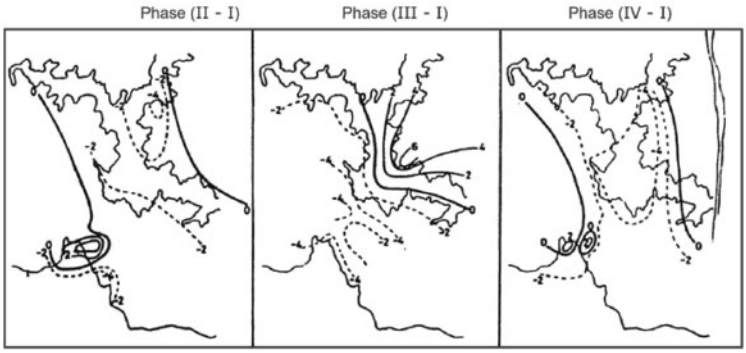

Figure 6.59. Contour map of temporal changes in residual geomagnetic field for three phases of measurements around Koyna reservoir (Arora, 1988).

by the reservoir. These results indicate that geomagnetic measurements in continuous mode can provide effective means of detecting precursory signals of earthquakes from Koyna region.

6.26 CO-SEISMIC INVESTIGATIONS—MAGNETIC AND ELECTRICAL ROCK PROPERTIES

Increased manifestation of Earth tremors both in seismic and aseismic areas makes it imperative to study this phenomenon more intensely. Magnetic and electrical properties of rocks are subjected to change with the stress imparted by impending earthquakes. Continuing worldwide efforts have shown that, from among the variety of geophysical precursors, geomagnetic and geoelectrical forewarnings lend good support to prediction programmes. Geomagnetic repeat surveys with high sensitive magnetometers in dense network configuration have proved effective in delineating long term (>few years) precursors.

Considering the recurrence of earthquakes in different parts of India including the seismically active Himalayan belt, and to isolate seismic precursors, an augmented plan has been put in place to monitor geomagnetic and geoelectrical parameters. Specifically, an increase in density of geomagnetic repeat stations, establishment of more digital geomagnetic observatories, electrical resistivity dipole and telluric current recordings supplemented by monitoring ionospheric parameters obtained from digital ionosonde (digisonde) and VHF receivers like ball antenna, form useful earthquake precursory experiments.

More frequent observations of magnetic field changes show better understanding of secular variation and help in delineation of stress induced changes in geomagnetic field. Noting that SV trend is locally distorted in seismic areas due to accumulating stress, a close network of repeat stations, as in Jabalpur, can be set up in other such areas. Efforts would need to transmit data

in real time by radio telemetry system to a centralized recording station where rapid on-line computerized analysis is organized for detecting short-term premonitory signals preceding an earthquake.

6.27 PREDICTING EARTHQUAKES

The goal of prediction is to issue warning of potentially damaging earthquakes early enough to allow appropriate response to the disaster for minimizing loss to life and property. The aim is to increase earthquake probability estimates within reasonable spatial and temporal accuracy. Earthquake probabilities are estimated in two ways: by studying the history of large earthquakes, and the rate at which elastic strain builds up in the rocks.

The frequency of past earthquakes is a pointer to future shocks. For example, if a region has experienced four M7 or larger earthquakes during 200 years of recorded history, and if these shocks occurred randomly in time, then it is assigned a 50% probability (just as likely to happen, as not to happen) to the occurrence of another M7 or larger quake in the region during the next 50 years.

But in many places, the assumption of random occurrence with time may not be true, because when strain is released along one part of the fault system, it may actually increase on another part; this reasoning is open to debate and controversy. For instance, four M6.8 or larger earthquakes and many M6.0-M6.5 tremors shook the San Francisco bay regions for 75 years between 1836 and 1911. For the next 68 years (until 1979), no earthquake of M6 or larger took place. Beginning with a M6 shock in 1979, earthquake activity in the region increased dramatically between 1979 and 1989, wherein four earthquakes of $M \geq 6$ struck, including the M7.1 Loma Prieta earthquake. This sort of clustering of earthquakes led scientists to estimate the probability of an M6.8 or larger earthquake to occur during the next 30 years in the San Francisco bay region to be ~67% (twice as likely as not).

Another way to estimate the likelihood of an impending earthquake is to study the rate of strain accumulation. When plate movements build the strain in rocks to a critical level, like pulling a rubber band too tight, the rocks suddenly break and slip to a new position. Scientists measure the amount of strain accumulating along a fault segment in a given time, say each year, the time passed since the last earthquake along the segment, and the quantity of strain released during the last earthquake. This information is then used to calculate the time required for the strain to build to the level capable of triggering an earthquake. This simple model is complicated by the fact that such detailed information regarding dynamic behaviour of faults is rare. Only the San Andreas fault system has adequate records for using this prediction method.

6.28 EARTHQUAKE PRECURSORY CHANGES

Forecast of earthquakes falls broadly in two categories: long and short range. For long range forecasting, a map showing all epicentres with spatio-temporal patterns of seismic activity is compiled. Figure 6.60 presents such a map along with major tectonic features and significant earthquakes (M ≥ 5) that helped identify main seismic belts in peninsular India. Statistical techniques are also employed to assess earthquake risks. The technique of short range forecast includes observation of foreshocks, space-time variation of earthquake activity, changes in seismic wave velocity, geomagnetic anomalies and others.

Some earthquakes in Russia, Japan, China and USA have been successfully predicted, though systematic precursory observations are very few. The science of earthquake prediction is still in its infancy. The current approach is to collect

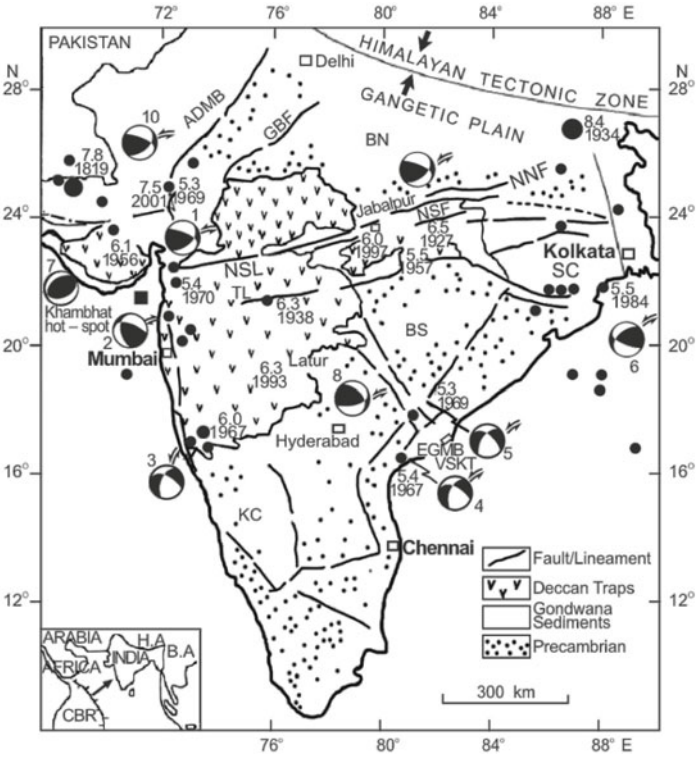

Figure 6.60. Epicentres of the major tectonic features and the significant earthquakes (M~5) in peninsular India; the recent damaging earthquakes are shown by star symbols. Preferred fault-plane solutions are shown by beachball symbols (1-6: after Chandra, 1977; 7: Chung and Gao, 1975; 8-10: USGS); the dark area indicates the zone of compression, and the blank area zone of dilatation, the fault movement is shown by arrows. NSL: Narmada Sone Lineament, NNF: Narmada North Fault, NSF: Narmada South Fault, TL: Tapti Lineament, KMF: Kutch Mainland Fault. Inset: Indian plate movement from theCarlsberg ridge (CBR), HA: Himalayan arc, BA: Burmese arc (Kayal, 2003).

data on all possible parameters and investigate possible correlations. This includes monitoring variations in seismic wave velocity, magnetic field, electrical resistivity, water level in wells, porosity/permeability, emanations of odours/gases and determination of ground deformation through tilt/strain measurements. In some cases even animal instincts (abnormal behaviour of certain animals) are reported to be helpful. For example, the Asian tsunami came as a complete surprise to humans, but the animals in the area had gone to higher ground hours before the tidal waves unleashed their wrath.

The physics of earthquake precursors is commonly described in terms of dilatancy-diffusion (DD) or crack-avalanche (CA) models. Non-universality of premonition signals is related to the diverse nature of earthquakes; shear-rupture or strike-slip motion. Because of limited information available on the nature of faults and lack of theoretical understanding of the growth, coalescence and recovery of fractures, the strategy for prediction depends upon observation of precursory changes. Delineation of active faults and knowledge of their

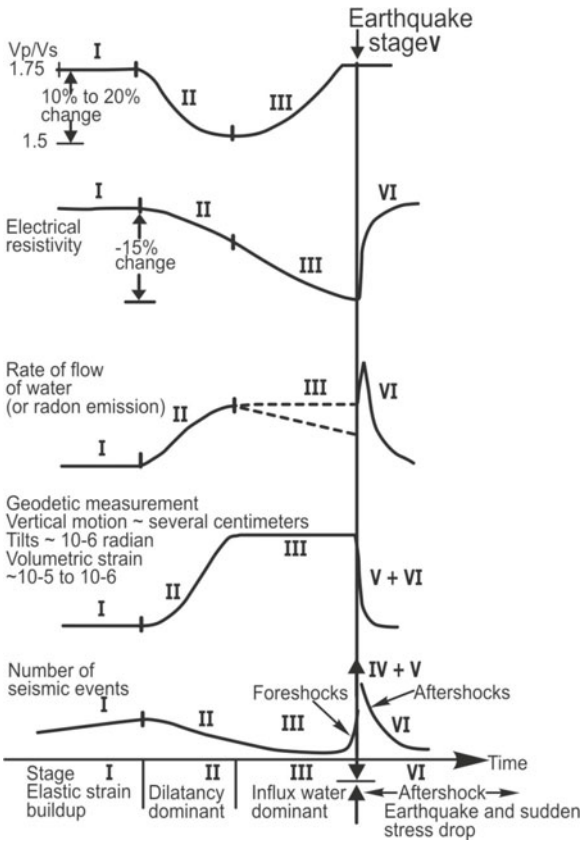

Figure 6.61. Predicted systematic changes in the rate of dilatancy, resistivity, volume, water flow and the number of seismic events as a function of time during earthquake cycle based on the dilatancy-diffusion model (Scholz et al., 1973).

stress distribution are of great help in optimizing forewarning observational networks.

The DD model developed experimentally by Scholz and his coworkers explains many of the premonitory phenomena (Fig. 6.61). They found that dilatancy is produced by the formation and propagation of cracks within the rock and these cracks begin to appear when stress level reaches nearly half of the fracture strength giving rise to changes in physical properties of rocks, such as permeability and electrical resistivity. This can be clearly seen from Fig. 6.61, which shows changes in Vp/Vs, electrical resistivity, radon emission, volumetric strain and number of seismic events (foreshocks). Stage I corresponds to the period of strain accumulation. This phase sees a steady increase in stress levels leading to an increase in volume of crustal rocks. During the phase of stage II, resistivity of rocks drops considerably due to an increase in the number and dimension of cracks and fluid flow into the dilatant zone. On the occurrence of an earthquake, there is a reduction in stress because of which cracks close and water flows out of the source region, resulting in the return of resistivity to its earlier values.

The CA model is also somewhat similar to DD model. In this model, physical properties change only slightly, marking the onset of phase I. After a certain critical density is reached, there is a marked increase in oriented fracture formation. There is thus an avalanche like rapid growth signifying the presence of phase II. The stage III begins with a further rise in strain accompanied by a drop in stress in the narrow zone of the future macro-fault. This also causes reduction in the stress throughout the volume of rock, dividing the area into two parts with differing properties. This model allows one to explain the relation between precursor times and the magnitude of impending earthquake.

The piezomagnetic theory explains the effect of stresses on magnetization of crustal rocks that causes anomalous changes in geomagnetic field in relation to seismic activity. The effects of stress on magnetic susceptibility and remanent magnetization are well understood. In general, the compression axis decreases while the transverse susceptibility tends to increase. The electrokinetic phenomenon, on the other hand, is based on the effect of water diffusion into newly created cracks in the dilatant region. The underground water, because of the effect of stress, is forced through the porous medium which creates a streaming potential inducing electric current flow. This current is strong enough to produce detectable variations in the electrical as well as magnetic fields at the Earth's surface.

6.29 EARTHQUAKE PRECURSORY CASE HISTORIES

Geomagnetic and geoelectric precursors have played a significant role in the prediction of earthquakes, for example in China, Greece and other parts of the world. The nature and duration of premonitory changes from its first appearance

till the time of earthquake suggest these two have large potential in medium and short-term, as well as in immediate prediction of earthquakes. However, the spatial extent and precursory time are seen to vary from one seismic zone to other. Inclusion of this aspect into earthquake prediction strategy in conjunction with other seismological and geophysical precursors would put these studies on a better footing from diagnostic (probabilistic) to prognostic (deterministic) level.

I. International Status

Secular variation anomaly in geomagnetic field prior to a large earthquake in Japan is given in Fig. 6.62, where station A is treated as a magnetic benchmark. Here the rate of SV during the decade of 1950-60 was ~7 nT/yr compared to the normal 2 nT/yr recorded at stations B and C. This anomalous behaviour disappeared after earthquakes of M6.1 and M6.4 close to station A, which showed up several years before and persisted up to the time of earthquake occurrence. A relation between the spatial extent of anomalous area and magnitude was obtained by Rikitake as: $\log r = 11.4 + 1.1\ M$, where r denotes the radius of the anomalous area in cm and M the magnitude.

Another example of short-term precursory change in geomagnetic field (Fig. 6.63) was detected in association with M5.2 earthquake on 28 Nov 1974 along an active fault in California. The plot gives the temporal variations in local geomagnetic field obtained by differencing the simultaneously observed field at two pairs of stations. In this process, the temporal variations associated

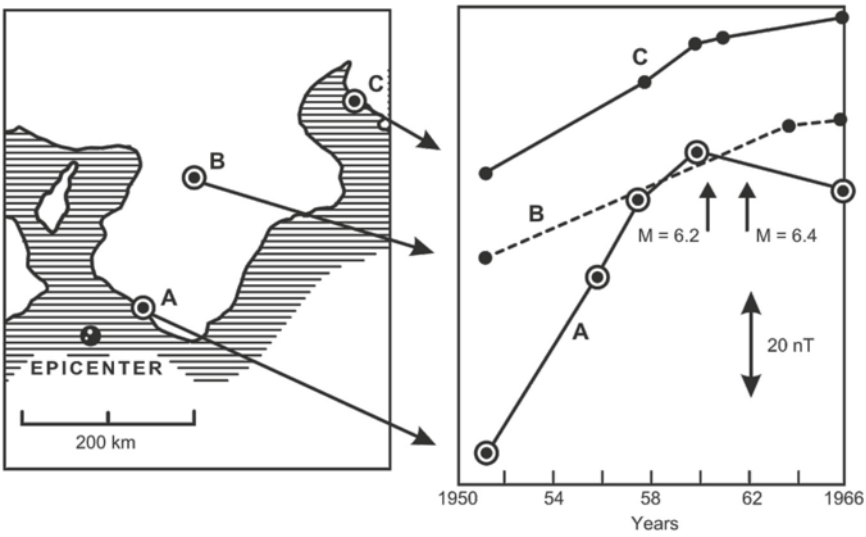

Figure 6.62. Typical example of anomalous behaviour of large secular variation in the geomagnetic field intensity observed in association with two earthquakes in Japan. Note secular change foreruns large earthquakes (Tazima, 1968).

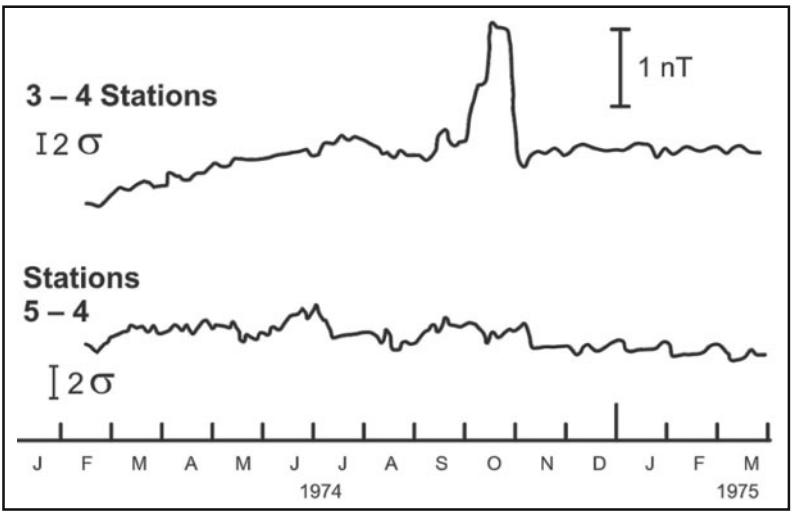

Figure 6.63. An example of mid-term precursory change in geomagnetic field detected in association with a magnitude 5.2 earthquake on 28 November 1974 along an active fault in California. Note a clear bay-shaped change in residual geomagnetic field intensity preceding the earthquake (Smith and Johnston, 1976).

with ionospheric and magnetospheric currents are effectively eliminated, leaving behind the component of tectonic origin. The plot shows a clear and distinct bay-shaped anomaly preceding the earthquake. It was seen that an increase in magnetic field began seven weeks before and returned to normal four weeks prior to the earthquake. The epicentral distance of this site was 11 km. Another place located only a few km away did not record any change. Such examples of precursory changes are many, but there are also instances, where no discernible change preceding an earthquake has been found.

The most popular techniques employed in China, Russia and USA for earthquake prediction are the measurement of telluric current, Earth potential and resistivity. In an experiment in China, electric potential difference between two pairs of electrodes aligned in NS and EW directions were measured daily, where potential difference between NS electrodes showed a sharp drop of 100 mV during ~2 to 3 days prior to the earthquake (M7.3) at Haicheng on 4 Feb 1975 (Fig. 6.64). At another station in the same region, but located at epicentral distance of 145 km, the NS component of telluric current had showed a 40 μAmp decrease ~10 hrs before the earthquake (Fig. 6.64). The anomaly lasted for 7 hrs and then the telluric current intensity recovered to the previous level, 3 hrs before the shock. Kamchatka in Russia is another area, where anomalies in telluric current forerunning impending earthquakes have been observed very often, which have now become one of the regular parameters for making short term predictions of earthquakes.

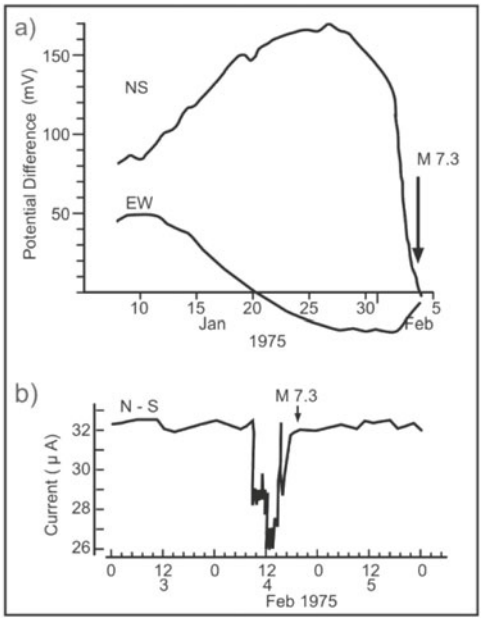

Figure 6.64. (a) Variation in self-potential differences between the NS and EW electrode pairs recorded in association with Haicheng earthquake at a station about 25 km from epicentre. Potential difference showed a sharp drop of >100 mV about 2–3 days before the earthquake. (b) Abrupt changes in electric current observed a few hours before Haicheng earthquake at a station located about 145 km from epicentre. Telluric current showed a 40 μA decrease about 10 hrs before the earthquake (Raleigh et al., 1977).

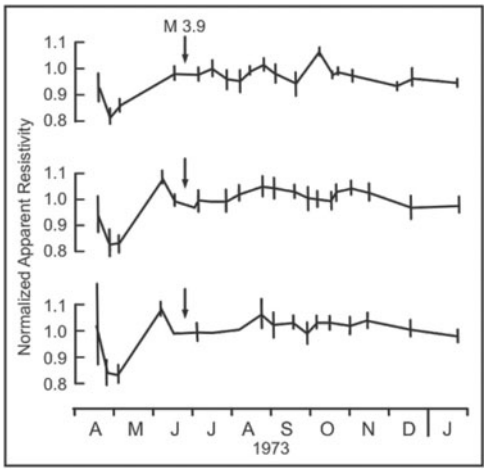

Figure 6.65. Changes in apparent resistivity observed in association with earthquake in the San Andreas fault region. Note a precursory change in resistivity amounting to 15% and lasting for 60 days before an earthquake of magnitude 3.9 (Mazzella and Morrison, 1974).

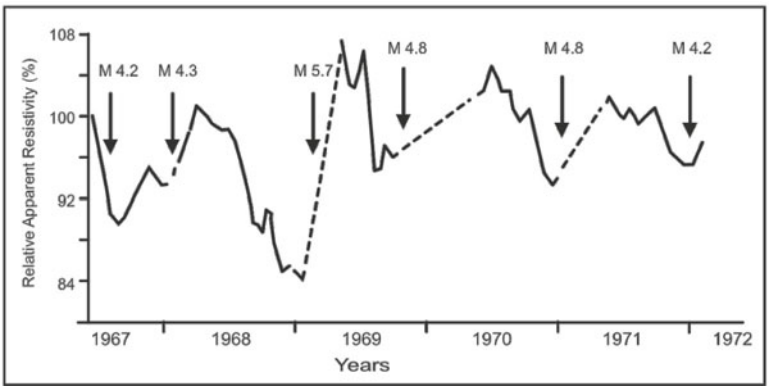

Figure 6.66. Temporal variation in apparent resistivity observed at Garm, central Asia and earthquake occurrence times of M>3. A strong correlation is evident between minima in electrical resistivity and earthquake occurrence time (Barsukov, 1974).

A strong correlation between minima in electrical resistivity and earthquake occurrence (Figs 6.65 and 6.66) is also found. A decrease in electrical resistivity is observed up to 20% for large/near earthquakes and up to 10% for small/distant earthquakes. The precursory time is seen to vary from ~2 to 7 months for earthquakes of M4.2 to M5.7, and it tends to be longer for larger earthquakes.

II. Results from Shillong, NE India

Geomagnetic field variations at Shillong, a place located in an intense seismic region, are examined for possible association with the felt earthquakes in its

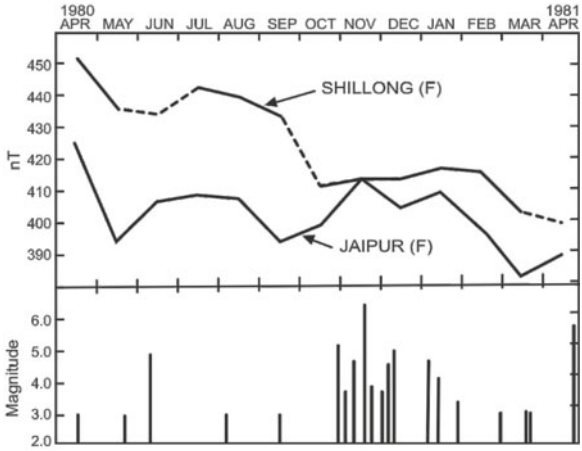

Figure 6.67. Changes of geomagnetic total field (F) at Shillong and Jaipur. The frequency of felt earthquakes during April 1980 to April 1981 is shown at the bottom and monthly variation in F (total geomagnetic field intensity) is shown at the top. Note the tectonomagnetic effect showing a systematic decrease in magnetic field at Shillong prior to earthquake during Sept to Oct 1980 (Chakrabarty, 1984).

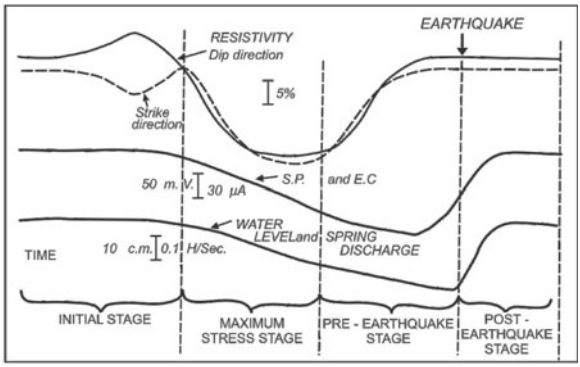

Figure 6.68. General trend of variation of geophysical (electrical resistivity, self potential and Earth current) and geohydrological (water level and spring discharge) parameters with the different stages of earthquake activity associated with M4.2 earthquake on 9 March 1980 near Shillong in NE India (Nayak et al., 1983).

vicinity. The results are compared with Jaipur, a station along the same latitude as Shillong, but differing in LT by one hour. It revealed a depression of the geomagnetic field prior to the shock, when epicentre of the earthquake is not too far away from Shillong (Fig. 6.67). The field change is most likely due to alteration in the crustal stress generated by NE Himalayas.

The geomagnetic field intensity curves for Jaipur and Shillong apparently display similar signatures (Fig. 6.67). However, a significant change in the total geomagnetic field intensity 'F' is observed at Shillong between Sept and Oct 1980. During this period Shillong shows –22 nT change, while Jaipur shows +5 nT change. The anomaly at Shillong is directly attributable to the earthquake occurrences during this interval (Sept-Oct 1980), which includes the largest M6.5 earthquake. Similar changes are also observed during other months as well. These observations thus reveal changes of regional geomagnetic field due to magnetization changes in subcrustal rocks.

Figure 6.68 gives changes in geoelectrical and geohydrological parameters such as electrical resistivity, self potential (S.P.), Earth current (E.C.), spring discharge and water level in dug wells recorded in association with 9 Mar 1980 earthquake (M~4.2) at a site near Shillong. Although precursory changes in all these measured parameters were seen preceding many earthquakes, the strongest precursory change was registered in resistivity, which gradually decreased by 25%. The precursory time in various parameters varied from 7 to 20 days.

III. Sunspot Activity and Earthquakes

Sunspot activity is also monitored to predict the occurrence of an earthquake. The sunspot hypothesis suggests certain changes in Sun-Earth environment affect the EMF that can trigger earthquakes in areas prone to it. During sunspot

activity, a huge mass (or energy) from the outer periphery of the sunspot is hurtled towards the Earth (Chapters 3 and 8). This disturbs the magnetic field and brings about changes in the atmosphere, ionosphere and geosphere. The changes associated with sunspot activity are known to take place typically ~24 to 36 hrs before a moderate earthquake and hence can be utilized to predict earthquakes. Such a change, for example, occurred on 24 Jan 2001 and two days later, a large earthquake measuring M7.7 hit Gujarat (Bhuj; on 26 Jan 2001).

6.30 PALAEOSIESMOLOGY: QUASI-EMPIRICAL EARTHQUAKE PREDICTION TECHNIQUE

'Palaeoseismology' is the study of prehistoric earthquakes in terms of their location (fault dislocation), timing (date) and size (magnitude). The probability of a future earthquake can be worked out, but not accurately predicted. To circumvent this lacuna, geoscientists study earthquakes of the geological past. The instrumental, historical and geological records reveal major quakes to recur after a gap of 100 years or more. The seismographs are not more than century old, which precludes the possibility of instrumental record beyond that timeframe. Historical earthquake records are scanty and do not go beyond 500 years. Religious scriptures have mentions of older earthquakes, but their veracity is difficult to confirm. But the earthquakes that go long back in time have left behind definite tell-tale marks, the study of which forms part of a comparatively new science called 'palaeo-seismology'. These signs are in the form of active faults, shifting of river courses, tilting of rock beds, displacement of strata, liquefaction of sediments (as sand dykes and sand blow), sudden change in sedimentation pattern in lakes and co-seismic land slides.

I. Methodology and Palaeoearthquake Studies

Sedimentary formations are normally deposited as layers and these are deformed if an earthquake occurs. While searching for past earthquakes, geoscientists search for clues that locate and identify deformational features called 'seismites'.

The study and methodology of palaeosiesmology involve identification of seismites, trenching and collecting relevant material for dating, and also cataloguing of stratigraphic sequences. Past earthquakes may generate a series of faults, hence it becomes necessary to ascertain the number of displacements (indicative of past earthquakes), which is done by excavating the trenches across the fault zone. The magnitude of a palaeoquake is judged by the amount of relative fault displacement. The age of the sediments displaced by the fault is then determined using various dating techniques. For example, the sample overlying the undeformed strata gives the minimum age, since it postdates the event. On the other hand, organic material deposited at the time of seismic event along with the deformed strata provides the coeval age, i.e. age pertaining to the palaeoseismic event. ^{14}C dates are then related to the geological signatures

to constrain the time of seismic occurrence along with measurement errors (uncertainties). Relative dating method of magnetostratigraphy is also undertaken to complement direct dating techniques.

Palaeoseimology also involves approximating probable magnitude, apart from estimating the timing of seismic event. The recurrence period of large earthquakes is then reconstructed from a set of events identified in a given area. This information helps in estimating the extent of areal threat experienced by the region in historical past, and serves to make realistic projections to mitigate the hazards.

II. Indian Palaeoseismological Studies

Palaeoseismological studies have recently started in India. An earthquake induced fault in Nainital was dated to 40 ka. Deformational structures (seismites) are mapped from Shillong plateau. The faulting due to M8.7 Shillong earthquake of 12 June 1897 shifted the course of Krishna river. Dated liquefied structures coincided with this earthquake timing. Studies also suggest the area quaked with similar magnitude 500, 1000 and 1500 years BP (1950 is taken as a reference year), suggesting recurrence period of 500 years. Similarly, a few notable studies show Latur was not just rocked for the first time in 1993, but damaging earthquakes had taken place in the area some 200 years ago too. Allah Bund is another palaeoseismological signature due to 1819 Kutch earthquake. Geologists investigating the 2001 Bhuj earthquake found a number of liquefaction features in the form of sand blows, ground fissures, mud craters and subsidence craters. Earthquake occurrences even much before the collision of the Indian and the Asian plate, some 120 Ma ago, have been found in deformational structures from the rocks of Chaibasa formation (2100 to 1600 Ma) of eastern India.

Since instrumental records are short and historical records sparse in India, it is necessary to understand the mechanism responsible for producing

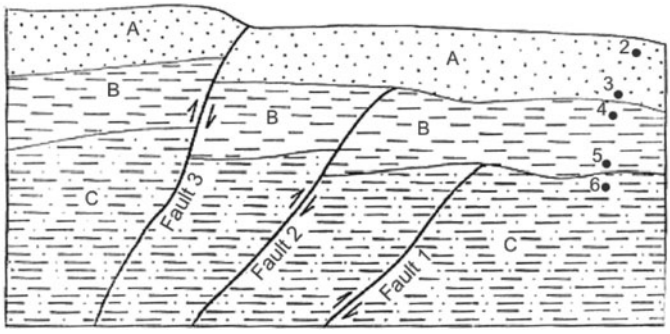

Figure 6.69. Dating faulted deposits. Trench exposure showing displacement of sand and gravel deposits. Fault 1 displaces only unit C, Fault 2 displaces B and C and Fault 3 displaces A, B, and C. Samples of 2, 3 (UB), 4, 5, and 6 (LB) are used for age estimation. UB - Upper bound, LB - Lower bound (Keller and Pinter, 1996).

catastrophic earthquakes and their repeat times from sedimentary sequences. Thus, palaeoseismological studies are of global relevance. Examples of palaeoearthquake age determination and an array of seismites are shown in Figs 6.69-6.72.

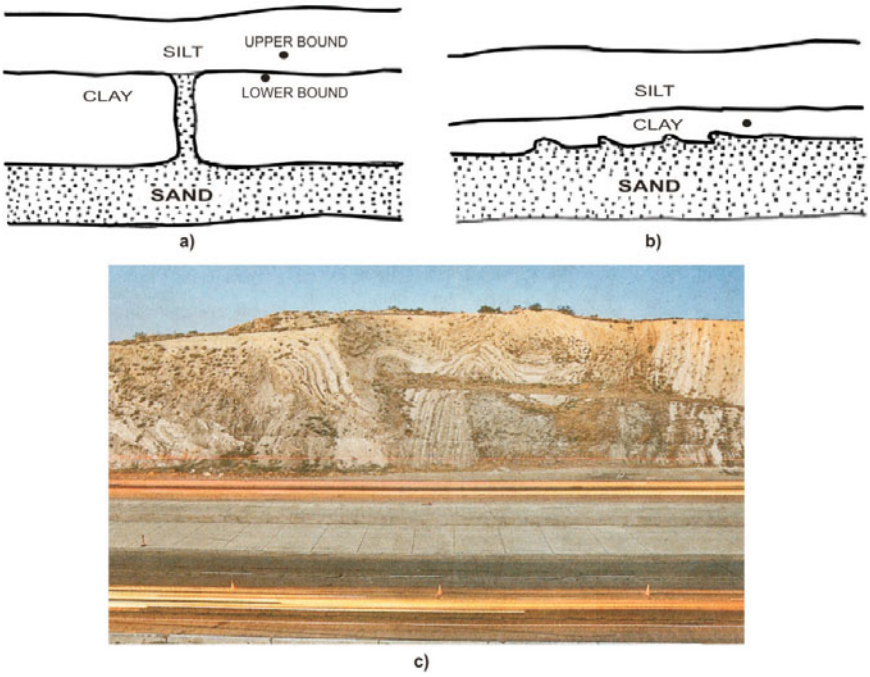

Figure 6.70. Dating of liquefaction features: (a) In case of sand dykes, (b) Penecontemporaneous event, and (c) Layers of earthquake-twisted ground seen at the San Andreas.

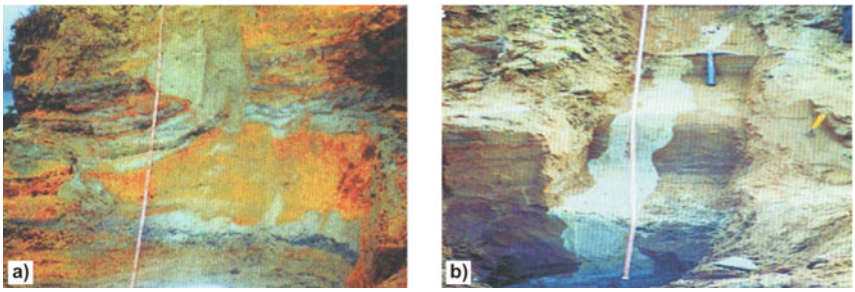

Figure 6.71. (a) Palaeoliquefaction feature at Nayapara site along the Krishna river, Shillong plateau, India. (b) A trench at Beltaghat meander showing multiple sand dykes originating from the sand bed below (Sukhija et al., 1999 a,b,c).

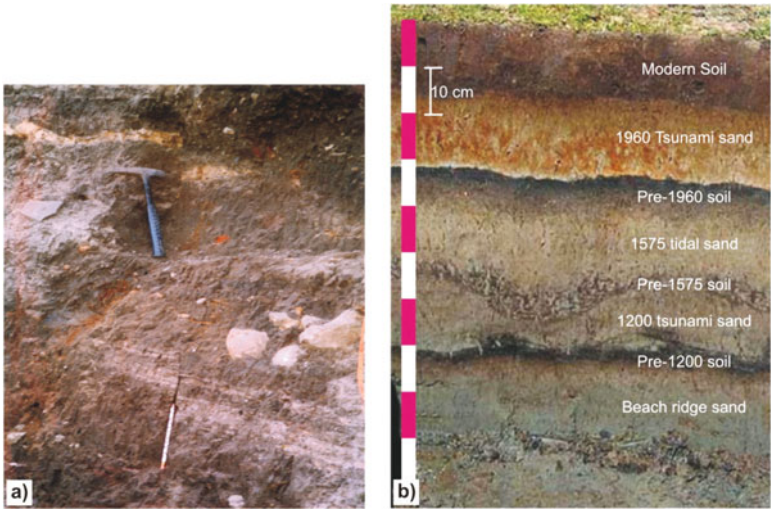

Figure 6.72. (a) A fault observed with a displacement of about 15–25 cm at Ther village, along Terna river. (b) Geological records of tsunamis from lithological field observations at Andaman Nicobar islands. Note that the sediments carried by the tsunami waves have an admixture of offshore and onshore material and are mainly composed of fine to medium sand layers.

6.31 GPS MEASUREMENTS AND GEODYNAMICS

The global positioning system (GPS) designed for military and civilian navigation has become a preferred method to study a wide range of geophysical phenomena. GPS measurements are now used to determine the motion of tectonic plates, deformation around active faults/volcanoes and to measure crustal isostatic adjustments in response to changes (past and present) in the mass of sediments/ice sheets. It is also used in combination with tide gauges to monitor global sea level changes. Because GPS signals are measurably delayed as they pass through the Earth's atmosphere, they are even able to contribute to atmospheric studies.

The tremendous growth in GPS research can be attributed to several reasons. It provides 3D relative positions with the precision of a few mm to a cm over baseline separations of hundreds of metres to thousands of kms. The 3D nature of GPS measurement allows to determine vertical as well as horizontal displacement at the same time and place. Previously, horizontal measurements were often made by trilateration and vertical measurements by spirit levelling. The two data types are almost never collected at the same time and place considerably complicating the analysis. Furthermore, the collective vertical and horizontal information often place more robust constraints on physical processes than do either data type alone. GPS receivers and antennas are portable, operate under essentially all atmospheric conditions, and do not require intervisibility between sites. The level of precision and accuracy are enhanced by using a combination of precise GPS satellite orbit information, dual-

frequency GPS receivers, advanced software packages for post-processing the GPS observations, and multipath-mitigating antennas, to name a few. With such a remarkable development, GPS found its way in the field of geophysics for studying crustal deformation.

GPS technology started out as a military tool. It was initiated in 1970s by the Department of Defense (DoD), and developed later to provide an invaluable navigational service in an alien terrain to save soldiers' time and life. In 1980, this utility was opened to civilian use as well. The remarkable development in space technology, radio science, and the experience with very long baseline interferometry (VLBI) greatly facilitated its development.

I. The GPS Constellation

The first of 24 satellites GPS network called NAVSTAR was launched in 1978. The cluster of NAVSTAR satellites orbits the Earth every 12 hours (twice a day), and emits continuous signals irrespective of weather conditions. These satellites run in a specific orbit, that is ~20,000 km above the ground, and travel as fast as 14,000 km/hr. The satellite orbits are distributed such that a set of at least four satellites are always visible from any point on the Earth at any given instant (with up to 12 visible at one time). Each satellite carries with it an atomic clock that 'ticks' with an accuracy of one nanosec (one billionth of a second). With proper equipment, any user can receive these signals to calculate time, location and velocity. Receivers have been developed for use in aircraft, ships and land vehicles. Portable ones are also available for hand carrying.

The navigation system uses radio frequencies that are sent out by the satellites to locate a transmitter. In this sense, signals transmitted from the satellites are 'trapped' by the GPS receivers, and then the time a signal was transmitted by a satellite is compared with the time it was received. The time difference, if any, tells the GPS receiver its distance from the satellite. With distance measurement from a few more satellites, the receiver determines the user's position and displays it on the unit's electronic map. In order to calculate latitude and longitude, receivers need information from three satellites. But if it has to determine altitude as well, then it has to receive information from four or more satellites. In addition, GPS can also provide other information such as sunset time.

GPS technology has now matured into a resource that goes far beyond its original visualized goals. These days scientists, sportsmen, farmers, soldiers, pilots, surveyors, hikers, delivery drivers, sailors, dispatchers, lumberjacks, fire-fighters, and people from many other walks of life are using GPS in ways that make their work more productive, safer, and sometimes even easier.

II. Principle

GPS satellites transmit synchronized signals on their position and real time (t) to the ground based receiver. The ground receiver however receives the signals

from a given satellite at a time ($t+\delta t$), where δt is the transmission delay between the satellite and the ground station. This delay at ground station is different for signals arriving from different satellites positioned at different places in space. The ground station processor uses these delays to compute its location with reference to the four 'best' satellites. The set of four satellites helps determine the four unknown parameters at the ground station, viz. the three position coordinates in space and the fourth, time. The error of measurement of these parameters is governed by various external parameters, such as the error in the position and time coordinates transmitted by a satellite, the constellation (spatial distribution of the satellites at the time of measurements), the topospheric refraction of the electromagnetic signals, etc.

III. GPS System and Sources of Errors

The GPS system has been designed to be as accurate as possible. But, it still gives out some errors. These errors, when compiled together, cause a deviation of ±50 as 100 m from the actual GPS receiver position. The source of errors is many, but the most significant ones are discussed below:

Atmospheric conditions, also known as ionosphere and troposphere, delay causing an inaccuracy due to reduced speed of propagation. Radio signals travel with the velocity of light in the outer space, but are slower through the ionosphere and troposphere. The GPS system uses a built-in model that calculates an average amount of delay to partially correct for this type of error.

Signal multipath occurs when the GPS signal is reflected off objects such as tall buildings or large rock surfaces before it reaches the receiver. This increases the travel time of signal, thereby causing errors. It is difficult to completely correct multipath error, even in high precision GPS units. Hence, this error has become a serious concern.

Satellite orbits: Although the satellites are positioned in very precise orbits, slight shifts are possible due to gravitation forces. The resulting error is very low, which is not >2 m.

Receiver clock errors: A receiver's built-in clock is not as accurate as the atomic clocks onboard the GPS satellite. Therefore it may have very slight timing errors.

Satellite geometry/shading refers to the relative position of the satellite at any given time. Ideal satellite geometry exists when the satellites are located at wide angles relative to each other. Poor geometry occurs when the satellites are located in a line or in a tight grouping.

6.32 OBSERVATIONAL PROCEDURE

GPS receivers and antennas: The ground-based GPS equipment is only a receiver, without any transmitting capability. The satellites do not contain any

Figure 6.73. GPS unit at Shillong.

database about their location or other parameters. They are equipped with only highly precise atomic clocks that generate some codes, which are transmitted to the Earth. The GPS receiver gets that code from multiple satellites which is slightly time shifted due to difference in the distance to the satellites. Using this difference, the receiver precisely calculates the geographic longitude and latitude of its own position. Indian scientists use both Trimble and Leica GPS receivers for data collection.

A GPS site is chosen such that it has exposed bedrocks with unobstructed view of the sky and a non-reflective environment. About 1 cm diameter and 6 cm deep hole is made into strong and sturdy bedrocks and a non-magnetic stainless steel pin is rigidly driven into the hole. A fine dot of 0.5 mm is made on the pin to aid accurate measurements (Fig. 6.73). Later, 2-channel dual frequency receivers are used in re-occupation mode. Microstripped omni directional (with 9 cm internal ground plate) GPS antenna is placed over the marks (fine dot made on the pin) using tripods. The sampling interval and cut-off angle of elevation (to receive signals from the orbiting satellites) are then fixed at 30 sec and 15^{o}, respectively. However, the sampling interval and cut-off angle of elevation can be changed according to the requirement and needs of the purpose.

6.33 METHODOLOGY, DATA ACQUISITION AND ANALYSIS

GPS satellites transmit signals on two carrier frequencies: the L1 carrier and L2 carrier. L1 carrier is 1575.42 MHz, used for civilian purposes and the L2 carrier is 1227.60 MHz used for more precise military purposes. These signals

travel by line of sight, i.e. they pass through clouds, glass and plastics, but cannot go through most solid objects such as buildings, mountains, etc. In every transmission the satellite sends three types of information: *Pseudo-random code* is an I.S. code that identifies which satellite the information is being sent from. *Ephemeris data* tells the receiver, where the satellite should be at any given time of day. The *Almanac data* is the part that is essential for determining the user's position. Almanac data is constantly transmitted by each satellite, and it contains important information about the status of satellite (healthy or unhealthy), the current date and time.

GPS methodology follows three different approaches: (i) *Estimating the strain field* in seismic zones using GPS receivers: Precise measurement of baselines between well defined ground markers is made. The methodology is such that the changes in position coordinates and baseline lengths in three orthogonal directions (coordinates)—computed with GPS data during two or more visits to the same place or during successive reoccupations—enable to assess crustal deformation in the survey region. Four to five sets of observations are required to estimate the strain field. In addition to the observed strain field, attempts are made to compute strain field for hypothetical stress distribution either by the method of least-square collocation or finite element method. This enables to relate the GPS results to the seismotectonics of the region. (ii) *Establishing certain prerequisites* in high precision geodesy, and (iii) *Establishing the ability of synthetic aperture radar (SAR) interferometry* for deformation measurements: SAR is a new technique in which the phases of two SAR scenes are made to interfere to generate interference fringes which relate to terrain elevations. This technique promises to revolutionize the study of active tectonics by providing high precision deformation measurements carried out remotely from space.

The GPS data is normally organized into 24 hrs covering Greenwich Mean Time (GMT) day. The data are processed using the GAMIT post-process software to produce estimates, and associated covariance matrix of station positions for each session. The site coordinates are constrained by surrounding International GPS Service for Geodynamics (IGS) stations. To get a combined solution for site positions and velocities, all such covariance matrices are input to GLOBK software, which is essentially a Kilman filter that gives the coordinates and velocity vectors at each site. Figure 6.74a shows the horizontal component of the velocity vector with 95% confidence error ellipses. The horizontal components of these velocity vectors are further used to estimate the horizontal strain field by least-squares prediction method in which two empirically deduced local covariance functions (corresponding to E-W and N-S components of horizontal crustal movement in Gaussian form) are used.

6.34 GPS: REPEAT CAMPAIGNS, PERMANENT SITES AND CASE STUDIES

I. Survey Design

GPS networks are operated all over the world to estimate crustal displacements. Permanent networks like CIGNET and the IGS network have proven their utility to the geodetic community for orbit determination, and have also been used for plate tectonic studies. India started GPS in 1995 and since then taken up campaign-style repeat surveys over a period of time in seismically active regions, viz. western Maharashtra, Bhuj, Chamoli, North-East India, Andaman & Nicobar Islands, and Antarctica (here focus is on glacial movements). Continuous GPS (or permanent GPS) monitoring is an essential complement of seismological observations (time unit: sec), and geological (time unit: a ka or a Ma). It is the only technique that can directly measure displacements about a few mm/year over distances of several hundred kms. In view of this, a network of 13 permanent GPS sites are established in different parts of the Indian subcontinent, four in Andaman-Nicobar Islands, and two in east Antarctica region. The GPS data obtained at these stations are used to detect ionospheric TEC perturbations associated with large vertical ground movements related to earthquakes.

II. Seismological Device

Before describing some results obtained with GPS data, its general role of crustal deformation measurements in the study of earthquakes is discussed. Measuring long term current displacements of the crustal blocks in an active zone of deformation like the Himalayas allows to know the amount of energy which accumulates at the active faults, which could be released during earthquakes. These measurements are complementary to seismological data because they document the full earthquake cycle, including interseismic and transient postseismic processes, as well as coseismic deformation. To directly monitor crustal deformation between (interseismic), during (coseismic) and after (postseismic) earthquakes, there are several well established and recognized space-borne geodetic (geodesy is the science of surveying and mapping the Earth's surface) techniques such as VLBI, satellite laser ranging (SLR), SAR interferometry, and GPS. Compared to these techniques, GPS is more widely used in deriving crustal displacement, velocity and strain distribution because its receivers are cost-efficient and highly portable allowing their deployment in large numbers and also in frequently repeating modes as warranted by the deformation status of a particular region. Apart from these factors, post-process softwares, which circumvent purposeful degradation of GPS signals by the DoD to reduce the accuracy and precise orbits from International GNSS Service (IGS), make it ideal to use GPS for geodynamic studies.

GPS data are used to accurately determine horizontal as well as vertical movements to characterize active fault regions, and to determine the position of centroid of the deformation zone. GPS records serve as equivalent tools to very low frequency seismograms. Recently, many countries have developed a way to use GPS satellites to monitor the environment, which could lead to better weather prediction models. They are also trying to develop a system using GPS signals to image things on the ground, measuring soil moisture, and the thickness of ice on the Earth's surface. Few GPS applications in studies of the weak crustal motion, geodynamics (velocity and strain field), and glacial movement are discussed here.

III. Plate Motions and Plate Boundary Deformation

The success of the GPS investigations depends to a large extent on the speed at which the crustal movements occur. In the absence of any significant movements in the crust, the GPS studies may not be conclusive. At present, the Indian continent is subducting below the Eurasian continent at a rate of 4 to 5 cm/yr. This fact has been established by the GPS studies, which have shown that the distance between Bangalore and Hanley (Ladakh) is decreasing at the rate of 4 to 5 cm/year. Thus, GPS data are vital to understand the compressive effects and estimate strain within different crustal blocks, which is possible by taking a NS trending profile across the entire Indian subcontinent.

It is instructive to examine geological and tectonic evidences after the 26 December 2004 Andaman-Sumatra giant earthquake. GPS data from Andaman & Nicobar Islands, nearby IGS sites, and some sites from the Indian subcontinent indicated thtat the south Indian shield shifted towards east by ~1.5 cm, and all the baselines cutting across the India-Burma interface have been shortened by 2-4 cm.

IV. Crustal Deformation in Deccan Trap Region

From GPS data, 2D strain field is estimated and modelled for crustal deformation. GPS has brought out an extensional regime along the western coast of Maharashtra including south of Koyna and Warna reservoirs, which transcend into a region of compressive strain towards the interior of the shield area. The extensional strain regime coincides with the west coast geothermal province, and intersecting fault system south of Koyna-Warna reservoirs. The crustal deformation strain rate has been estimated to be in the range of 40 to 60 mm/year (Fig. 6.74a) with an average of 51 mm/year in N47°E and compressive strain of ~0.4 μ-strain/year (Fig. 6.74b). Strain pattern in the Deccan trap region is a reflection of the transmitted stress field caused by northward continental collision between Indian and Eurasian plates along the Himalayan arc in NS to NNE-SSW direction (Fig. 6.74a).

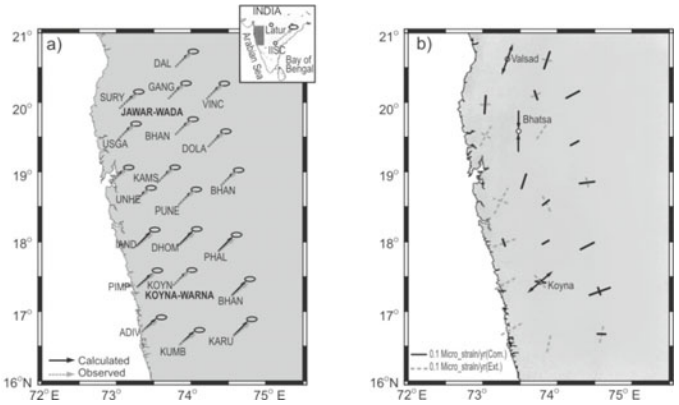

Figure 6.74. (a) Observed and calculated horizontal velocity vectors at 21 sites in Deccan volcanic province. The velocity vector for IGS site IISC (Bangalore) is shown in the inset. (b) Principal axes of strain at GPS sites corresponding to the dilatation strain rate. Note the axes of compressional and extensional strain rates (Reddy et al., 2000).

V. Crustal Deformation in Bhuj Region

Bhuj earthquake affected region is investigated for evaluation of seismotectonics of the region. A compressive strain of ~0.1 μ-strain/year in the epicentral region is established, and the crustal deformation strain rate is estimated to be about 50 mm/year in N-NE direction (Fig. 6.75). The residual velocity of 11.62 mm/year in N-NW direction and 5.24 mm/year towards south is seen at sites south and north of the epicentre. This indicates localized ongoing convergence in the epicentral region. The results also suggest ongoing transpressional deformation across the area with a blocked structure embedded between the north and south Wagad fault. This deformation is believed to be

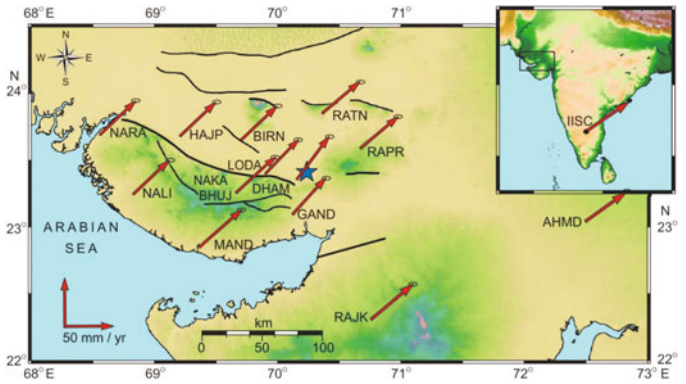

Figure 6.75. GPS derived velocity vectors in ITRF2000 estimates from Bhuj. Star (blue coloured) indicates the 2001 earthquake. The study region and velocity of IISC (IGS site) are shown in inset.

related to the present neotectonic compressive stress regime of the Indian plate due to its NNE movement against the collision front in the north, and its proximity to the triple junction in the western continental margin of the study area.

VI. Antarctic Schirmacher Glacier Movement

GPS studies on ice-sheet dynamics of the Schirmacher glacier (east Antarctica) have revealed that the magnitude of horizontal velocities of the glacier sites lie between 1.89±0.01 m/year and 10.88±0.01 m/year to the N-NE with an average velocity of 6.21±0.01 m/year. The velocity and strain-rate distributions across the GPS network in Schirmacher glacier are spatially correlated with topography, subsurface undulations, fracture zones/crevasses and the partial blockage of the flow of nunataks and the Schirmacher oasis (Fig. 6.76).

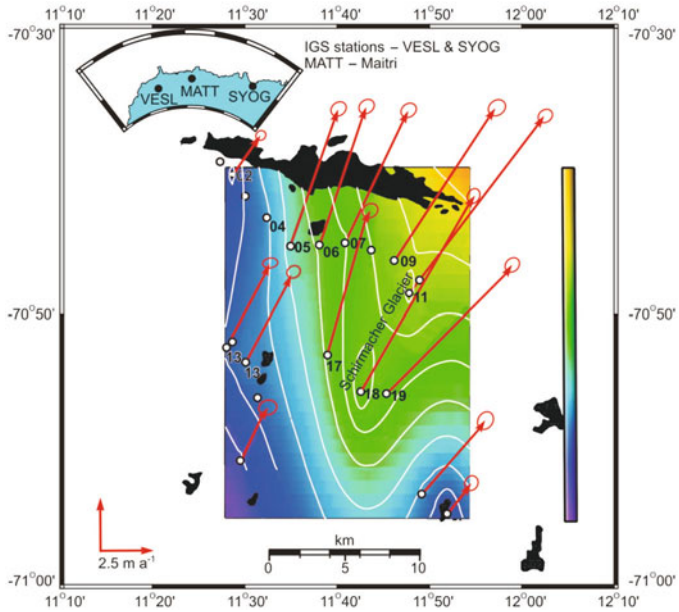

Figure 6.76. Horizontal velocity vectors (with 95% confidence ellipses) for the GPS network on Schirmacher glacier, superposed on a shaded relief velocity–distribution map with 1 m contour interval obtained from the GPS velocity field. The scale represents the glacier flow rate corresponding to the velocity shaded relief (m/yr). The black patches indicate the Schirmacher oasis and nunataks (Sunil et al., 2007).

APPENDIX 6.1

Maxwell's Equations

To understand the propagation and attenuation of electromagnetic waves, it is necessary to use Maxwell's equations relating to electric and magnetic field vectors.

Name	*Differential form*	*Integral form*
Gauss's law	$\nabla \cdot \mathrm{D} = \rho$	$\oint_s \mathrm{D} \cdot d\mathrm{A} = \int_v \rho d\,\mathrm{V}$
Gauss' law for magnetism (absence of magnetic monopoles)	$\nabla \cdot \mathrm{B} = 0$	$\oint_s \mathrm{B} \cdot d\mathrm{A} = 0$
Faraday's law of induction	$\nabla \times \mathrm{E} = -\frac{\partial \mathrm{B}}{\partial t}$	$\oint_\mathrm{C} \mathrm{E} \cdot d\mathrm{I} = -\frac{d}{dt}\int_s B \cdot d\,\mathrm{A}$
Ampère's law (with Maxwell's extension)	$\nabla \times \mathrm{H} = \mathrm{J} + \frac{\partial \mathrm{D}}{\partial t}$	$\oint_\mathrm{C} \mathrm{H} \cdot d\mathrm{I} = \int_s \mathrm{J} \cdot d\,\mathrm{A} + \frac{d}{dt}\int_s \mathrm{D}$

Symbol	**Meaning**	**SI Unit**
E	electric field	V/m
H	magnetic field also called the auxiliary field	A/m
D	electric displacement field also called the electric flux density	C/m^2
B	magnetic flux density also called the magnetic induction also called the magnetic field	Tesla or Wb/m^2
ρ	*free* electric charge density, not including dipole charges bound in a material	C/m^3
J	*free* current density, not including polarization or magnetization currents bound in a material	A/m^2

APPENDIX 6.2

Transfer Function Estimates

The transfer functions showing the relationship between seafloor station horizontal components (X_{SF} and Y_{SF}) and land station horizontal components (X_L and Y_L) are estimated from the magnetic storm and sub-storm (bays) by using tensor analysis. The relationship between the horizontal field components and transfer function is given by

$$X_{SF} = A\,X_L + B\,Y_L$$
$$Y_{SF} = C\,X_L + D\,Y_L$$

where the subscripts SF stands for seafloor station while L for land reference station. The analysis has been carried out in frequency domain. A, B, C, and D are thus the frequency dependant complex numbers and are known as transfer functions, for the north and east components of geomagnetic field variation between land and seafloor station. Transfer functions are computed by using tensor analysis technique. Single station vertical transfer functions are calculated from

$$Z = Txx\,X + Tyy\,Y$$

where X, Y and Z are time varying magnetic fields observed at that particular station. The following assumptions are made in order to calculate the transfer functions: (i) The normal inducing field (X_n,Y_n) is nearly equal to the observed field X and Y, i.e. (X_n,Y_n) = (X,Y) and (ii) in low and middle geomagnetic latitudes the normal Z-component is zero and hence total recorded Z can be taken as wholly anomalous, i.e. $Z_a = Z$.

APPENDIX 6.3

Trembles that Shook Mumbai in the Past

Year	*Month*	*Intensity (MMI)/Magnitude (RS)*
1618	May	IX
1832	Oct	VI
1906	March	VI
1929	February	V
1933	July	V
1951	April	VIII
1966	May	V
1967	April	4.5
1967	June	4.2
1993	September	6.4
1998	May	3.8
2005	March	5.1
2005	June	3.7
2005	August	4.1

APPENDIX 6.4

Major Earthquakes in the History of the Indian Subcontinent

Year	*Location*	*Magnitude*	*Intensity*	*Death Toll*
1618	Mumbai	-	-	2000
1720	Delhi	6.5	-	2000
1737	Bengal	-	-	3000
1803	Mathura	6.5	-	Hundreds, shock felt up to Calcutta
1803	Kumaon	6.5	-	200-300
1819	Kutch, Gujarat	8.0	XI	Thousands, chief towns of Tera, Kathara and Mothala razed to the ground
1828	Srinagar, Kashmir	6.0	-	1000
1833	Bihar	7.7	X	Hundreds
1848	Mt.Abu, Rajasthan	6.0	-	Few people killed
1869	Assam	7.5	-	Affected an area of 2,50,000 sq. miles
1885	Srinagar, Kashmir	7.0	-	1,600
12 June 1897	Shillong	8.7	XII	1600
4 April 1905	Kangra, Himachal	8.0	XI	20,000
1906	Himachal Pradesh	7.0	-	Heavy damage
1916	Nepal	7.5	-	All houses at Dharchula in Pithoragarh, India collapsed
8 July 1918	Assam	7.6	-	Heavy damage
1930	Dhubri, Meghalaya	7.1	IX	Heavy damage in Dhubri
15 August 1934	Northern Bihar-Nepal	8.3	XI	20,000
1935	Quetta, Pakistan	7.5	IX	25,000
26 June 1941	Andaman Islands	8.1	X	Very heavy damage
1947	Dibrugarh	7.8	-	Heavy damage
15 August 1950	Assam	8.6	XII	>1,500
1952	Northeast India	7.5	-	Heavy damage
1956	Bulandshahar, Uttar Pradesh	6.7	VIII	Many killed
1956	Anjar, Gujarat	7.0	VIII	Hundreds of people killed
1958	Kapkote, Uttaranchal	6.3	VIII	Hundreds of people killed

(Contd.)

Year	*Location*	*Magnitude*	*Intensity*	*Death Toll*
10 December 1967	Koyna, Maharashtra	6.5	VIII	200, Koyna Nagar razed to ground
1969	Bhadrachalam, Andhra Pradesh	6.1	I	Moderate damage
19 January 1975	Kinnaur, Himachal Pradesh	6.2	-	42
1980	Dharchula, Uttaranchal	-	-	Heavy damage
1980	Jammu, J&K	-	-	12
1986	Dharamshala, H.P.	5.7	VIII	Heavy damage
1988	Almora, Uttaranchal	-	-	1000
1988	Assam	7.2	XI	Few people killed
21 August 1988	Bihar- Udaypur (Nepal)	6.5	VIII	Large number of people killed
20 October 1991	Uttarkashi, Uttaranchal	6.6	VIII	768, heavy damage to property
30 September 1993	Latur, Osmanabad, Maharashtra	6.4	VIII	>9,000, heavy loss of property
22 May 1997	Jabalpur, Madhya Pradesh	6.0	VIII	40, heavy damage to property
29 March 1999	Chamoli, Uttarakhand	6.8	VIII	100, heavy loss of property
26 January 2001	Bhuj, Gujarat	7.7	X	>20,000, huge devastation
25 October 2005	Mujaffarabad, Pakistan and Kashmir, India	7.6	X	73,000 dead including both countries. Heavy loss of property